

KfK 2840  
EUR 5758 e  
Februar 1980

**9<sup>ème</sup>**  
**Journée des Actinides**  
**May 31 - June 1, 1979**

**Editors:**  
**B. Kanellakopoulos, L. Manes**  
**Institut für Heiße Chemie**  
**Europäisches Institut für Transurane**

**Kernforschungszentrum Karlsruhe**



KERNFORSCHUNGSZENTRUM KARLSRUHE

Institut für Heiße Chemie

KfK 2840

EUR 5758 e

9<sup>ème</sup> Journée des Actinides

May 31 - June 1, 1979

Editors: B. Kanellakopulos  
L. Manes<sup>x)</sup>

<sup>x)</sup> European Institute for Transuranium Elements

Kernforschungszentrum Karlsruhe GmbH, Karlsruhe

Als Manuskript vervielfältigt  
Für diesen Bericht behalten wir uns alle Rechte vor

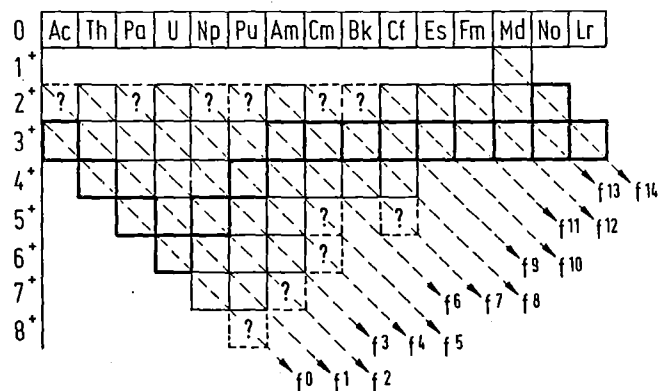
Kernforschungszentrum Karlsruhe GmbH  
ISSN 0303-4003

# 9ème JOURNEE DES ACTINIDES

May 31 - June 1, 1979

PLACE:

SCHULE FOR KERntechnik  
KFK KARLSRUHE



ORGANIZATION:

B. Kanellakopoulos, KFK-KARLSRUHE/IHCH

L. Manes, EUROP. INSTITUTE FOR TRANSURANIUM ELEMENTS

## Introduction

The series of the "Journées des Actinides", coming now to its ninth edition, have represented a useful occasion for researchers of different European Laboratories to exchange results and ideas. They have been mostly dedicated to the physics, chemistry and physical chemistry of the solid state of actinides, metals and compounds. They have taken place at different sites, sponsored, in turn, by a different Laboratory or Institution: thus, personal contacts and discussions have been stimulated.

The special feature of these conferences has been their informality. In the "Journées", researchers may present, at their will, completed works or just work being performed and even puzzling results or ideas, in the hope of being enlightened and helped, during the Journées, by others. Another feature has always been the strong interdisciplinarity of these conferences: in them, the physicist learns, for instance, how difficult the preparation of the "exotic" sample is, which he uses for his measurements, the chemist deepens his knowledge by following "exotic" theoretical treatments of the actinide physics.

In presenting the Proceedings of the "9<sup>ème</sup> Journée des Actinides", held in Karlsruhe from May 31 to June 1, 1979, we are happy to realize that the features above mentioned have been amply respected: in fact, they are essential to the success of the "Journée". In addition, we are happy to see that the field of actinide research is continuously expanding, as proved by the interest and the work of Laboratories not present in precedent editions, and by the inspiring results in all fields, which have been discussed.

It is necessary to clarify the spirit of the Proceedings that we offer; they respect the feature of informality of the Journée. They contain therefore already published work (which is referenced) as well as uncomplete results and even abstracts. It is reminded that the choice, whether to appear with a written text or with an abstract only was left to individual authors.

In concluding these introductory remarks, we express the hope that new and inspiring "Journées" will take place, giving other Laboratories the chance (and the head-ache) of organizing and us the opportunity of learning.

We wish to thank all Participants, and the Organizations sponsoring  
the Journée:

Basil KANELLAKOPULOS

Kernforschungszentrum Karlsruhe GmbH,  
Karlsruhe

Livio MANES

European Institute for Transuranium  
Elements, Joint Research Center of  
the European Commission, Karlsruhe

Contents

	Page
1) Reactions des ions d'elements f en solution aqueuse avec des ligands a soufre atome donneur R. FITOUSSI, C. MUSIKAS	5
2) Eu(II) complex formation in solution G. LE MAROIS, C. MUSIKAS	17
3) Preparation and x-ray analysis of $(\eta^5\text{-C}_5\text{H}_5)\text{UCl}_3 \cdot 2\text{HMPA}$ : Trichloro- $(\eta^5\text{-cyclopentadienyl})\text{bis}(\text{hexamethylphosphoramide})\text{Uranium(IV)}$ F. BENETOLLO, G. BOMBIERI, G. DE PAOLI, P. ZANELLA	18
4) Chemistry of mendelevium: monovalent state of mendelevium is not observed in aqueous solution F. DAVID, K. SAMHOUN, E.K. HULET, P.A. BAISDEN, R. DOUGHAN, J.H. LANDRUM, R.W. LOUGHEED, J.F. WILD, G.D. O'KELLEY	19
5) Preparation and single crystal growth of protactinium arsenides by chemical vapour transport G. CALESTANI, J.C. SPIRLET, J. REBIZANT, W. MÜLLER	30
6) Quelques résultats récents des recherches sur les composés d'actinides A. WOJAKOWSKI	42
7) Analyse des impuretés métalliques dans les actinides de pureté élevée par spectrographie d'émission au moyen d'un plasma d'argon induit par haute fréquence (ICAP-OES) R. GAUTHIER, H. KUTTER, F. KINNART	43

- 8) Phase transition of  $\text{ThBr}_4$  and  $\text{ThCl}_4$  51  
P. DELAMOYE, S. HUBERT, S. LEFRANT, J.C. KRUPA
- 9) Etude des fluorures et oxyfluorures de plutonium 57  
par thermochromatographie  
B. JOUNIAUX, Y. LEGOUX, J. MERINIS, G. BOUISSIÈRES
- 10) Magnetic and electric properties of  $\text{Pu}_2\text{O}_2\text{Y}$  compounds 65  
(Y = O, S, Se, Te)  
J.M. COSTANTINI, D. DAMIEN, C.H. de NOVION,  
COUSSON, ABAZLI, PAGES, A. BLAISE, R. GUILLAUMONT
- 11) Enthalpy of formation of americium dioxide and 76  
estimate of enthalpy of formation of aqueous  
americium(IV) ion  
L.R. MORSS, J. FUGER
- 12) Low temperature specific heat of plutonium carbides 77  
R.O.A. HALL, H.R. HAINES, J.A. LEE, M.J. MORTIMER,  
D. McELROY
- 13) News from the uranium-sulfur system: On the synthesis 92  
and the magnetic properties of the uranium polysulfide  
 $\text{U}_2\text{S}_5$   
H. NOËL
- 14) Magnetic Properties of  $\text{NpAs}_2$  93  
M. BOGÉ, J. CHAPPERT, A. BLAISE, J.M. FOURNIER,  
D. DAMIEN, J. REBIZANT, J.C. SPIRLET
- 15) Magnetic susceptibility of pentavalent uranium oxyhalides 94  
J.C. LEVET, H. NOËL
- 16) EPR of  $\text{Gd}^{3+}$  in actinide compounds 95  
G. AMORETTI, D.C. GIORI, V. VARACCA

- 17) Neutron diffraction study of  $^{243}\text{AmO}_2$  105  
A. BOEUF, J.M. FOURNIER, J.F. GUEUGNON, L. MANES,  
J. REBIZANT, F. RUSTICHELLI
- 18) E.S.C.A. Study of uranium(IV) Halides 109  
E. THIBAUT, J.P. BOUTIQUE, J. VERBIST,  
H. NOËL, J.C. LEVET
- 19) Surface studies by photoemission of the laves 117  
phases  $\text{UAl}_2$  and  $\text{UCo}_2$   
J.R. NAEGELE, L. MANES, N. NOLTE, J.M. FOURNIER
- 20) State of Angular resolved photoemission on the compound 133  
 $\text{USb}$   
Y. BAER, R. BAPTIST, M. BELAKHOVSKY, M.S.S. BROOKS,  
O. VOGT
- 21) Preliminary observation of low temperature defect 134  
interactions in cubic  $^{241}\text{AmO}_2$  from  $^{237}\text{Np}$  Mössbauer  
emission spectroscopy  
J. FRIEDT, R. POINSOT, J. REBIZANT
- 22) Mössbauer effect and magnetic susceptibility studies 137  
of the non stoichiometric neptunium oxides:  $\text{NpO}_{2+x}$   
J. GAL, C. MUSICAS, A. COUSSON, J. JOVÉ, M. PAGÈS
- 23) Mössbauer effect and magnetisation studies of the 138  
monoclinic  $\text{NpSe}_3$   
J. JOVÉ, A. COUSSON, M. PAGÈS, R. POTIER, D. DAMIEN,  
C. COSTANTINI, J. GAL
- 24) Strongly correlated electron bands and magnetism in 139  
transition metals  
Application to actinide metals and compounds  
K.A. LONG

25)	On the regularity of the cohesive energy of the lanthanide elements B. JOHANSSON	164
26)	Kondo effect in U, Np and Pu metals V. DALLACASA	165
27)	Self-consistent band structure calculations for fluorite structure compounds M.S.S. BROOKS, P.J. KELLY	194
	List of participants	204

REACTIONS DES IONS D'ELEMENTS F EN SOLUTION AQUEUSE  
AVEC DES LIGANDS A SOUFRE ATOME DONNEUR

---

R. FITOUSSI, C. MUSIKAS

---

Centre d'Etudes Nucléaires  
de Fontenay-aux-Roses

1 - Introduction

Les composés et complexes des ions d'actinides et de lanthanides avec le soufre sont intéressants à étudier du fait de la faible différence d'électronégativité entre le soufre et les ions des éléments f. Celle-ci doit permettre d'observer des liaisons à électrons plus délocalisés qui n'existeront pas dans les composés où l'atome donneur du ligand est plus électronégatif. Sur la figure 1 sont rassemblés deux graphiques montrant la variation des paramètres de maille pour des composés isostructuraux oxygénés et soufrés des éléments 4 f et 5 f [1]. Dans les sesquioxides, on a une variation sensiblement parallèle des distances métal-ligand pour les deux séries, alors que dans les monosulfures le paramètre de la maille cubique varie différemment dans les deux séries.

En première approximation, on peut supposer que les différences d'aptitude à la délocalisation des électrons 4 f et 5 f sont révélées pour les sulfures, alors qu'elles sont masquées pour les oxydes à cause de la forte ionicité des liaisons métal-oxygène.

En solution aqueuse, les sulfures d'éléments f sont décomposés car la compétition soufre-oxygène pour les sites de coordination du métal est en faveur de ce dernier. En milieu anhydre et sous atmosphère inerte Holah et Brown [2] ont préparé des complexes d'actinides trivalents et tétravalents avec les ions dithiocarbamates. Sur la figure 2 est représenté le polyèdre de coordination du neptunium dans le composé  $\text{Np}(\text{DTC})_4 \text{N Et}_4$ .

Les complexes d'actinides hexavalents avec les dithiocarbamates tels que  $UO_2 (DTC)_2$  [3] et  $UO_2 (DTC)_3$  N Et 4 [4] ont également été étudiés (figure 2).

Par extraction Curtui et al [5 et 6] ont mis en évidence des complexes de l'uranium avec des acides dialkyldithiophosphoriques, tel que  $UO_2 (DTP)_2$ , ROH et  $UO_2 (DTP)_2$ , TBP. Nos travaux [7] sur l'extraction de l'uranium à partir d'un milieu acide phosphorique concentré, par un mélange acide dialkyldithiophosphorique - composé organophosphoré neutre ayant l'oxygène pour atome donneur ont également permis de montrer qu'un complexe de formule  $UO_2 (H_2PO_4) (DEHDTP) (R_3PO)$  était obtenu en phase organique.

## 2 - Partie expérimentale.

Tous les produits utilisés sont de qualité Normapur.

Les acides dialkyldithiophosphoriques ont été synthétisés par l'I.R.C.H.A.

L'étude de la complexation des actinides par les dithiophosphates en milieu aqueux, a été réalisée en utilisant deux techniques :

- spectroscopie UV-visible (Cary 17) par la méthode des solutions correspondantes. On a effectué les mesures de densité optique à une longueur d'onde de 380 nm, sur la bande de transfert de charge soufre-uranium.

- spectroscopie d'émission Raman (Coderg). On a étudié les variations de la bande de vibration symétrique uranium-oxygène à  $870 \text{ cm}^{-1}$  en fonction de la concentration en dithiophosphate. Un étalon interne est nécessaire afin de normaliser les spectres du fait des fluctuations d'intensités émises et des rendements de la détection qui peuvent varier d'une expérience à l'autre.

## 3 - Résultats.

Nous allons présenter les résultats d'études de complexes avec les dialkyldithiophosphates dont la formule développée est montrée sur la figure 4.

Par rapport aux dithiocarbamates, ils présentent les avantages suivants :

- les dithiocarbamates sont rapidement décomposés en mi-

lieu acide pour donner  $CS_2$  et l'amine protonée, alors que les dialkyldithiophosphates sont beaucoup plus stables [8].

- Les pKa des dialkyldithiophosphates sont plus petits que ceux des dithiocarbamates ce qui permettra d'étudier les complexes en milieu plus acides. (Tableau I)

R	DTC	DTP
$CH_3$	3.66	1.55
$C_2H_5$	4.04	1.62
$C_3H_7$	4.79	1.75
$C_4H_9$	5.19	1.82

Tableau I : pKa des acides dialkyldithiocarbamiques et dialkyldithiophosphoriques.

DTC : Acides dialkyldithiocarbamiques

DTP : Acides dialkyldithiophosphoriques

- Uranium (VI)

On a déterminé la première constante de complexation régie par l'équation suivante :

$$K_1 = \frac{[(UO_2 \quad S_2P(OR)_2)]}{[UO_2^{2+}] [(RO)_2 \quad PS_2]} = 1 \pm 0,2$$

On trouve une constante de complexation =  $1 \pm 0,2$  avec les dialkyldithiophosphates ayant pour radical,  $CH_3$ ,  $C_2H_5$  ou  $C_4H_9$ . On peut voir sur la figure 5, un spectre Raman d'une solution d'uranium  $5.10^{-2}$  M. La bande à  $870 \text{ cm}^{-1}$  correspond à la vibration de l'ion aqueux et celle à  $860 \text{ cm}^{-1}$  à celle du complexe 1 : 1.

Alors qu'avec les dialkyldithiophosphates ayant pour radical  $CH_3$  ou  $C_2H_5$ , nous n'observons la formation que d'un complexe 1 : 1, il se forme avec le dibutyldithiophosphate un second complexe qui demixe. Cette demixion peut être attribuée au fait que le complexe est neutre, et par ailleurs que les chaînes butyl sont hydrophobes. Le spectre Raman de ce complexe, montre que la bande de vibration Uranium-oxygène est déplacée à  $845 \text{ cm}^{-1}$ .

- Neptunium (V)

Un phénomène de précipitation est mis en évidence avec le Neptunium V. En effet nous n'observons pas de formation de complexe entre les ions Np (V) et dimethyl ou diethyldithiophosphate. Par contre avec l'ion dibutyldithiophosphate on obtient la précipitation du complexe 1 : 1. Il a été étudié par la méthode de solubilité. La solubilité des ions Np (V) est montrée sur la figure 6 en fonction de la concentration en ions  $DTP^-$  dans le surnageant. On a vérifié par spectrophotométrie que la solution ne contient que des ions  $NpO_2^+$ .

La concentration des ions  $\text{NpO}_2^+$  en solution obéit à la loi du produit de solubilité.

$$K_s = (\text{NpO}_2^+) \cdot (\text{DTP}^-)$$

Tableau II : Comparaison des produits de solubilité des dibutylphosphates et dibutyldithiophosphates de neptunium (V).

Complexe	Ks	ref
$\text{NpO}_2$ (DTP)	$9 \cdot 10^{-5}$	-
$\text{NpO}_2$ (DBP)	$5.2 \cdot 10^{-7}$	191

On a consigné Tableau II les produits de solubilité des composés peu solubles neptunium (V) dibutylphosphate et neptunium (V) dibutyldithiophosphate. On peut remarquer l'insolubilité plus grande du complexe formé avec le donneur oxygéné.

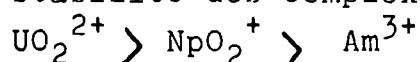
L'étude spectrophotométrique a montré que les deux ions trivalents ne forment pas de complexes en solution aqueuse avec les ions dialkyldithiophosphates.

#### 4 - Conclusion

Notre étude a montré que le complexe  $\text{UO}_2(\text{DTP})^+$  existe en solution aqueuse. Des complexes plus riches en ligand sont observés dans des phases organiques en contact avec des solutions aqueuses.

Dans le cas des ions pentavalents on peut précipiter le composé  $\text{NpO}_2(\text{DTP}) \cdot x\text{H}_2\text{O}$  avec le radical butyl. Lorsque le radical est éthyl ou méthyl aucun solide n'est observé. Comme dans le cas de la formation du second complexe de l'uranium (VI), un effet dû à la longueur des chaînes organiques du ligand est observé.

En l'état actuel de nos travaux, on peut dresser la séquence de stabilité des complexes dialkyldithiophosphoriques.



Cet ordre est le même que celui des complexes azotures ou sulfocyanures (11). La faible stabilité des complexes observés est en accord avec l'idée qu'on se fait d'un ion de type "a" d'après la classification de Chatt, Arhland et Davies (10). Les valeurs du Tableau III permettent de comparer la stabilité des complexes des ions  $\text{UO}_2^{2+}$  (type a) et  $\text{Pb}^{2+}$  (type b) avec les ions dibutylphosphate et dibutyldithiophosphate.

Tableau III : Comparaison des constantes de formation des complexes 1 : 1 des ions  $\text{UO}_2^{2+}$  et  $\text{Pb}^{2+}$  avec les ions dibutylphosphates et dilentylolithiophosphates.

	DBDTP <sup>-</sup>	DBP <sup>-</sup>
$\text{UO}_2^{2+}$	$10^0$	$10^{4.43}$
$\text{Pb}^{2+}$	$10^{29.4}$	$10^{1.3}$

BIBLIOGRAPHIE

- [1] D. DAMIEN. Thèse présentée à l'Université de Clermont-Ferrand II. (1976)
- [2] D. BROWN. D.G. HOLAH, C.E.F. RICKARD, J. Chem. Soc. 1970, 786
- [3] L. MALATESTA, GAZZ. Chim. Ital., 1939, 69, 752
- [4] R.A. ZINGARO, J. Am. Chem. Soc., 1956, 78, 3568  
K. BROWMAN, Z. DARI, Chem. Commun., 1968, 636
- [5] G.H. MARCU, M. CURTUI, I. HAIDUC, J. Inorg, Nuclear Chem. 1977, 39, 1415
- [6] I. HAIDUC, G.H. MARCU, M. CURTUI, Rev. Roum. Chim. 1977, 22, 625
- [7] R. FITOUSSI, C. MUSIKAS, B. F. 78.33 544, 1978
- [8] W. BODE, Z. ARNSWALD, Anal. Chem., 1962, 188, 1979
- [9] C. MUSIKAS, G. Le MAROIS, J. RACINOUX, Colloque International sur la thermodynamique des matières nucléaires. Juliers (1979) I.A.E.A. SM 236 (à paraître)
- [10] S. ARHLAND, J. CHATT, N.R. DAVIES, Quart. Rev. 1958, 12, 265
- [11] C. MUSIKAS, M. MARTEAU, Radiochem. Radioanal. Lett. 30.(4) 1977. 271.

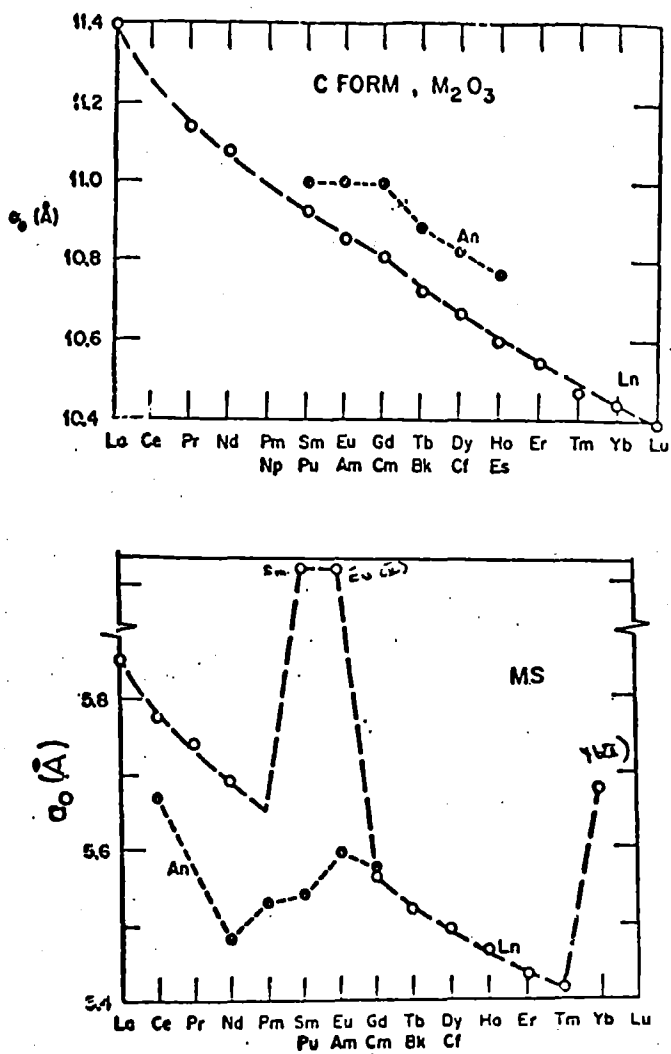


Figure 1 : Comparaison des paramètres de maille des sesquioxides et des monosulfures d'éléments 4 f et 5 f.

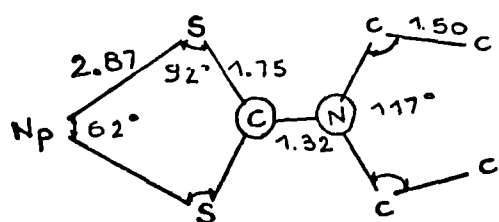
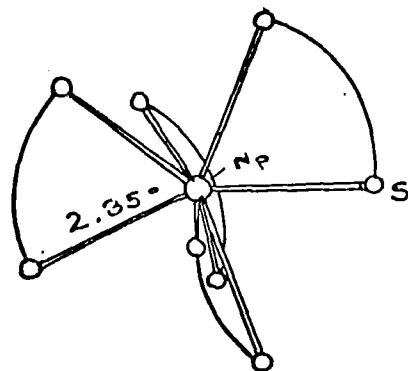


Figure 2 : Polyèdre de coordination des ions Np (III) dans le composé  $\text{Np}(\text{DTC})_4 \text{N}(\text{Et})_4$

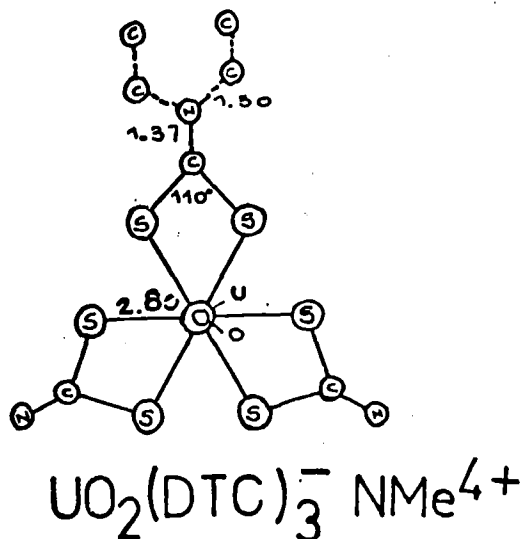


Figure 3 : Polyèdre de coordination de l'uranium (VI) dans le dithiocarbamate d'uranium et de tétraméthylammonium.

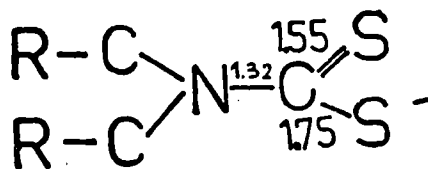
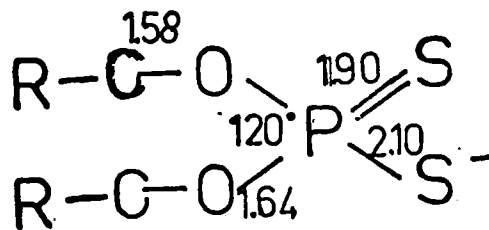


Figure 4 : Taille des ions dialkyldithiocarbamate et dialkyldithiophosphate.

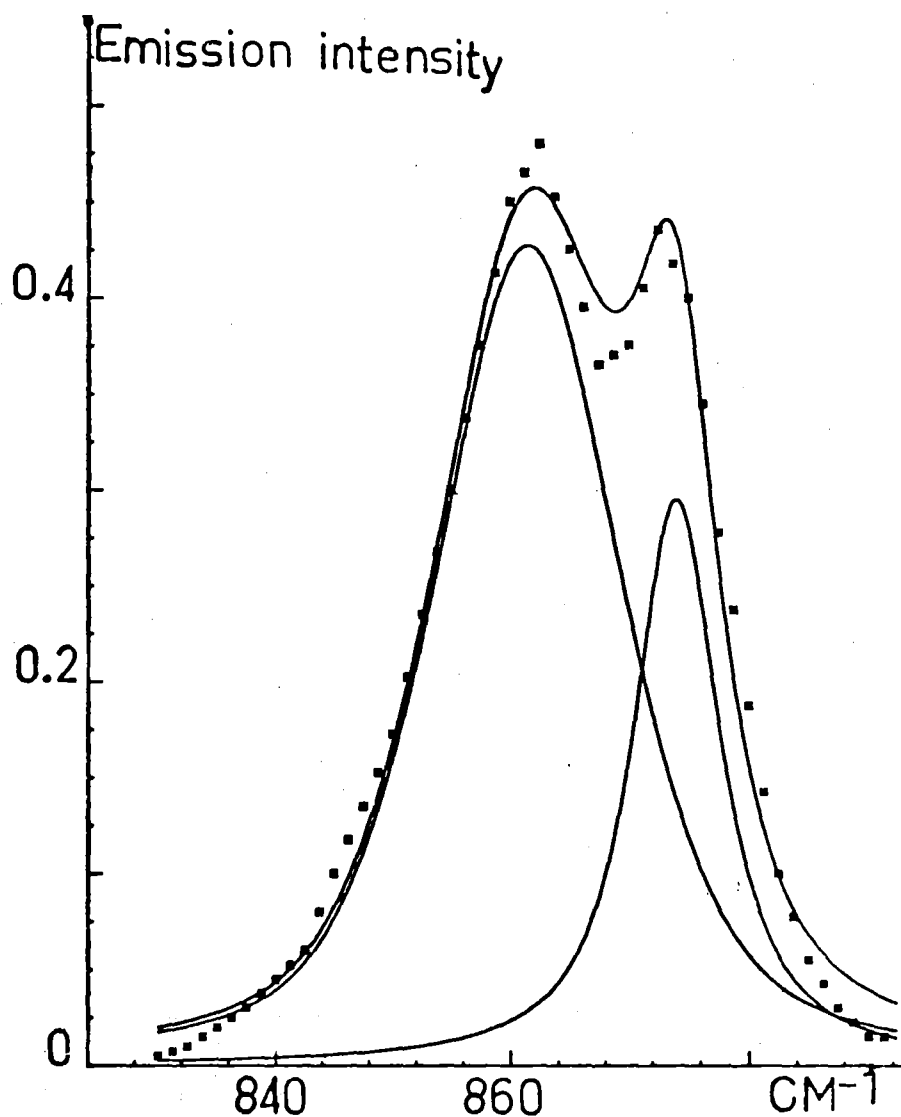


Figure 5 : Spectre Raman de l'uranium (VI) en présence d'ions diethyldithiophosphate.

$C_{\text{UO}_2^{2+}}$  :  $5 \cdot 10^{-2}$  M

$C_{\text{DEDTP}^-}$  : 1.2 M

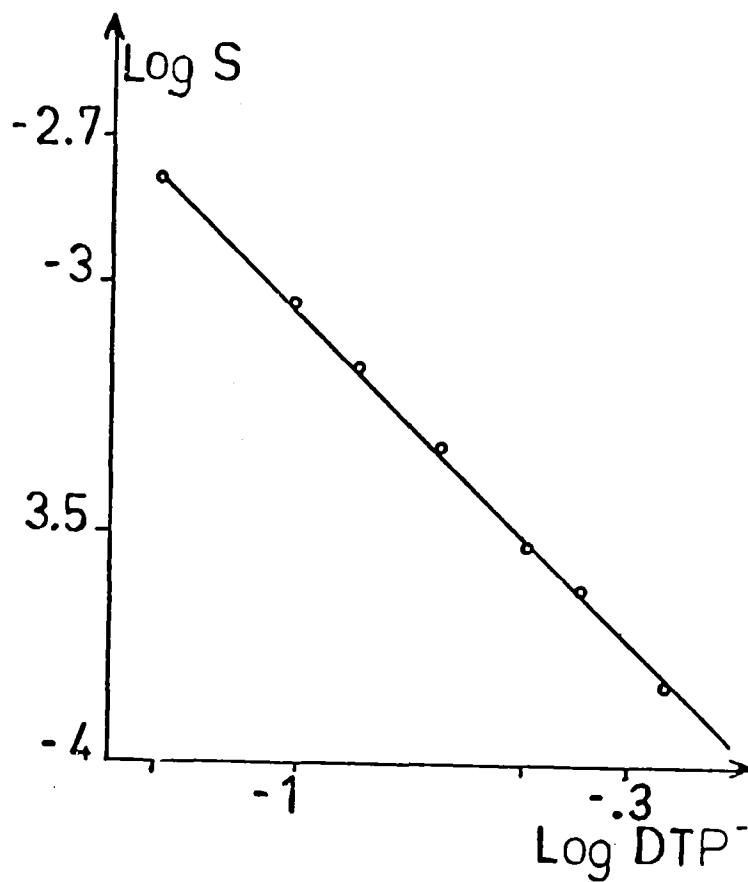


Figure 6 : Solubilité des ions Np(V) en milieu dibutyldithiophosphorique.

## Eu (II) COMPLEX FORMATION IN SOLUTION

G. LE MAROIS, C. MUSIKAS

Centre d'Etudes Nucléaires  
de Fontenay-aux-Roses

The complex chemistry of f block element in the divalent state has not been investigated extensively. Generally it is supposed that Eu (II) behaves like Sr (II) the alkaline earth ion which has the closest ionic radius. We shall report a study of Eu (II) complex ions with orthophenanthroline.

The main conclusions drawn from that study are :

- Eu (II) give complexes with orthophenanthroline which are more stable than Eu (III) ones and Sr (II) ones.

This can be probably imputed to the 4 f electrons participation to the bonds which is probably important in the case of the rather soft orthophenanthroline ligand. In addition to thermodynamic stabilization, coordination to orthophenanthroline slow down the rate of oxidation of Eu (II) by oxygen or water.

PREPARATION AND X-RAY ANALYSIS OF  $(\eta^5\text{-C}_5\text{H}_5)\text{UCl}_3 \cdot 2\text{HMPA}$ : TRICHLORO-  
 $(\eta^5\text{-CYCLOPENTADIENYL})\text{BIS}(\text{HEXAMETHYLPHOSPHORAMIDE})\text{URANIUM(IV)}$ .

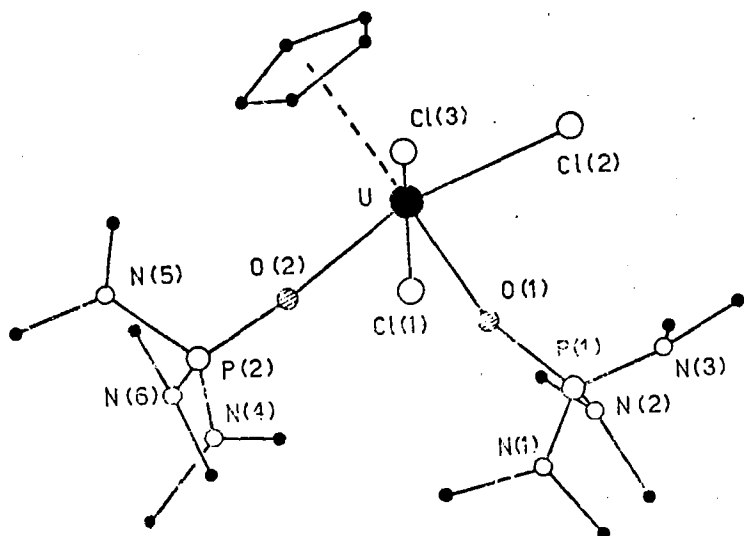
F. Benetollo, G. Bombieri, G. De Paoli and P. Zanella  
*Laboratorio di Chimica e Tecnologia dei Radioelementi del C.N.R.*  
*Corso Stati Uniti - 35100 PADOVA - Italy*

K. W. Bagnall

*Chemistry Department, University of Manchester, MANCHESTER*  
*M13 9P1 - England*

Following a research program on oxygen-donor complexes of cyclopentadienyl uranium(IV) halides<sup>1</sup>, the compound  $(\eta^5\text{-C}_5\text{H}_5)\text{UCl}_3 \cdot 2\text{HMPA}$  (HMPA = Hexamethylphosphoramide) was prepared by reacting  $\text{UCl}_4 \cdot 2\text{HMPA}$  and  $(\eta^5\text{-C}_5\text{H}_5)\text{Tl}$  (molar ratio = 1) in tetrahydrofuran at room temperature. Prismatic green crystals were obtained by crystallization of the crude product from a mixture of n-pentane and tetrahydrofuran.

Crystal data.  $(\eta^5\text{-C}_5\text{H}_5)\text{UCl}_3(\text{HMPA})_2$ , monoclinic,  $a = 9.942(6)$ ,  $b = 32.005(15)$ ,  $c = 9.576(6)$  Å,  $\beta = 106.3(1)^\circ$ ,  $Z = 4$ . Space group  $P2_1/n$ ,  $\text{MoK}\alpha$  radiation,  $R = 0.077$  for 4170 observed intensities.



The structure consists of discrete molecules of  $(\eta^5\text{-C}_5\text{H}_5)\text{UCl}_3(\text{HMPA})_2$  in which the uranium atom has a coordination geometry quite similar to that of the TPPO derivative (TPPO = triphenylphosphine oxide)<sup>2</sup>. A view of the molecule is given in figure. The coordination octahedron

is formed by two oxygen atoms of the HMPA ligands in *cis*-position, three chlorine atoms and the cyclopentadienyl ring. The substitution of the HMPA for TPPO does not influence the coordination geometry around the uranium atom.

1. K.W.Bagnall, J.Edwards and A.C.Tempest, *J. Chem. Soc., Dalton*, 295, 1978 and ref. therein.
2. G.Bombieri, G. De Paoli, A.Del Pra and K.W.Bagnall, *Inorg.Nucl. Chem.Letters*, 14, 359 (1978).

CHEMISTRY OF MENDELEVIUM : MONOVALENT STATE OF  
MENDELEVIUM IS NOT OBSERVED IN AQUEOUS SOLUTION.

F. David, K. Samhoun (Institut de Physique Nucléaire, Orsay),

E.K. Hulet, P.A. Baisden, R. Doughan, J.H. Landrum,  
R.W. Lougheed, J.F. Wild (Lawrence Livermore Laboratory),

G.D. O'Kelley (Oak Ridge National Laboratory)

Abstract

A radiopolarographic study of mendelevium has been performed at Lawrence Berkeley Laboratory following the Oak Ridge work. The element is studied with  $^{241}\text{Am}$ ,  $^{249}\text{Cf}$ ,  $^{254}\text{Es}$ ,  $^{255}\text{Fm}$  and  $^{256}\text{Fm}$  in non complexing aqueous medium : tetramethylammonium perchlorate and the influence of  $\text{Cl}^-$  and citrate ions are examined.

In non complexing medium, the measured half wave potential of mendelevium is  $-1.74 \text{ V/S.C.E.}$  which agrees with the one deduced from previous radiocoulometric experiments in acetic medium. The presence of  $\text{Cl}^-$  ions does not introduce a shifting of the wave.

Moreover, the number of produced atoms ( $\sim 10^6$ ) is sufficient to get the logarithmic transformed wave. As with fermium, one measure a 30 mV slope which agrees with a  $2 \rightarrow 0$  process.

In presence of citrate ions, the observed shift of the wave is similar to the shift measured with Fm.

These experimental data show that, at a very negative potential ( $-1.74 \text{ V/S.C.E.}$ ), mendelevium cannot be considered as a  $\text{Cs}^+$  or silver like ion. Therefore, one has to reconsider the discovery of the monovalency of mendelevium.

---

The scheme of the "Journées des Actinides" correlates redox properties of actinides with electronic configuration (Fig. 1). Since it is not possible to get macroamounts of elements as heavy or heavier than fermium, the only

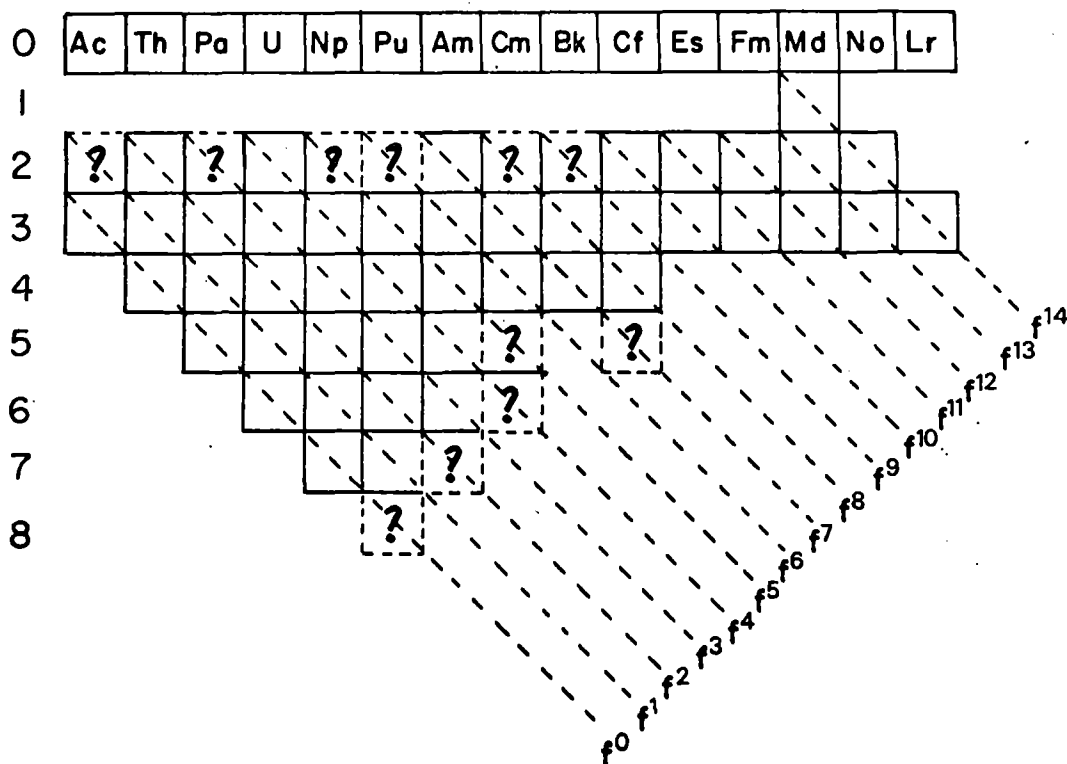


Fig. 1 - Actinide scheme.

way to study such heavy elements is radiochemistry. We will present here new experimental data obtained at Lawrence Berkeley Laboratory which concern redox properties of mendelevium.

Last year at Liege, radiocoulometric data obtained at Oak Ridge (1) have been presented. Fig. 2 shows the plot of the ratio  $\tau_d/\tau$  versus potential.  $\tau$  being the half time of the reduction process and  $\tau_d$  the limiting value of  $\tau$ . One can demonstrate that such curve is similar to a polarographic wave (2).  $^{256}\text{Fm}$  and  $^{256}\text{Md}$  are studied in acetate and citrate medium. They show a very similar behavior in these conditions. The observed shift with citrate ions led us to conclude that Md cannot be considered as a cesium like element as Mikheev et al. proposed in 73 (3).

However for a definitive answer on the question of the monovalency of mendelevium in aqueous solution, one has to consider the possibility of a monovalent  $\text{Md}^+$  ion which could have a particular behavior like  $\text{Ag}^+$  or  $\text{Cu}^+$ .

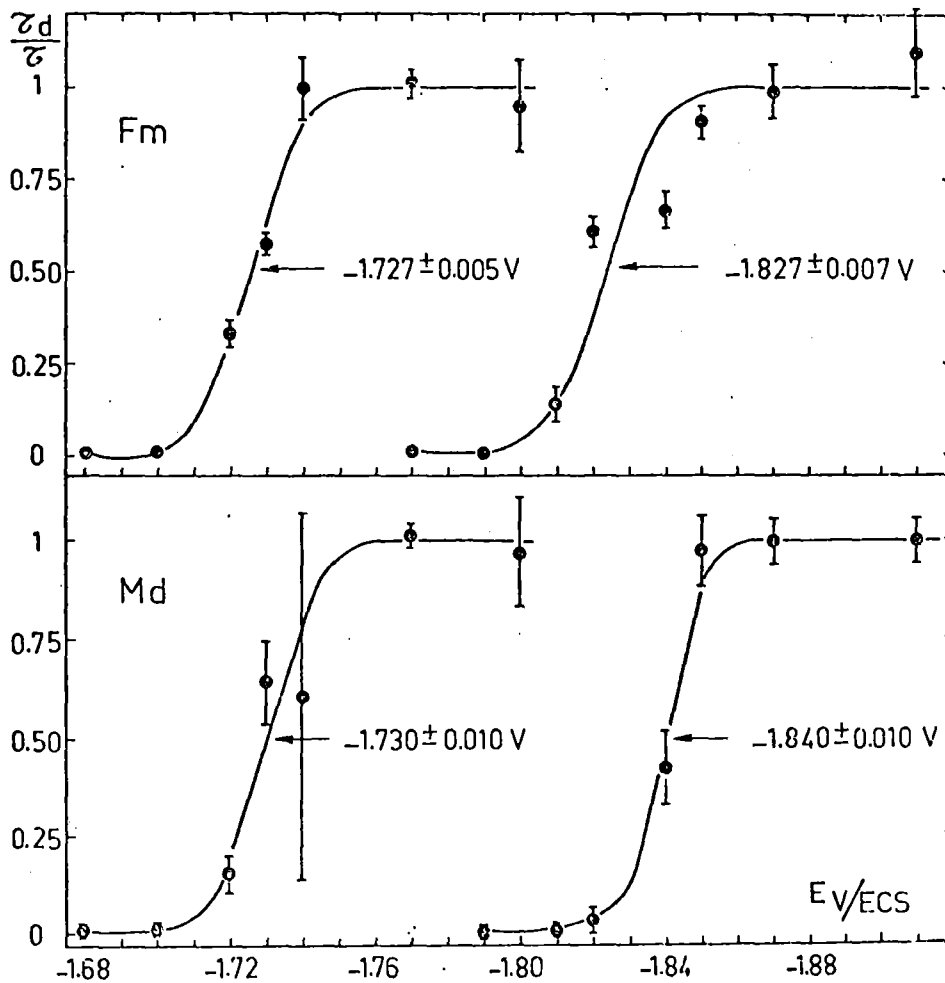


Fig. 2 - Equivalent current-potential curves of  $^{256}\text{Fm}$  and  $^{256}\text{Md}$  obtained in 0.1 M ammonium acetate buffer (left) and 0.1 M ammonium citrate at  $\text{pH} \sim 6$  (right).

This possibility would be related to the fact that the electronic configuration of  $\text{Md}^+$  should be a complete f14 subshell similarly to silver + which has a completed d subshell.

Therefore it is necessary to consider a particular possibility of complexation of  $\text{Md}^+$ .

This is the reason why new experiments were performed at Berkeley. It was possible to get  $10^6$  Md atoms per irradiation which are necessary for radiopolarographic experiments.

To decide if Md could be a silver like ion, we used the properties of these ions to be strongly complexed with  $\text{Cl}^-$ . Therefore, radiopolarograms were obtained in a non complexing medium : tetramethylammonium perchlorate and in presence of  $\text{Cl}^-$  and citrate ions.

The production of Md is performed at the 88 inch cyclotron of Lawrence Berkeley Laboratory.

With a cross section of the order of the mb, one produce  $10^6$  atoms of  $^{256}\text{Md}$  and  $^{257}\text{Md}$  which are collected on a Be foil ( $4.9 \text{ mg/cm}^2$ ). They are both 90 % electronic capture and 10 %  $\alpha$ , which make  $\alpha$ -measurements difficult. More over  $\alpha$ -energy of the produced atoms are close as shown on Table 1 (% branching is given in ( )).

Table 1

	$T_{1/2}$	Decay	Energy of $\alpha$ in MeV
$^{255}\text{Fm}$	201 h	$\alpha$	7.03
$^{256}\text{Fm}$	157 mn	SF (92), $\alpha$ (8)	6.86
$^{255}\text{Md}$	27 mn	EC (90), $\alpha$ (10)	7.34
$^{256}\text{Md}$	77 mn	EC (90), $\alpha$ (10)	7.20
$^{257}\text{Md}$	5.4 h	EC (90), $\alpha$ (10)	7.07

To get internal monitor inside the experimental solution, one added known amounts of  $^{241}\text{Am}$ ,  $^{249}\text{Cf}$  and  $^{254}\text{Es}$  with the same radioactivity level as that of the studied isotopes.

The general flowsheet of the separation of mendelevium isotopes is given on Fig. 3.

Produced atoms of mendelevium and fermium and the einsteinium knock out the target are collected on a Be foil which is dissolved by 6 M HCl. Separation of Be is achieved by precipitation of lanthanum fluorides. After dissolution, precipitation of the hydroxides and a new dissolution, a cation exchange column gives a good separation of heavy actinides.

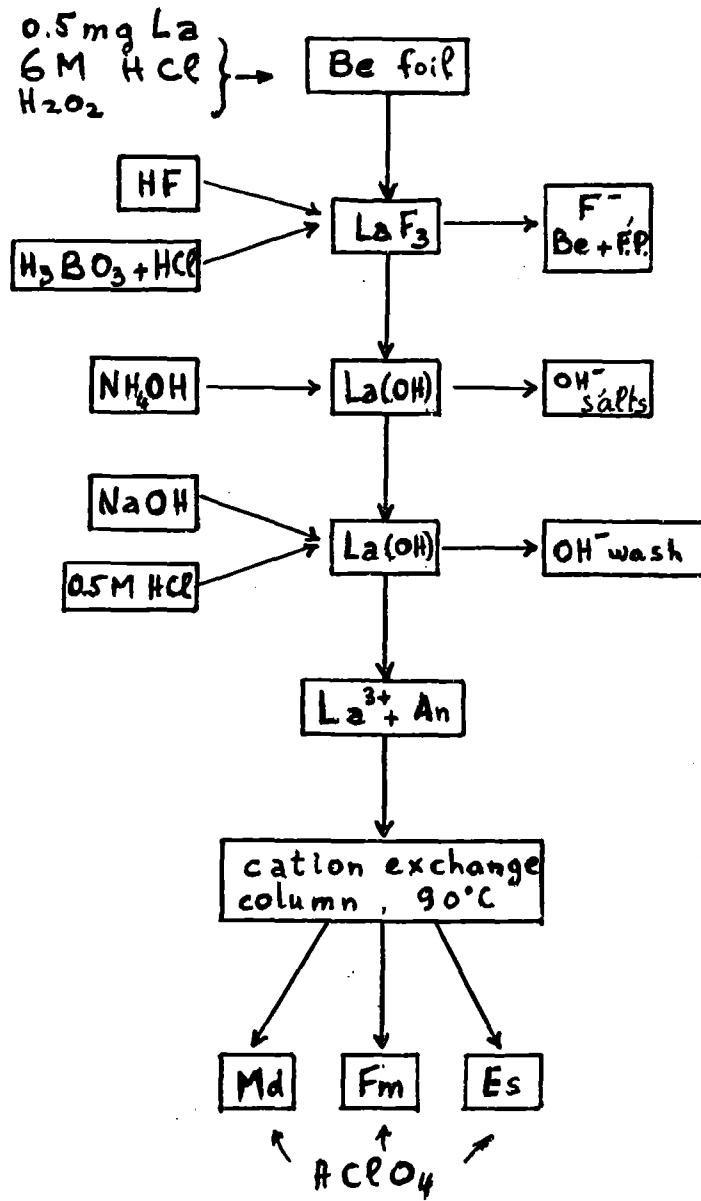


Fig. 3 - Chemical separation flowsheet.

The atoms are recovered with  $\text{HClO}_4$  first, to eliminate organic compounds and  $\text{Cl}^-$  ions, and after with the polarographic medium which contains equivalent quantities of  $^{241}\text{Am}$ ,  $^{249}\text{Cf}$  and  $^{254}\text{Es}$ .

Mendelevium could be measured through two different methods since  $\text{Md } 256$  has a 10 %  $\alpha$ -branching with 90 % electronic capture and  $^{256}\text{Fm}$ , the daughter, decreased mostly by spontaneous fission.

On Fig. 4, one sees an  $\alpha$ -spectrum of a sample. In the spectrum which is taken several hours after irradiation, one has mostly  $^{256}\text{Fm}$  and  $^{257}\text{Md}$ . But 2-3 days after, one measures mostly  $^{255}\text{Fm}$  which has a 20.1 h half-life.

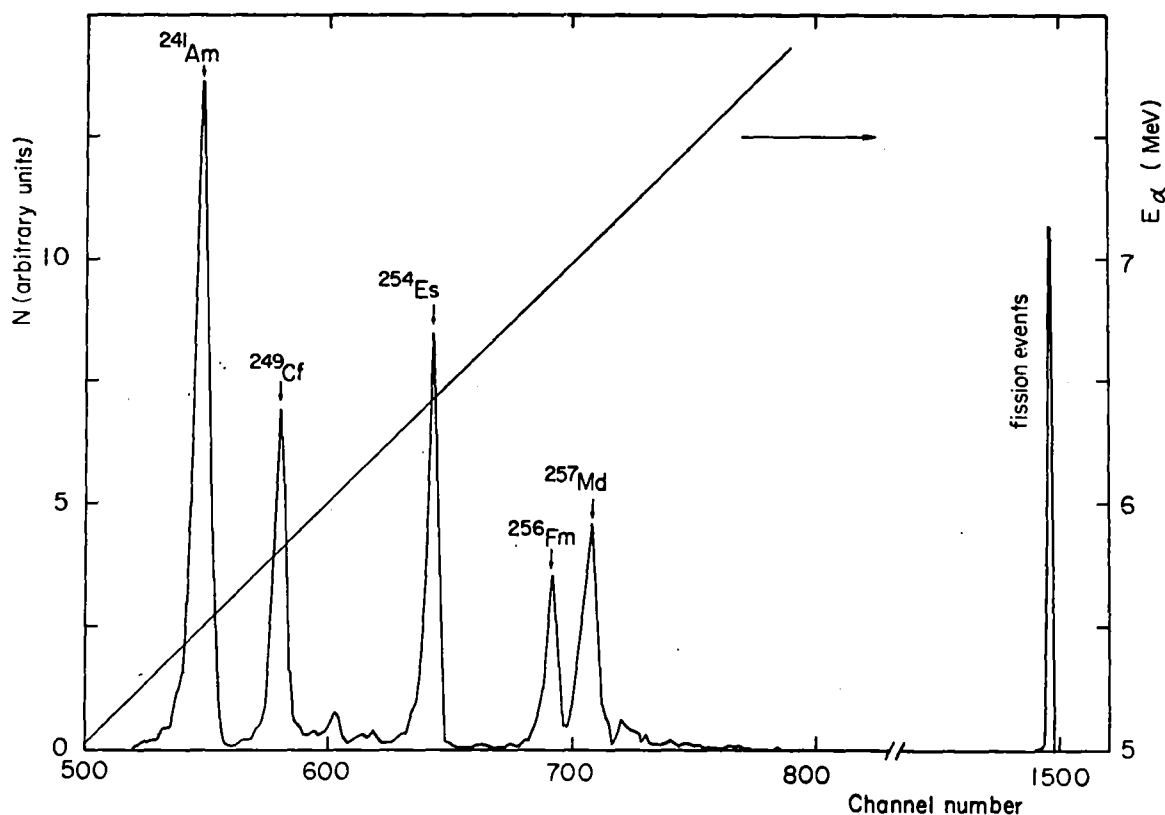


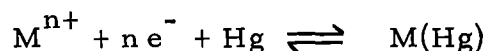
Fig. 4 -  $\alpha$ -spectrum of a sample.

Moreover the  $\alpha$ -contribution of  $^{256}\text{Fm}$  can be calculated precisely from the fission events since the ratio  $\alpha/\text{F.S.}$  is known (that ratio is chosen arbitrarily on Fig. 4).

Therefore one gets the  $\alpha$ 's due to mendelevium isotopes by a subtraction from the total  $\alpha$  measured between 6.8 and 7.8 MeV and those due to Fm.

The second way of measuring Fm and Md atoms in each sample is the analysis of growth and decay curve of fissions due to  $^{256}\text{Fm}$  with a least-mean square fitting. A comparison of both methods shows a good agreement in the obtained data.

The electrochemical reaction :



is studied by the radiopolarographic method which has been exposed previously (see for example (4)). Radiopolarograms, similar to polarographic waves, are obtained by plotting the number of reduced atoms or radioactivity  $A$  versus the applied potential at the dropping mercury electrode.

Fig. 5 gives example of waves obtained in a non complexing medium (pH 2.3) for Am, Cm, Bk, Cf and Es.

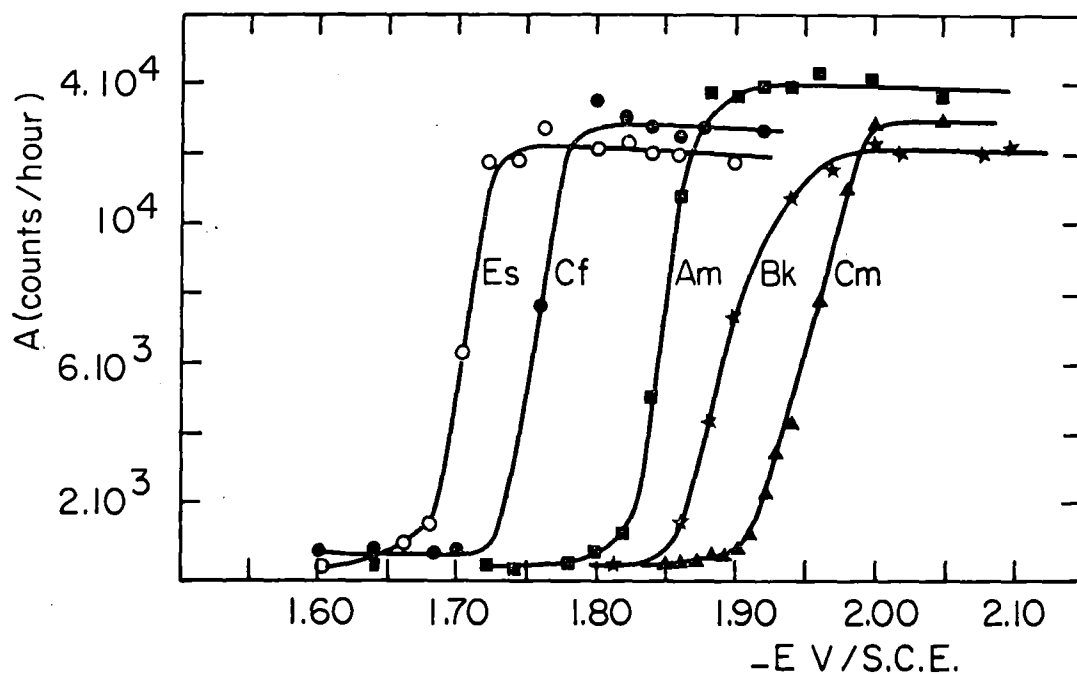


Fig. 5 - Radiopolarograms of Am, Cm, Bk, Cf and Es in 0.1 M LiCl, pH 2.2 at 25° C.

Since one has about  $10^5$  atoms of mendelevium after the chemical separation it was necessary to use a microcell in order to accommodate a volume of solution as small as possible.

The experimental device is shown on Fig. 6. A volume of solution of about 200  $\mu$ l is hung in contact with the mercury drop, the compartment of reference electrode and of the anode. This is done by a slight lowering of pressure which is adjusted by the height of water in the reservoir.

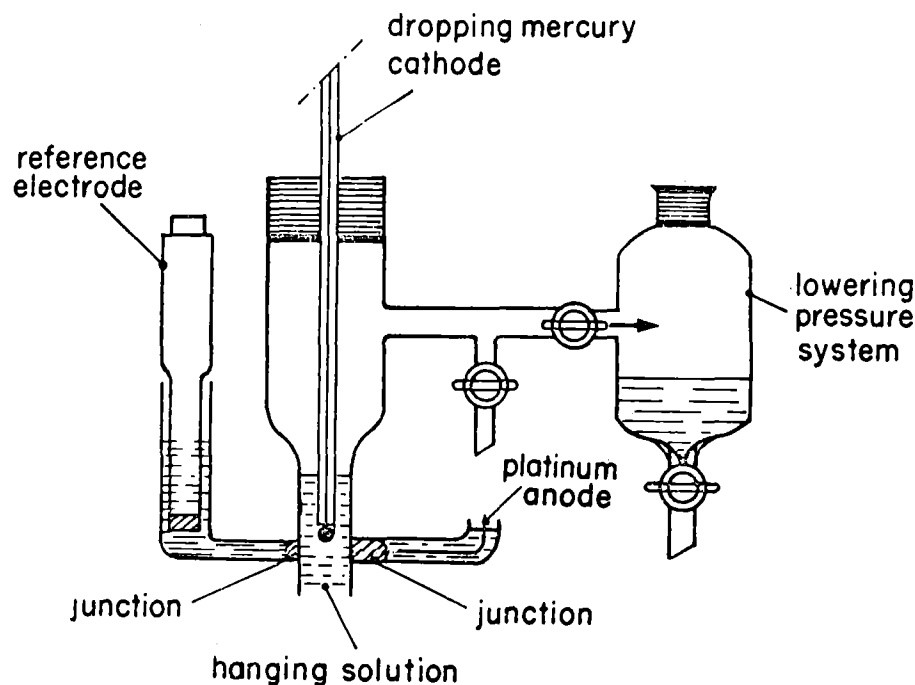


Fig. 6 - Radiopolarographic device.

The mercury drops are collected dry by going through the interphase aqueous-solution-air and a filter paper funnel.

Each wave is obtained with 8 points and 2 different irradiations.

Waves of Cf, Es, Fm and Md are obtained simultaneously. As example, we have here Cf and Es waves (Fig. 7) determined with such experimental device for the medium 0.1 M TMA ClO<sub>4</sub> at pH 2.4.

The logarithmic transformed wave is also reported. The measure of half wave potential and slopes are consistent with previous data for non complexing medium.

Therefore, these elements are used as internal monitor for radio-activity measurement and for potential calibration as well.

Fig. 8 shows a wave of Fm with the same medium. Data are again consistent with previous measurement : we have here a 2 → 0 reduction process as expected.

Finally, on Fig. 9 one has a wave of mendelevium with the same

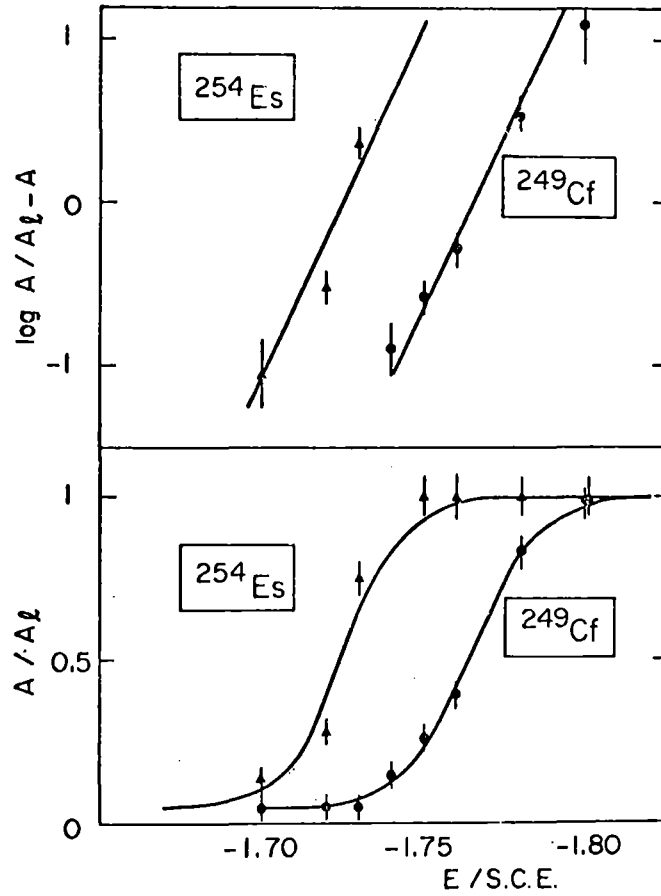


Fig. 7 - Radiopolarogram of <sup>249</sup>Cf and <sup>254</sup>Es in 0.1 M tetramethylammonium perchlorate, pH 2.4. log A/A<sub>l</sub> - A vs -E is plotted for each wave.

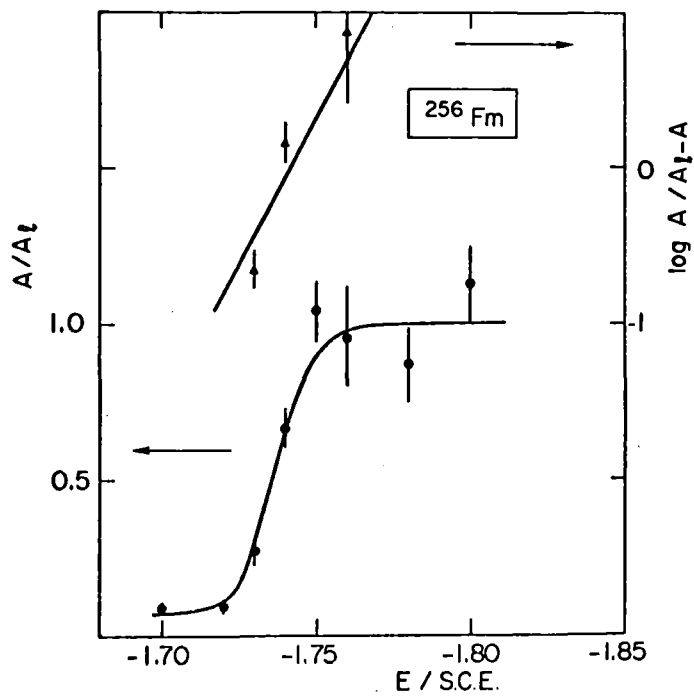
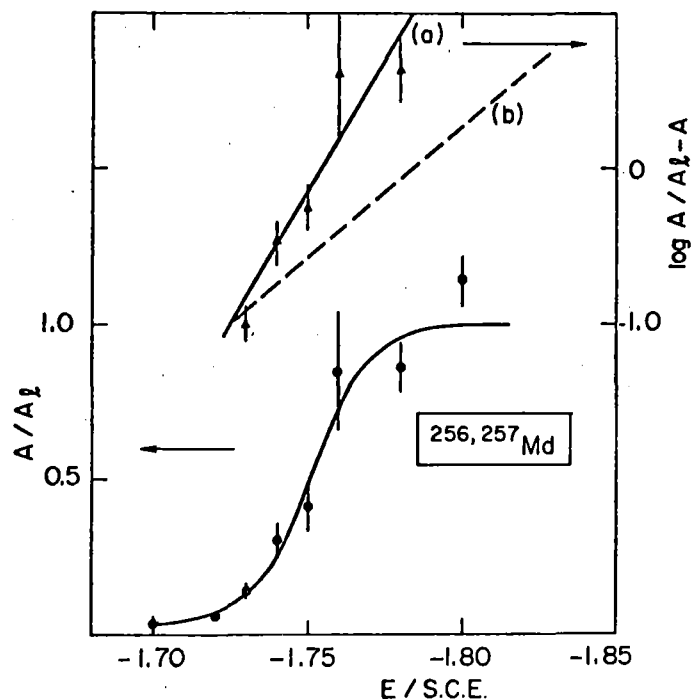


Fig. 8 - Radiopolarogram and logarithmic transformed wave of Fm (same conditions as in Fig. 7).



**Fig. 9** - Radiopolarogram and logarithmic transformed wave of Md (same conditions as in Fig. 7).

Line a : slope corresponds to 30 mV.  
 Line b : slope corresponds to 59 mV.

**TABLE 2**

Experimental half-wave potentials

Exp. Element	$- E_{1/2}/SCE$			
	1	2	3	4
$^{249}Cf$	1.75 (2)	1.765 (5)	1.786 (5)	-
$^{254}Es$	1.71 (1)	1.723 (5)	1.715 (5)	-
Fm	1.72 (1)	1.740 (5)	1.726 (5)	$\sim 1.82$
Md	1.73 (1)	1.755 (5)	1.755 (5)	$\sim 1.80$

Exp. (1) : 0.1 M T.M.A.  $ClO_4$ , pH 2.4  
 Exp. (2) : 0.1 M T.M.A.  $ClO_4$ , pH 2.4  
 Exp. (3) : 0.1 M LiCl, pH 2.4  
 Exp. (4) : 0.1 M LiCl,  $5 \times 10^{-3}$  M  $Li_3Cit$ , pH 6.5

medium. Half wave potential is essentially the same as deduced from radiocoulometric measurement in acetic medium. The slope  $a$  of  $\log A/A_{\lambda} - A$  is 30 mV as in case of Fm. The slope  $b$  corresponds to 59 mV. It is obvious that it cannot fit the experimental points.

On table 2 we have the measured half wave potential of the studied elements, for TMA  $\text{ClO}_4$ , LiCl and lithium citrate.

The data confirmed the values measured previously by radiocoulometry. Half wave potential of Md is about 10 mV more negative than Fm and no significant difference is observed between  $\text{ClO}_4^-$  and  $\text{Cl}^-$  medium. Therefore, it is demonstrated that  $\text{Cl}^-$  doesn't complex significantly Md ions.

Moreover :

- the shift of 90 mV measured with the same citrate medium is similar to the one observed for Fm and Ba ions ;

- the slope of  $\log A/A_{\lambda} - A$  versus  $E$  is 30 mV for both elements in non complexing medium.

Both observations show that the reduction process of Md which occurs in aqueous solution at a very negative potential corresponds to a  $2 \rightarrow 0$  process. Therefore, there is no experimental fact to conclude that mendelevium is monovalent in aqueous solution.

#### References.

1. K. Samhoun, F. David, R.L. Hahn, G.D. O'Kelley, J.R. Tarrant and D.E. Hobart, 8ème Journées des Actinides, Liège, 1979 ; same authors, J. Inorg. Nucl. Chem. (to be published).
2. K. Samhoun and F. David, to be published.
3. N.B. Mikheev, V.I. Spitsyn, A.N. Kamenskaya, I.A. Rumer, B.A. Gvozdev, N.A. Rozenkevich and L.N. Auerman, Dokl. Akad. Nauk, SSSR (in English) 208, 1146 (1973).
4. K. Samhoun and F. David, J. Inorg. Nucl. Chem. 41, 357 (1979).

Preparation and Single Crystal Growth of  
Protactinium Arsenides by Chemical Vapour Transport

G. Calestani, J.C. Spirlet, J. Rebizant and W. Müller

Commission of the European Communities  
Joint Research Centre  
European Institute for Transuranium Elements  
Karlsruhe Establishment  
Postfach 2266  
D-7500 Karlsruhe  
Federal Republic of Germany

SUMMARY

Single crystals of protactinium arsenides ( $\text{PaAs}_2$ ,  $\text{Pa}_3\text{As}_4$  and  $\text{PaAs}$ ) were prepared from the elements by chemical vapour transport using iodine as transporting agent. In a van Arkel process, the protactinium arsenides were deposited on an induction-heated tungsten support. Depending on the compounds deposition temperatures ranged from 1000 to 2200 °C, whereas the quartz bulb was kept at 400 to 450 °C. The single phase deposits were identified and characterized by X-ray diffraction methods. The values of the lattice parameters, compared with the values of the corresponding compounds of the actinide series, are discussed in terms of delocalization of the 5f electrons..

## 1. INTRODUCTION

Starting with van Arkel protactinium prepared at the gramme scale /1,2/, protactinium pnictides are being synthesized for solid state studies in order to complete an investigation of the pnictides of lighter actinides.

For many solid state property measurements, single crystals are required. Single crystals of the higher uranium and neptunium pnictides can be grown by chemical vapour transport in sealed quartz bulbs using iodine as transporting agent /3,4,5,6/. Attempts to prepare thorium pnictides and the monopnictides of uranium and protactinium by this method resulted in the attack of the quartz wall /5,7/, even at temperatures as low as 800 °C. Reaction with the wall material could be avoided by using a Van Arkel type procedure for direct synthesis of actinide pnictides /8/ : starting from the elements and in presence of iodine as transporting agent, single crystals and films can be grown on a radiofrequency heated tungsten support (temperature  $T_2$ ) whereas the quartz bulb is maintained at a lower temperature ( $T_1$ ).

We report here the application of this method for the preparation of single crystals of the protactinium arsenides :

$\text{PaAs}_2$ ,  $\text{Pa}_3\text{As}_4$  and  $\text{PaAs}$ .

## 2. EXPERIMENTAL

All experiments were performed in inert atmosphere glove boxes because of the radiotoxicity of  $^{231}\text{Pa}$  and the chemical reactivity of the element and its pnictides.

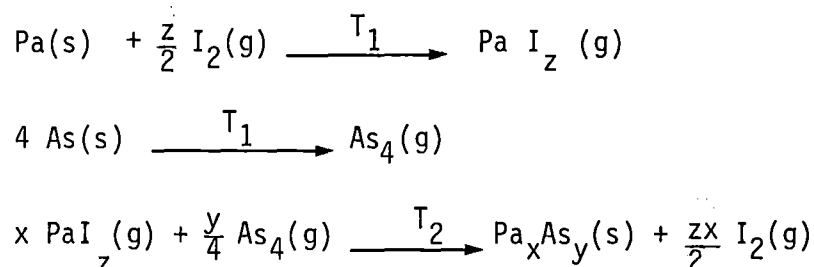
### 2.1. Materials

High purity Pa metal ( $\text{O} < 20$  ppm,  $\text{N} < 15$  ppm,  $\text{Si} = 300$  ppm) was prepared by a modified Van Arkel procedure /1,2/. Pure "pro analysi"

arsenic and "suprapure" iodine (Merck A.G., Darmstadt) were further purified by sublimation at  $10^{-6}$  torr. The tungsten supports, fabricated from a single crystal (Materials Research Corporation, Orangeburg, New York) were electropolished /9/.

## 2.2. Van Arkel process for pnictide synthesis : equipment and conditions.

The van Arkel process is carried out in an evacuated ( $10^{-6}$  torr) quartz bulb, which contains the tungsten support, the elements and a quartz capillary with the transporting agent (fig. 1). The process can be described as follows :



where  $T_1$  and  $T_2$  ( $T_2 > T_1$ ) are the temperatures of the furnace (i.e. of the quartz bulb) and of the tungsten support, respectively. In reality the process is more complicated. During the heating of the bulb to temperature  $T_1$ , further reactions between arsenic and iodine leading to arsenic iodide, and between this and the protactinium metal leading to protactinium iodide and arsenic are observed. It is unknown which protactinium iodide is involved in the transport, although our observations point to the more volatile pentaiodide. The evidence consists of i) a lower bulb temperature for the preparation of protactinium pnictides than for thorium pnictides /8/ ; ii) dark brown vapours typical of  $\text{PaI}_5$  ; iii) non transported products containing traces of an orthorhombic compound with lattice parameters attributed previously to  $\text{PaI}_5$  /10/.

The temperature  $T_1$  determines the vapour pressure of the iodide and, together with  $T_2$ , controls the deposition rate at the support. The

temperature  $T_2$  determines, in addition, the composition of the deposited compound. The conditions for the synthesis of protactinium arsenides are summarized in table 1.

### 2.3. X-ray analysis

The single phase deposits were identified and characterized by X-ray diffraction methods. X-ray powder patterns were taken at room temperature using standard Debye-Scherrer and Gandolfi /11/ cameras of 114.6 mm diameter, with filtered copper radiation. Ilford G X-ray film was used. Line intensities were visually estimated ; line positions were read using a micrometer with 0.02 mm precision. After indexing the various reflexions, the lattice parameters were calculated by the least squares method, using the LCR-2 program /12/. The Nelson-Riley extrapolation function was used. Error limits indicated correspond to one standard deviation.

## 3. RESULTS AND DISCUSSION

In all cases small single crystals (0.1-0.2 mm) were obtained. The measured lattice parameters are presented in table 2 compared with literature data /13/. For PaAs<sub>3</sub>, prepared for the first time, the observed and calculated reflexions are listed in table 3.

As can be seen from figs. 2 and 3, the lattice parameters of protactinium arsenides, unlike the case of mononitrides, are similar to those of the corresponding uranium compounds. This can be ascribed to the increase of the occupation number of the protactinium 5f band with increasing atomic number (and with the corresponding decreasing of electronegativity) of the bonded pnictogen. In analogy with PaC, for which the measurements of magnetic susceptibility <sup>(14)</sup> show temperature independent diamagnetism and the probable absence of 5f electrons, we can suggest that for PaN, the occupation number is very low.

The jump observed in the lattice parameters of the arsenides going from thorium to protactinium suggests the presence of bonding 5-f electrons. By comparing the lattice parameters of the actinide monoarsenides with the corresponding lanthanide compounds (localised 4-f electrons) the protactinium 5-f electron bonding seems moreover to be a maximum in the series.

#### Acknowledgements

Acknowledgements are due to Mr. E. Bednarczyk for help in the compounds preparation and to Dr. L. Manes and Dr. M.S.S. Brooks for useful discussions. One of us (G. Calestani) wishes to express his thanks to the Commission of the European Communities for financial support during this work.

Compound	$T_1(^{\circ}\text{C})$	$T_2(^{\circ}\text{C})$
$\text{PaAs}_2$	400	1000
$\text{Pa}_3\text{As}_4$	400	1500
$\text{PaAs}$	450	> 2000

Table 1

Table 1. Experimental conditions for growing protactinium arsenides single crystals.

Compounds	Symmetry	Space Group	Lattice Parameters (Å)	
			measured	literature /13/
PaAs <sub>2</sub>	tetragonal	P4/nmm	a = 3.9748 ± 0.0003 c = 8.159 ± 0.001	a = 3.978 c = 8.154
Pa <sub>3</sub> As <sub>4</sub>	b.c.c.	I43d	a = 8.5224 ± 0.0004	a = 8.524
PaAs	f.c.c.	Fm3m	a = 5.7560 ± 0.0003	-

Table 2

Table 2. Crystal structure and lattice parameters of protactinium arsenides.

h k l	2 $\theta$ observed	2 $\theta$ calculated	I observed
1 1 1	26.86	26.83	m
2 0 0	31.12	31.08	vs
2 2 0	44.60	44.52	vs
3 1 1	52.78	52.74	m
2 2 2	55.34	55.28	m
4 0 0	64.91	64.78	m
3 3 1	71.51	71.44	w
4 2 0	73.60	73.59	vs
4 2 2	82.03	82.01	s
5 1 1	88.19	88.20	w
4 4 0	98.52	98.51	m
5 3 1	104.64 $\alpha_1$	104.69	m
	105.00 $\alpha_2$	105.05	w
6 0 0	106.86 $\alpha_1$	106.82	s
	107.32 $\alpha_2$	107.20	m
6 2 0	115.65 $\alpha_1$	115.63	s
	116.15 $\alpha_2$	116.08	m
5 3 3	122.66 $\alpha_1$	122.69	vW
	123.23 $\alpha_2$	123.21	vW
6 2 2	125.19 $\alpha_1$	125.16	s
	125.81 $\alpha_2$	125.71	m
4 4 4	136.01 $\alpha_1$	135.98	vW
	136.67 $\alpha_2$	136.68	vW
5 5 1	145.77 $\alpha_1$	145.75	s
	146.69 $\alpha_2$	146.68	m
6 4 0	149.58 $\alpha_1$	149.58	s
	150.66 $\alpha_2$	150.64	m

Table 3

Table 3. Observed and calculated X-ray reflexions of PaAs (CuK $\alpha$  radiation).

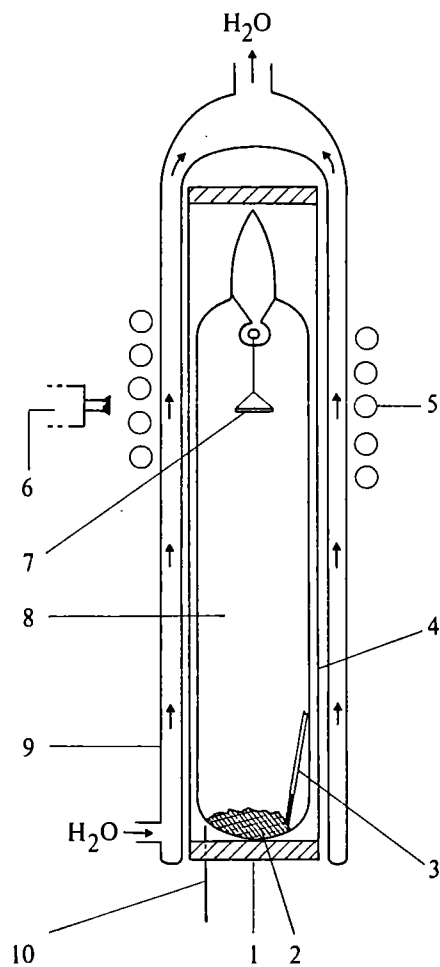


Fig. 1. Van Arkel process equipment : 1, thermal insulation ; 2, starting materials ; 3, iodine capillary ; 4, resistance heater (quartz tube with a heating coil) ; 5, HF induction coil ; 6, optical pyrometer ( $T_2$ ) ; 7, tungsten support ; 8, Van Arkel bulb ; 9, watercooling protection ; 10, thermocouple ( $T_1$ ).

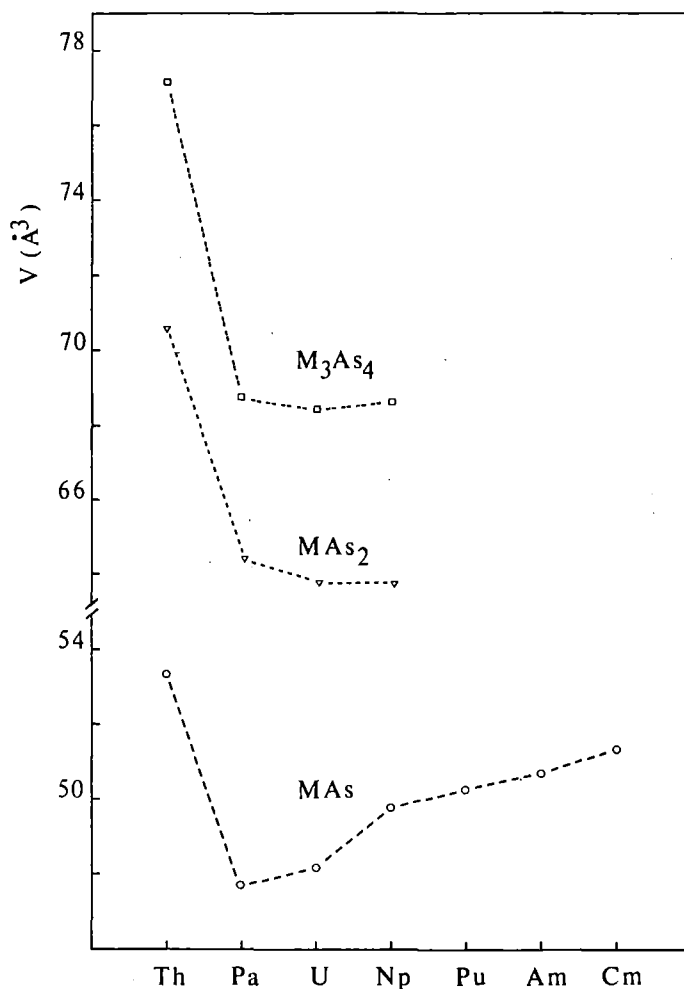


Fig. 2. Volume per formula weight containing one actinide versus atomic number for actinide arsenides : MAs<sub>2</sub> (anti-Fe<sub>2</sub>As structure type), M<sub>3</sub>As<sub>4</sub> (Th<sub>3</sub>P<sub>4</sub> structure type) and MAs (NaCl structure type)

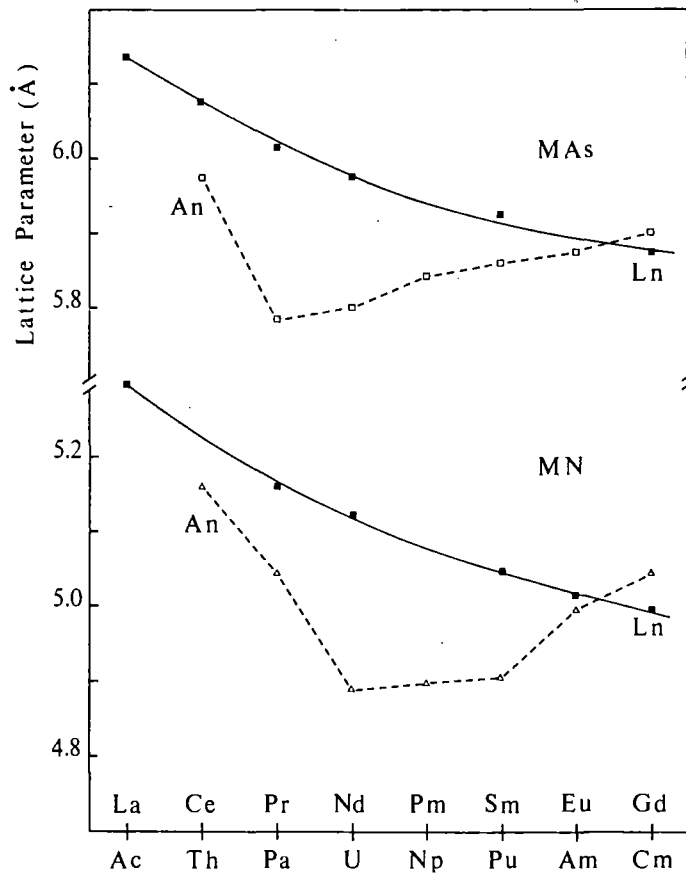


Fig. 3. Lattice parameter vs. atomic number for mononitrides and monoarsenides of the actinides and the corresponding lanthanides.

References

- / 1/ J. Bohet and W. Müller, *J. Less Common Metals*, 57(1978)185.
- / 2/ J.C. Spirlet, *J. Physique, Colloq.*, 40 C4(1979),87.
- / 3/ Z. Henkie, *Rocznichi Chem.* 42(1968)363.
- / 4/ Z. Henkie, *Technologia monokryształów (Polish Scientific Editions, Warsaw)*, 2(1974)56.
- / 5/ E. Bednarczyk and J.C. Spirlet, unpublished results (1976).
- / 6/ J.P. Charvillat, Thesis, Univ. de Clermont-Ferrand (France) 1977.
- / 7/ Z. Henkie and J.P. Markowski, *J. Crystal Growth*, 41(1977)303.
- / 8/ G. Calestani, J.C. Spirlet and W. Müller, *J. Physique Colloq.*, 40 C4(1979)106.
- / 9/ J.M. Weaver, C.G. Olson and D.W. Lynch, *Phys. Rev. B12* (1975)1293.
- /10/ D. Brown, J.F. Easey and P.J. Jones, *J. Chem. Soc. A* (1967)1698.
- /11/ G. Gandolfi, *Miner. Petrogr. Acta*, 13(1967)67.
- /12/ D. Williams, Ames Laboratory Report, IS-1052 (1964).
- /13/ Y. Hery, D. Damien, M. Haessler and C.H. de Novion, *Radiochem. Radioanal. Letters*, 32(1978)283.
- /14/ Y. Hery, A. Wojakowsky, M. Boidron and C.H. de Novion, *Proc. 2nd Int. Conf. Electr. Str. Actin.*, Eds. J. Mulak, W. Suski and R. Troć, Wrocław, Poland, 1976, p. 343.

Quelques résultats récents des recherches sur  
les composés d'actinides

Andrzej Wojakowski  
Institut des Basses Températures et des Recherches  
Structurales,  
de l'Académie Polonaise des Sciences, 50950 Wrocław,  
P.O. Box 937, Pologne

Résumé

L'arseniure de thorium  $\text{Th}_3\text{As}_4$  et leur solutions solides avec l'arseniure d'uranium isotype ont été obtenus par la méthode de van Arkel modifiée. Les propriétés électriques de  $\text{Th}_3\text{As}_4$  et de  $(\text{Th}_x\text{U}_{1-x})_3\text{As}_4$  ( $1 \leq x < 0.85$ ) ont été mesurées et leurs propriétés semiconductrices ont été montrées.

La qualité des monocristaux de  $\text{USb}_2$  obtenus par différentes méthodes (transport chimique, cristallization de solution liquide U-Sb ou U-Sb-Sn) a été étudiée.

Analyse des impuretés métalliques dans les actinides de pureté élevée par spectrographie d'émission au moyen d'un plasma d'argon induit par haute fréquence (ICAP-OES)

René Gauthier\*, Horst Kutter, François Kinnart

Commission des Communautés Européennes  
Centre Commun de Recherche  
Etablissement de Karlsruhe  
Institut Européen des Transuraniens  
Postfach 2266  
D-7500 Karlsruhe  
République Fédérale d'Allemagne

\* FB8 Technische Schule Darmstadt  
Hochschulstr. 4  
6100 Darmstadt

Abstract

Après avoir passé en revue les méthodes déjà existantes d'analyse de traces des composés d'actinides, nous avons décrit celles qui utilisent le plasma d'argon induit par haute fréquence (ICAP). Nous avons également mis en évidence et décrit un certain nombre de conditions requises à la manipulation des composés d'actinides. Les problèmes techniques et pratiques d'installation d'un ICAP en boîte à gants (couplage optique et refroidissement des gaz) sont décrits et discutés. Nous avons résumé les conditions choisies pour notre installation et comparé les limites de détection déduites de notre travail avec celles de la littérature. Des échantillons d'américium et de protactinium ont été analysés. Nous donnons également les résultats d'analyse pour quelques éléments.



On subdivise généralement ces méthodes en deux groupes importants. Selon nos critères et nos impératifs, la seule méthode optique utilisable est celle employant le plasma induit par haute fréquence.

Description du plasma

Un plasma est un gaz dont une fraction significative des éléments constitutifs est à l'état ionisé. Dans le type de plasma que nous avons choisi, une fréquence de 25 à 150 MHz créée par effet de peau, un plasma dont la forme est toroïdale alors qu'une fréquence inférieure à 5 MHz donne un plasma en forme de goutte.

Les avantages de la forme toroïdale par rapport aux autres résident surtout dans:

1. l'injection axiale aisée de la substance analysée
2. le passage de l'échantillon dans le plasma s'effectuant dans un tunnel à gradient radial de température faible, entouré d'une zone plus chaude.

Les températures obtenues dans les plasmas utilisés à des fins analytiques, sont généralement comprises entre 6000 et 10 000 K. Il s'avère donc nécessaire d'isoler le plasma des parois de la torche qui sont en quartz. Cette isolation est réalisée par la technique du Vortex, créée par un flux tangentiel d'argon.

Du point de vue spectroscopique, on distingue trois zones dans ce type de plasma (fig. 1):

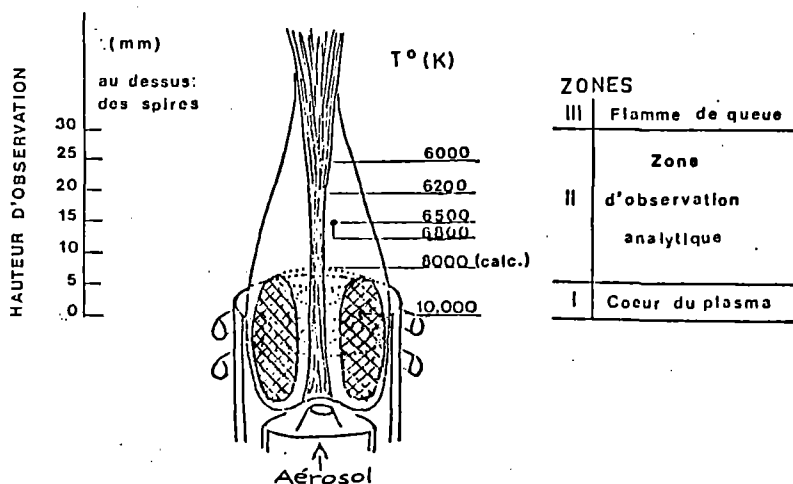


Fig.1: Diagramme de distribution spatiale des températures

La zone No. 1 de couleur blanche opaque émet un continuum très intense.

La zone No. 2 est beaucoup plus transparente et permet de réaliser des analyses.

La zone No. 3 possède les mêmes caractéristiques qu'une flamme classique, mais les turbulences dont elle est le siège lui donnent peu de valeur analytique.

### Installation en Boîte à Gants

L'analyse d'actinides de hautes puretés et de hautes radioactivités spécifiques requiert l'installation de l'ICAP Stand en boîte à gants.

Afin de permettre l'utilisation alternative de l'ICAP et de la "carrier distillation" avec le même spectrographe, les boîtes à gants sont montées sur des supports spéciaux. Ces supports sont mobiles sur rails fixés au sol pour fournir un déplacement et un alignement doux, rapide et reproductible en face du spectrographe Ebert 3,4 m. Le meilleur alignement s'opère à l'aide d'un petit laser He/Ne qui tolère une erreur maximale de déplacement (axes y,z) de  $\pm 0,5$  mm.

Le mise en boîte à gants de l'ICAP proprement dite pose quelques problèmes particuliers auxquels s'ajoutent également les impératifs ayant attrait aux règles de sécurités.

Les problèmes spécifiques sont:

1. La transmission par câble coaxial d'une puissance développée de 4 kW par le générateur aux spires.
2. Le refroidissement énergétique des gaz s'échappant du brûleur à des températures de 8000 à 12000°C pour obtenir 30°C aux filtres de sortie de la boîte à gants.
3. L'ajustement et la manipulation du système d'aérosolisation.
4. Le recueillement du drain et du condensat provenant des solutions analysées.

La figure 2 donne une vue générale de l'ICAP.

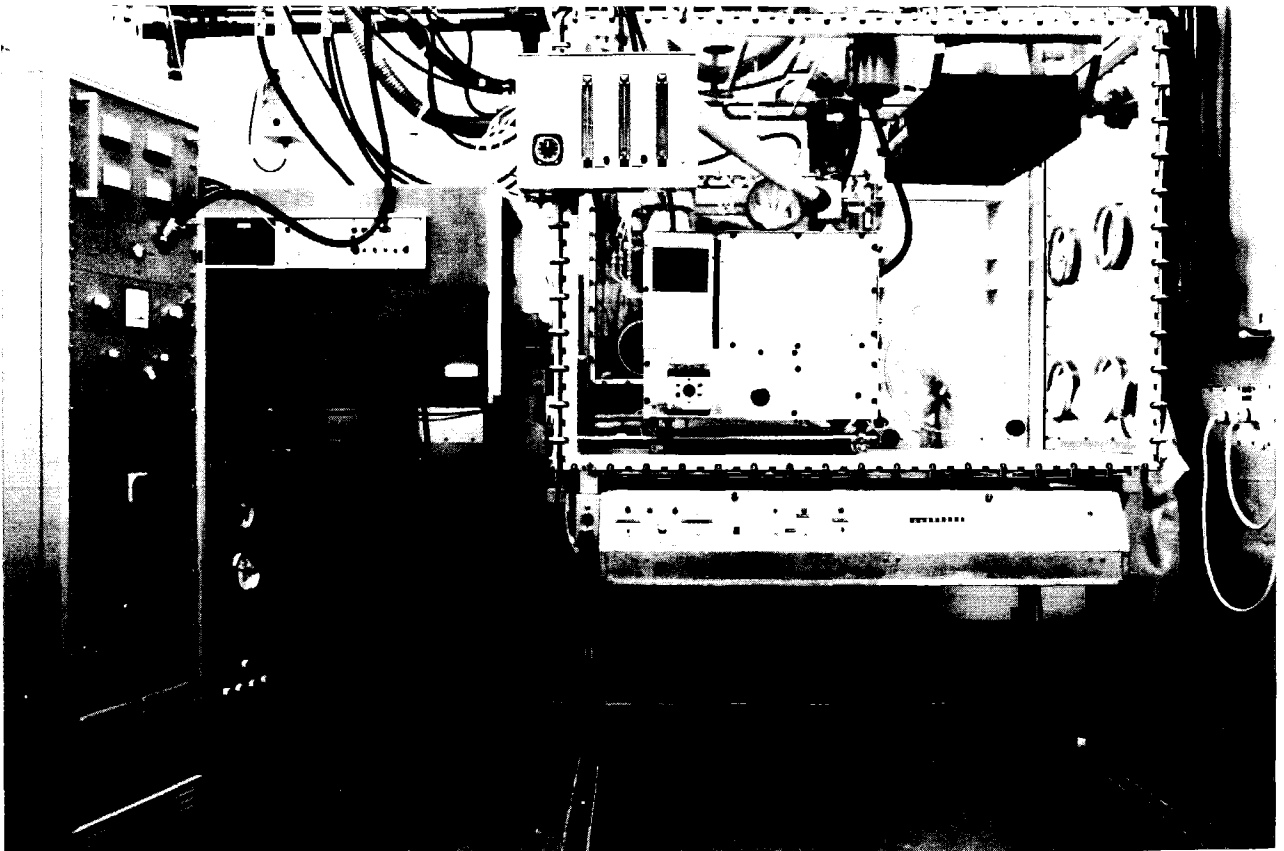


Fig.2. Vue générale de l'ICAP. Générateur haute fréquence de 27 MHz, 4 kW; Spectrographe type EBERT 3,4 m; Boîte à plasma (de gauche à droite).

### Choix du Système d'aérosolisation

La solution à analyser est introduite dans le plasma sous forme d'aérosol. Parmi les quatre nébuliseurs les plus couramment employés (Concentric glass nebulizer - CGN, cross flow nebulizer - CFN, fritted disk nebulizer - FDN, ultrasonic nebulizer), trois sont pneumatiques, le quatrième est ultrasonique. Celui-ci, bien que sa qualité d'aérosol soit excellente, l'emploi en est malaisé. Nous avons expérimenté le CGN et FDN; ce dernier, malgré son rendement exceptionnel, n'a pas été choisi car son temps de mémoire était beaucoup trop long et son emploi trop délicat. Le CFN exigeant un réglage de capillaires qui n'est pas facile à faire en boîte à gants, nous avons opté pour CGN qui, malgré son rendement médiocre, est d'une extrême facilité de manipulation en boîte à gants. La chambre de nébulisation est de modèle Scott et Fassel à deux tubes coaxiaux. On a veillé à une optimalisation de

- la ségrégation des gouttelettes formées,
- la stabilisation du brouillard formé,
- l'homogénéisation de l'aérosol,
- vaporisation de l'aérosol.

### Analyse paramétrique de l'ICAP et limite de détection

Le travail analytique est sujet essentiellement aux trois paramètres suivants;

- La puissance transmise au plasma (kW)
- Le débit de gaz porteur d'aérosol (l/min)
- La hauteur d'observation dans le plasma (mm).

La puissance transmise détermine la température du plasma, qui selon la loi de répartition de Boltzmann pour des températures de l'ordre de 6000 à 8000 K, favorise les niveaux énergétiques supérieurs et donc l'intensité des raies ioniques par rapport aux raies fondamentales.

Le débit d'argon, gaz porteur d'aérosol, influence le temps de séjour des atomes dans le plasma mais également la température du coeur du plasma et la hauteur d'observation.

Ces trois paramètres s'influencent mutuellement et retentissent différemment sur l'intensité des raies d'analyse et du bruit de fond. On trouvera donc pour chaque installation un optimum particulier par le rapport signal sur bruit de fond (S/N).

La hauteur d'observation optimum varie donc aussi bien pour des raies d'éléments différents que pour les raies ioniques et atomiques d'un même élément.

En ayant optimisé les conditions pour chaque élément (cas idéal), on peut obtenir les limites de détection suivantes (Tab. 2), qui sont comparées à celles de l'absorption atomique avec flamme. On remarquera la supériorité très nette de l'ICAP pour tous les éléments difficiles comme les terres rares et les éléments réfractaires.

Tab. 2. **COMPARAISON DES LIMITES DE DETECTION**  
**I.C.A.P [analyse multiélémentaire]**  
**F.A.A.S [analyse élémentaire]**

< 1 ppb		1 - 10 ppb		10 - 100 ppb		100 - 500 ppb		> 500 ppb	
I.C.A.P	F.A.A.S	I.C.A.P	I.A.A.S	I.C.A.P	F.A.A.S	I.C.A.P	F.A.A.S	I.C.A.P	F.A.A.S
Al	Mo	Be	Ag Si	Ag	Au	Al	Si		Dy
B	Na	Ca	As Sn	Ba	Hf	As	Sn		Hg
Ba	Nb	Cd	Bi Th	Co	In	Au	Te		Tm
Be	Ni	Mg	Dy Tm	Cr	Nd	Bi	Ti		Zr
Ca	Sr	Mn	Er	Cu	P	Er	Th		
Cd	Ti	Zn	Eu	Fe	Pr	Eu	V		
Ce	V		Gd	Na	Pt	Ga	Y		
Co	W		Hg	Nb	Sm	Ho	Yb		
Cr	Y		Hf	Ni	Ta	In			
Cu	Yb		Lu	Pb	Tb	Mo			
Fe	Zn		Pb	Sr	Te	Pd			
Ga	Zr		Pd		Tl	Pt			
Ge			Rh		U	Rh			
La			Sb			Sb			
Mg			Sc			Sc			
Mn			Se			Se			

Analyse multiélémentaire par ICAP

Pour des analyses simultanées de plusieurs éléments, l'étude préalable des paramètres fait apparaître la nécessité d'une solution de compromis. Nos conditions sont les suivantes:

Puissance ( $W_r$ ) : 1,4 Kw  
 Débit de gaz porteur ( $d_p$ ) : 2,3 L/min  
 Hauteur d'observation ( $H_{obs}$ ): 12 mm.

Des exemples d'analyses d'oxide commercial d'américium et de protactinium de haute pureté sont données dans le tableau 3. Les limites de détection sont élaborées avec des solutions propres de chaque élément, mais avec les conditions de compromis mentionnées ci-dessus.

Tab. 3. Analyse d'oxide d'américium et de protactinium métal

ÉLÉMENTS	AMÉRICIUM	PROTACTINIUM	LIMITES DE DÉTECTION
	oxide commercial	métal purifié	
	(ppm) ± 10%	(ppm) ± 10%	mg l <sup>-1</sup>
B	5	0,4	0,01
Ba	18	2,5	0,01
Cr	20	11	0,01
Fe	5	25	0,005
Hf	2	1,5	0,025
Hg	60	15	0,01
Mg	4	0,08	0,001
Mn	0,4	0,1	0,001
Mo	2400	0,4	0,015
Pt	13	70	0,005
U	1000	22	1

PHASE TRANSITION OF  $\text{ThBr}_4$  AND  $\text{ThCl}_4$

P. Delamoye, S. Hubert, S. Lefrant\* and J.C. Krupa

Institut de Physique Nucléaire, Laboratoire de Radiochimie,  
Bâtiment 100, Université de Paris-Sud, 91406 Orsay (France)

\* Laboratoire de Physique Cristalline, Université de Paris-Sud,  
Bâtiment 490, 91405 Orsay (France)

I. Introduction.

The optical spectra of the actinide ions, incorporated as isolated ions in crystals, are not as well understood as those of the lanthanides or 3d elements. The main problem is that the energies of the crystal field, inter-electron repulsion and spin-orbit interactions are comparable (1, 2, 3).

The most studied actinide ion is  $\text{U}^{4+}$  since the  $f^2$  configuration is the simplest case in which, using the crystal field model, there are more energy levels than parameters. We have obtained absorption and emission spectra of  $\text{U}^{4+}$  in  $\text{ThBr}_4$  (4, 5) and  $\text{ThCl}_4$ . At 4 K the spectra consist of many more lines than could be reasonably attributed to zero phonon electronic transition. To help separate vibrational from electronic transition and to be sure there is no change in the structure between room temperature and 4 K, we investigated Raman scattering and I.R. absorption of  $\text{U}^{4+}$  in  $\text{ThBr}_4$  and  $\text{ThCl}_4$  in the temperature range 300 to 4 K.

II. Experimental results.

Raman scattering experiments were performed on  $\text{ThBr}_4$ ,  $\text{ThBr}_4 : \text{U}^{4+}$ ,  $\text{ThCl}_4$  and  $\text{ThCl}_4 : \text{U}^{4+}$  single crystals.

$\text{ThBr}_4$  and  $\text{ThCl}_4$  are tetragonal crystals belonging to the space group  $D_{4h}^{19}$  (6). The two  $\text{ThBr}_4$  or  $\text{ThCl}_4$  per unit cell support 30 modes of vibration. The representation formed by cartesian displacement coordinates has the following structure :

$$\Gamma_{30} = 2A_{1g} + A_{2g} + B_{1g} + 3B_{2g} + 4E_g + A_{1u} + 3A_{2u} + B_{1u} + 2B_{2u} + 4E_u$$

The modes belonging to the species  $A_{1g}$ ,  $B_{1g}$  and  $E_g$  are Raman active while the  $A_{2u}$  and  $E_u$  are infrared active.

Raman spectra were recorded from 5 to 400  $\text{cm}^{-1}$ . We have used a right angle geometry and by choosing the appropriate polarization for the incident and scattering light, the Raman tensor components can be determined. According to group theory,  $A_{1g}$ ;  $A_{1g}$  and  $B_{1g}$ ;  $B_{2g}$  and  $E_g$  modes are allowed for  $\alpha_{zz}$ ;  $\alpha_{xx}$ ,  $\alpha_{yy}$ ;  $\alpha_{xy}$  and  $\alpha_{xz}$ ,  $\alpha_{yz}$  respectively. Taking into account the possible mixing of species, we have assigned the room temperature observed frequencies to the different modes. As the spectra obtained with  $U^{4+}$  doped and undoped crystals are quite similar, we will discuss only  $\text{ThBr}_4$  and  $\text{ThCl}_4$  crystals (Fig. 1). These assignments are summarized in table 1.

Table 1

Experimental results ( $\text{cm}^{-1}$ )		
	$\text{ThBr}_4$	$\text{ThCl}_4$
$A_{1g}$	108, 194	181, 297
$B_{1g}$	45	57
$B_{2g}$	66, 135, 183	70, 214, 301
$E_g$	38, 82, 122, 187	57, 98, 188, 260

As the temperature is lowered, there is essentially no change in the frequency of lines and no anomalous spectrum until 92 K for  $\text{ThBr}_4$  and 70 K for  $\text{ThCl}_4$ . Below these temperatures the spectra become very different and several additional Raman lines are observed. This is due to a phase transition (Fig. 2).

A better proof for the existence of a phase transition is the observation of a soft mode or unstable optical phonon. In the low temperature phase, we have observed a band shifting from 5  $\text{cm}^{-1}$  at 88 K to 19  $\text{cm}^{-1}$  at 4 K. The temperature dependance of a such a mode, lowering its frequency with the

increasing of the temperature leads to a dynamical instability of the crystal.

Fig. 3 summarizes the Raman spectra observed at different temperatures where the soft mode decreases in frequency toward zero as the phase transition was approached from below. Above the transition temperature, the soft mode does exist and increases its frequency from zero but becomes Raman inactive in the high temperature form.

In the case of soft modes, we expect that the frequency  $\omega = A(T_c - T)^\beta$  over a substantial temperature range near the phase transition temperature  $T_c$ . To get  $\beta$  and  $T_c$ , we have plotted  $\omega^{1/\beta}$  versus  $T$  (fig. 4). From this figure we can deduce that the temperature dependence is given by  $\omega = A(92 - T)^{1/3}$ .

### III. Conclusion

The existence of a soft mode clearly demonstrates the existence of a phase transition at 92 K for  $\text{ThBr}_4$  and 70 K for  $\text{ThCl}_4$ . Although Raman and infrared experiments permitted us to separate some vibrational transitions from pure electronic transitions, it is still necessary to know the structure and specially the symmetry site of  $\text{U}^{4+}$  in the low temperature form in order to interpret the visible spectrum.

X-ray experiments are now in progress. Up to now the only thing we can say about the structure is that in the new phase, the fourfold axis is preserved.

### References

1. D.J. Mackey, W.A. Runciman and E.R. Vance, Phys. Rev. B 11, 211 (1975).
2. R. Mc Laughlin, J. Chem. Phys. 36, 2699 (1962).
3. I. Richman, P. Kisliuk and E.Y. Wong, Phys. Rev. 155, 262 (1967).
4. M. Genet, P. Delamoye, N. Edelstein, J. Conway, J. Chem. Phys. 67, 1620 (1977).

5. P. Delamoye, S. Hubert, M. Hussonnois, J.C. Krupa, M. Genet, R. Guillaumont, N. Edelstein, J. Conway, Journal de Physique : "3rd International Conference on the Electronic Structure of the Actinides", C<sub>4</sub> (1979), p. 173.
6. D. Brown : "Halides of Lanthanides and Actinides", John Wiley (1968), p. 191 ;  
D. Brown, T.L. Hall and P.T. Moseley, J. Chem. Soc. 6, 686 (1973).

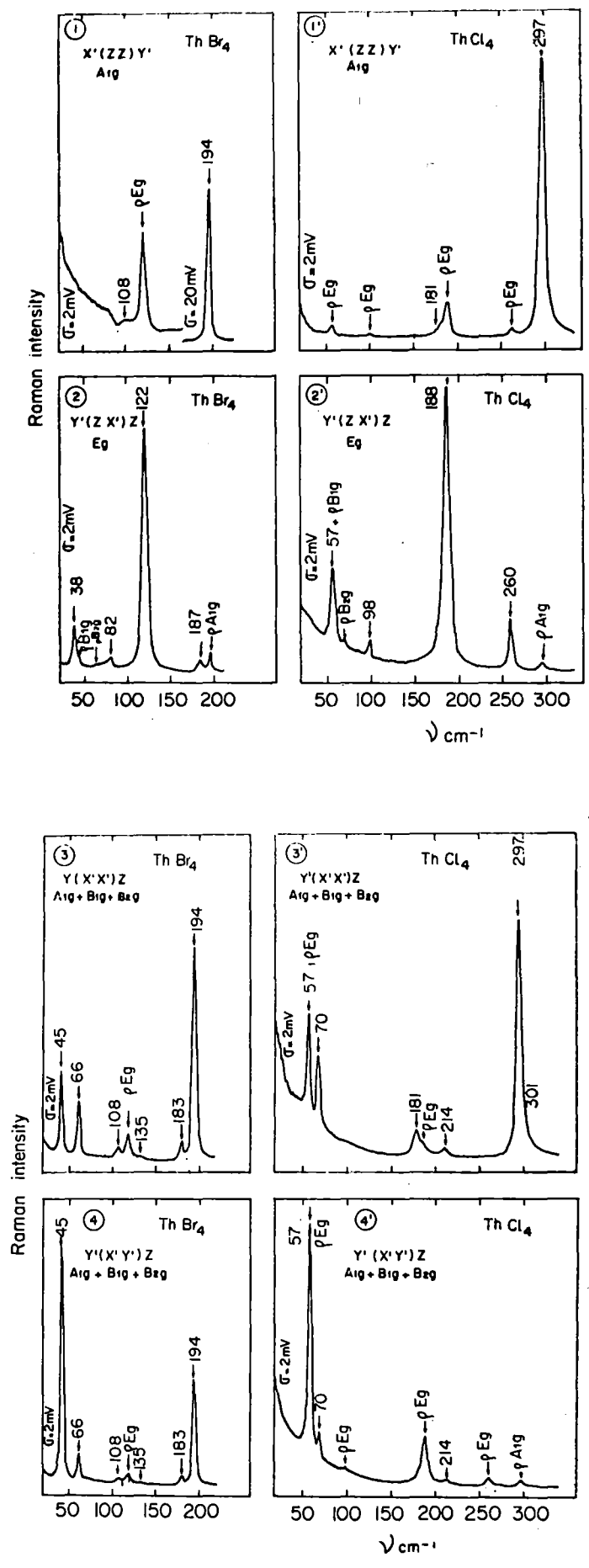


**Fig. 1** - Stokes Raman spectra of  $\text{ThBr}_4$  at  $300^\circ\text{K}$  for right angle scattering.

A : incident beam direction.  
 B : incident polarization.  
 C : scattered polarization.  
 D : scattered beam direction.

$\sigma$  : 2 mV, 20 mV sensitivity.  
 $\rho$  : depolarization lines.

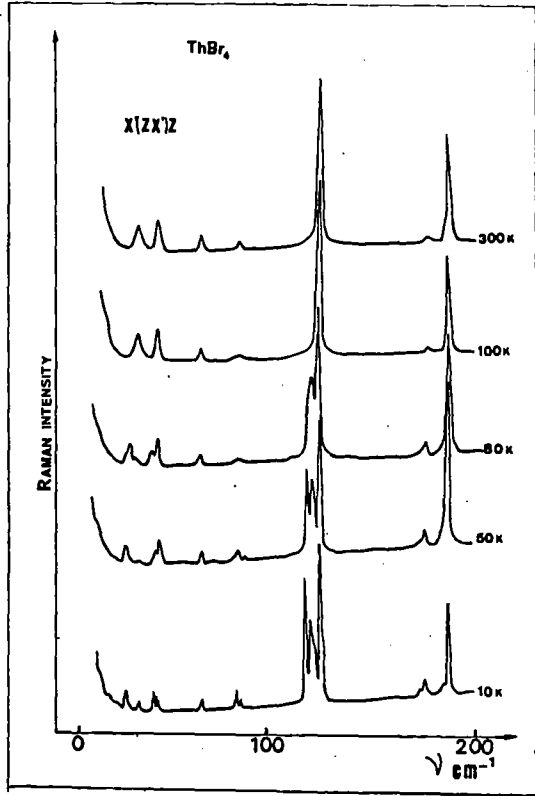


Fig. 2 - Temperature dependence of part of the E<sub>g</sub> spectrum above and below the phase transition.

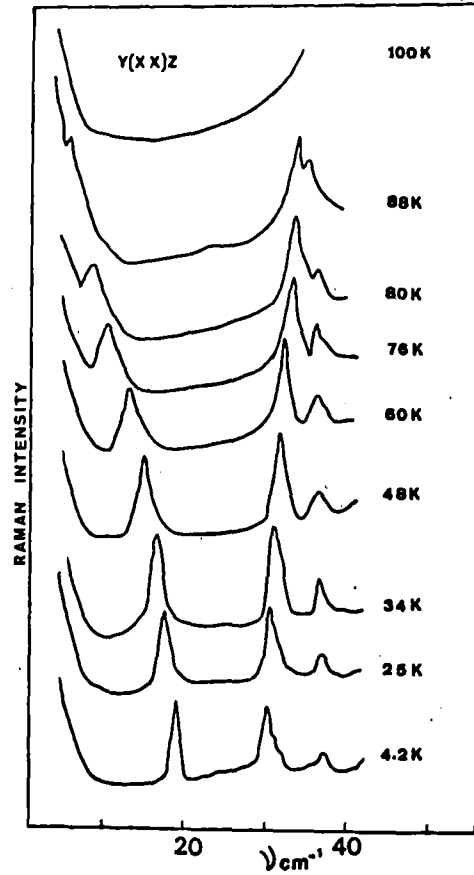


Fig. 3 - Temperature evolution of the polarized low frequency Raman spectra of ThBr<sub>4</sub> (stokes component).

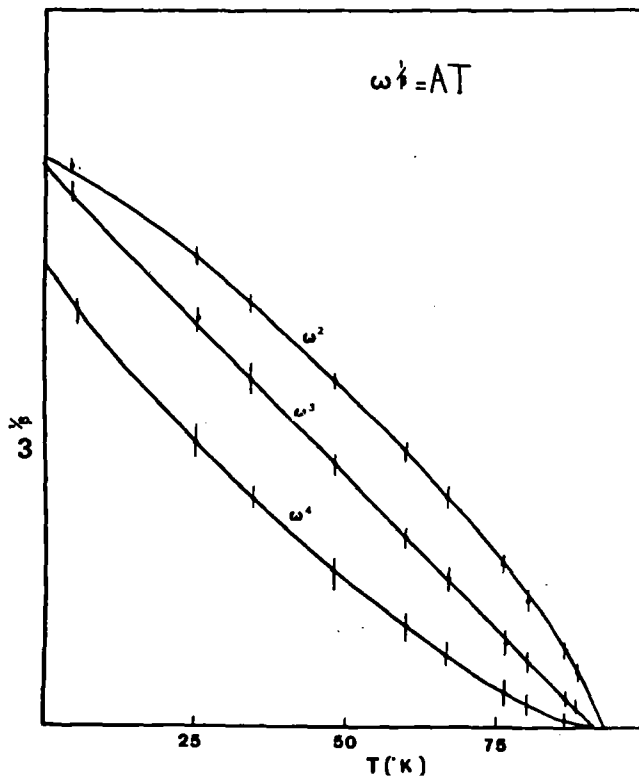


Fig. 4 - Temperature dependence of the soft mode frequency  $\omega$ .

ETUDE DES FLUORURES ET OXYFLUORURES DE PLUTONIUM  
PAR THERMOCHROMATOGRAPHIE

B. Jouniaux, Y. Legoux, J. Merinis, G. Bouissières

Laboratoire de Radiochimie, Institut de Physique Nucléaire

B. P. N° 1, 91406 Orsay, France

Après une étude par thermochromatographie (1) des chlorures des éléments : actinium à fermium, nous avons entrepris avec un appareillage adapté, celle des composés fluorés et oxyfluorés de ces mêmes éléments (2). Le plutonium a retenu plus spécialement notre attention, et nous rapportons ici les résultats concernant cet élément.

Techniques expérimentales.

La partie centrale du thermochromatographe (fig. 1) est constituée d'un tube de cuivre calorifugé extérieurement, de 90 cm de longueur, 1 cm d'épaisseur de paroi, 0,5 cm de diamètre intérieur. L'une des extrémités est chauffée jusqu'à environ 750° C par un four électrique de 2 kW asservi à un dispositif de régulation automatique de la température. L'autre extrémité est refroidie par un courant d'azote liquide circulant dans une enceinte soudée sur le tube et munie intérieurement d'ailettes en cuivre. Dans cette partie, la température est maintenue à - 100° C à  $\pm 1^\circ$  C près, par un dispositif de régulation cryogénique automatique. Dans l'axe de cette gaine métallique, on introduit un tube de nickel de 0,4 cm de diamètre extérieur et 0,2 cm de diamètre intérieur, préalablement nettoyé et séché, qui est parcouru du point chaud au point froid par un gaz fluorurant (HF ou F<sub>2</sub>) dont la vitesse est de l'ordre de 1 cm.s<sup>-1</sup>.

---

Ce travail a été réalisé dans le cadre d'un contrat CEA N° BC-1294. Nous tenons à exprimer nos remerciements à MM. Chesné et Lucas qui ont proposé cette étude.

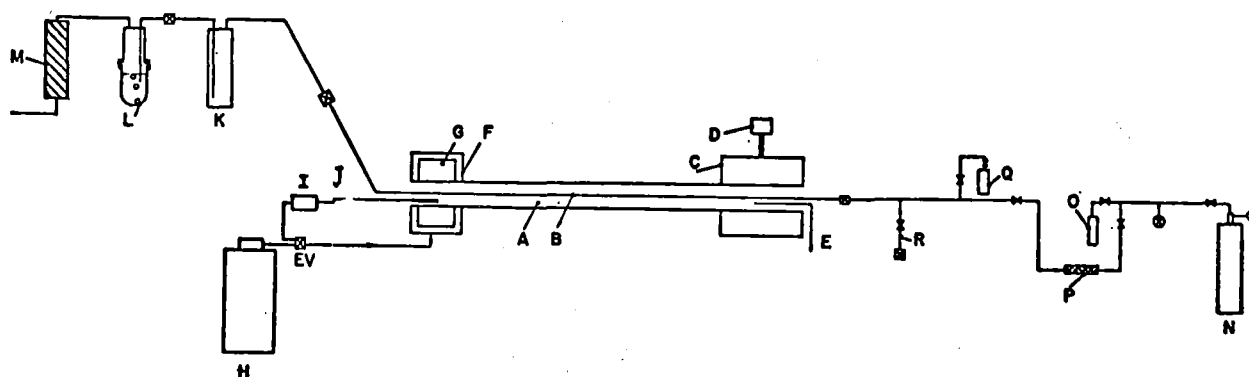


Fig. 1

- |  |  |
|--|--|
| A - barre de cuivre  | I - régulation cryogénique                                     |
| B - tube de nickel   | J - sonde à résistance de Pt (100 Ω)                           |
| C - four électrique (1 ou 2 kW)                              | K - tube de garde (inox)                                       |
| D - régulation de la température du four                     | L - compte-bulles, débitmètre                                  |
| E - thermocouple de contrôle                                 | M - piège à fluor (alumine activée)                            |
| EV - électrovanne  | N - bouteille de fluor   |
| F - enceinte cryogénique (-150° C à + 20° C)                 | O - réserve de fluor   |
| G - ailettes de refroidissement                              | P - piège à HF (KF)  |
| H - réservoir d'azote liquide (200 l)<br>à pression réglable | Q - bouteille de HF  |
|  | R - entrée gaz divers : O <sub>2</sub> , N <sub>2</sub> , Ar . |

Le fluor, délivré à partir d'une bouteille commerciale, est stocké dans un réservoir à pression contrôlée, puis purifié de ses traces de HF par passage sur du fluorure de sodium sec, et enfin dirigé vers le thermochromatographe. Sa teneur en oxygène est de l'ordre de 1 %.

Le fluorure d'hydrogène, de pureté 99,9 % (des traces d'hydrogène sont présentes) est prélevé directement dans une bouteille du commerce placée dans un circuit dérivé qui est réchauffé jusqu'à environ 30° C pour éviter les condensations du gaz dans les canalisations.

Une entrée secondaire permet d'introduire dans l'appareil de l'azote sec obtenu par distillation d'azote liquide. Toutes les canalisations, réservoir, manomètres et vannes diverses sont réalisées en acier inoxydable, soigneusement dégraissées, séchées par étuvage, et passivées progressivement par du fluor.

<sup>238</sup>Pu est déposé par évaporation d'une solution sur l'extrémité d'une

baguette de nickel de 0,1 cm de diamètre qui est ensuite placée dans le tube de nickel du thermochromatographe. La quantité de radioélément mise en oeuvre est inférieure à  $10^{-7}$  gramme. En fin d'expérience, la distribution de  $^{238}\text{Pu}$ , émetteur  $\alpha$ , se détermine commodément en mesurant l'activité  $\alpha$ , centimètre par centimètre, de la baguette (fig. 2).

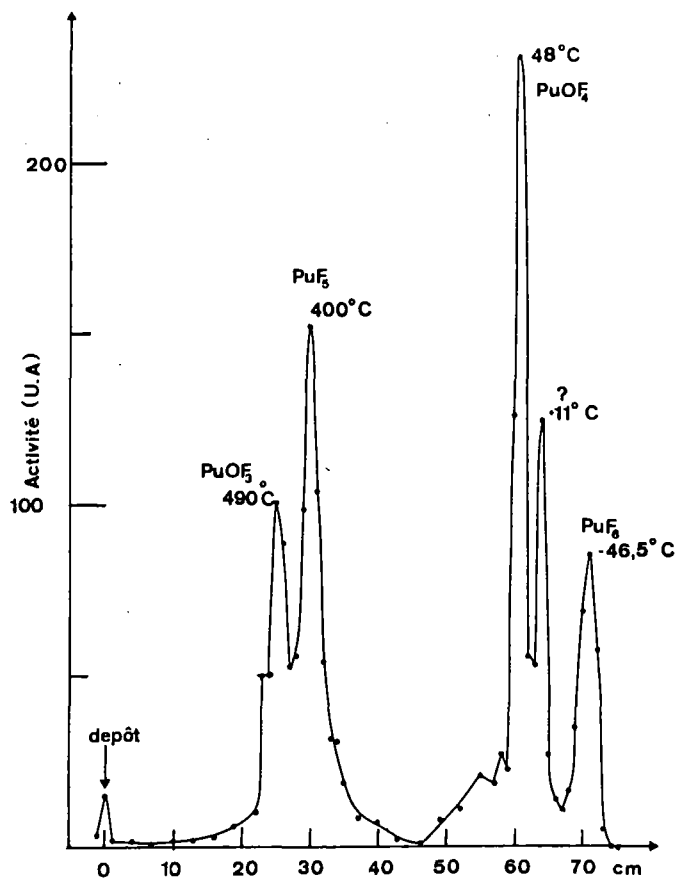


Fig. 2 - Répartition du plutonium le long du tube après six heures de fluoration de  $\text{PuO}_2$ .

Avant chaque série d'expériences, la température est mesurée, centimètre par centimètre, en enfonçant à l'intérieur du tube de cuivre une sonde thermosensible. La courbe de température ainsi obtenue montre un maximum suivi d'une décroissance exponentielle (fig. 3). Le dépôt initial du radioélément est placé dans la région du tube qui correspond au maximum de température et que l'on prend comme origine des distances pour mesurer le déplacement du radioélément.

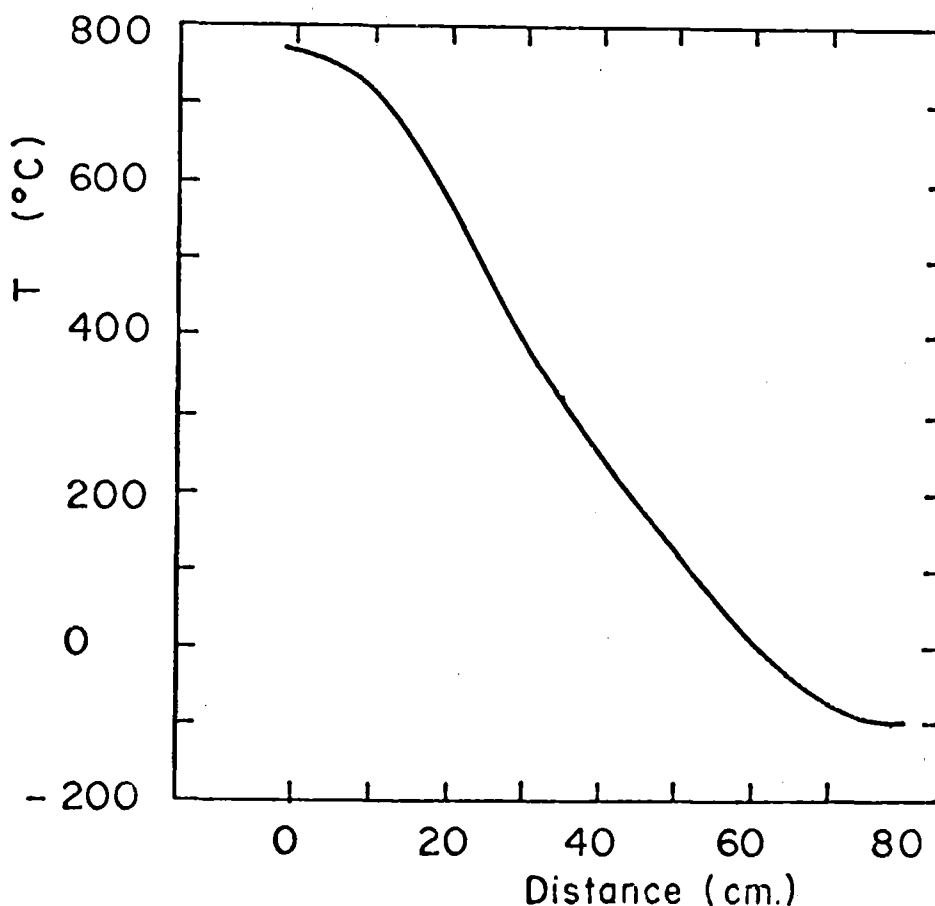


Fig. 3 - Répartition de la température le long du thermochromatographe.

Deux modes opératoires ont été pratiqués selon que le produit initial devant être attaqué par le fluor est un oxyde ou un trifluorure.

1 - Produit initial sous forme d'oxyde.

Le dépôt initial de  $^{238}\text{Pu}$  est effectué sous la forme d'un nitrate qui, chauffé dans l'appareil jusqu'à  $750^\circ\text{C}$  en présence d'air, conduit à l'oxyde  $\text{PuO}_2$ . Le courant de fluor est établi quand l'équilibre de température est atteint, et maintenu pendant six, dix ou vingt heures.

2 - Produit initial sous forme de trifluorure.

Le dépôt de  $^{238}\text{Pu}$  obtenu par évaporation d'une solution nitrique sur la baguette de nickel, est chauffé progressivement dans le thermochromatographe jusqu'à  $750^\circ\text{C}$  sous un courant de  $\text{HF}$ , pour former  $\text{PuF}_3$ , l'extrémité froide de l'appareil étant maintenue à  $25^\circ\text{C}$  pour éviter la condensation

du gaz. Le tube est ensuite purgé de toute trace de HF par passage d'un courant d'azote sec. On refroidit alors l'extrémité du thermochromatographe jusqu'à - 100° C, tout en maintenant le point chaud à 750° C. Quand l'équilibre de température est réalisé, le fluor est admis dans l'appareil pour une durée de six à vingt heures.

Quel que soit le mode opératoire choisi, en fin d'expérience le courant de fluor est arrêté et le tube est balayé par de l'azote contenant environ 10 vpM d'eau, admis sous un faible débit. Les espèces volatiles sont alors décomposées et restent ainsi fixées dans la zone de leur dépôt final.

### Résultats

Un ensemble de résultats obtenus dans une étude antérieure (2) permet d'identifier plusieurs des composés fluorés et oxyfluorés de plutonium produits dans nos conditions expérimentales, d'après la température de la zone du tube de nickel dans laquelle ils se déposent (température caractéristique de dépôt :  $T_C$ ). Ces données sont réunies dans le Tableau 1.

Tableau 1

Zônes de dépôt définies dans le thermochromatographe, par l'étude de divers éléments, de chaque type de composé fluoré

Types de composés	Eléments	$T_C$ °C
$M F_4$	M : Ce, U, Np, Pu Am, Cm, Cf	600 à 700
$M F_5$	M : Ta, Pa	300 à 400
$MO_2 F_2$	M : Np	150
$MOF_4$	M : U, Np	20 à 80
$MF_6$	M : U, Np	- 80 à - 30

Les résultats du présent travail sont reportés dans le Tableau 2.

Tableau 2 - Plutonium : résultats expérimentaux

Systèmes Composés formés	$F_2 + PuO_2$					$F_2 + PuF_3$				
	6 heures		20 heures		6 heures		10 heures		20 heures	
	$T_C$	% $A_{tot}$	$T_C$	% $A_{tot}$	$T_C$	% $A_{tot}$	$T_C$	% $A_{tot}$	$T_C$	% $A_{tot}$
Dépôt initial		1				7		7		
$PuF_4$					697°	≈ 2				
	490°	17					528°	7		
$PuF_5$	400°	28	★		384°	9	370°	44	370°	21
				38	320°	18			260°	16
$PuO_2F_2$					218°	20	183°	38	110°	31
$PuOF_4$	48°	24	35°	42	73°	29			38°	26
	11°	13	1°	13	30°	16	11°	5	0°	7
$PuF_6$	- 47°	13	- 57°	7						

★ Activité éparse le long du tube (non rassemblée)

Les températures caractéristiques de dépôt relevées dans les différentes expériences conduisent, d'après le Tableau 1, à conclure à la formation en phase gazeuse des composés  $PuF_4$ ,  $PuF_5$ ,  $PuO_2F_2$ ,  $PuOF_4$  et  $PuF_6$ . Notons que  $PuF_5$  n'avait jamais été observé auparavant.

Il est intéressant de remarquer que si l'on porte sur un graphique (figure 4) la température caractéristique de dépôt de ces composés en fonction du nombre d'atomes de fluor présents dans la molécule, les points représentatifs des espèces  $PuF_4$ ,  $PuF_5$  et  $PuF_6$  sont bien alignés. Il en est de même pour les composés hexavalents :  $PuO_2F_2$ ,  $PuOF_4$  et  $PuF_6$ .

Ce type de diagramme permet d'avancer une interprétation du dépôt de plutonium à 490-530° C. Ce dernier doit correspondre à un composé de volatilité intermédiaire entre celle de  $PuF_4$  et celle de  $PuF_5$ , donc vraisemblablement à un oxyfluorure de  $Pu^V$ . Or, le diagramme de la figure 4 est en faveur de  $PuOF_3$  et non de  $PuO_2F$ . En effet, d'après les droites en pointillé

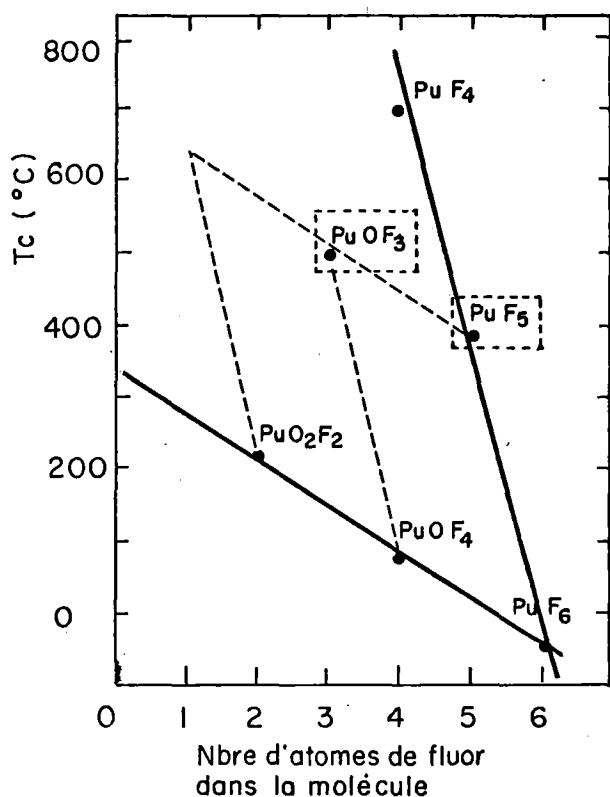


**Fig. 4** - Température caractéristique de dépôt des composés de Pu en fonction du nombre d'atomes de fluor présents dans la molécule.

A la valence VI, compte tenu des produits déjà identifiés : PuF<sub>6</sub>, PuOF<sub>4</sub>, PuO<sub>2</sub>F<sub>2</sub>, on pourrait penser à un composé du type Pu<sub>2</sub>OF<sub>10</sub>. A la valence VII, si PuF<sub>7</sub> est exclu pour des raisons de volatilité, les oxyfluorures PuOF<sub>5</sub>, PuO<sub>2</sub>F<sub>3</sub>, PuO<sub>3</sub>F sont envisageables. Par analogie avec NpOF<sub>5</sub> qui a été obtenu par Drobyshevskii et al. (3) et dont la volatilité serait comprise entre celle de NpOF<sub>4</sub> et NpF<sub>6</sub>, on serait tenté de retenir PuOF<sub>5</sub>. Cependant, il semble par comparaison avec les oxyfluorures de Pu<sup>VI</sup> que ce composé devrait se déposer à une température beaucoup plus basse que celle qui est observée. En revanche, la formation de PuO<sub>3</sub>F, de même que celle de Pu<sub>2</sub>OF<sub>10</sub>, ne seraient pas incompatibles avec les données de la figure 4. Des expériences supplémentaires seraient nécessaires pour lever cette indétermination.

tracées parallèlement aux droites établies précédemment, la T<sub>C</sub> de PuOF<sub>3</sub> devrait être proche de 500° C alors que celle de PuO<sub>2</sub>F serait bien plus élevée.

L'interprétation des deux dépôts de plutonium à 260-320° C et à -1 - 30° C semble délicate.

Pour le dépôt à 260-320° C on pourrait penser au dimère (PuF<sub>5</sub>)<sub>2</sub> car dans le travail déjà cité (2), on a noté, dans la même zone de température, un dépôt de <sup>182</sup>Ta attribuable, dans les conditions où nous opérons, à (TaF<sub>5</sub>)<sub>2</sub>.

Enfin, le dépôt qui apparaît vers -1 - 30° C, donc entre PuOF<sub>4</sub> et PuF<sub>6</sub>, doit être un oxyfluorure de Pu<sup>VI</sup> ou de Pu<sup>VII</sup>.

### Conclusion

L'étude par thermochromatographie du comportement du plutonium sous fluor montre la formation de nombreux dérivés parmi lesquels deux nouveaux composés :  $\text{PuF}_5$  et  $\text{PuOF}_3$  ont été identifiés en phase gazeuse.

### Références.

- (1) J. Merinis, Y. Legoux, G. Bouissières, Radiochem. Radioanal. Letters 3/4 (1970) 255.
- (2) B. Jouniaux, Thèse de 3ème cycle, Université de Paris VI, 1979.
- (3) Yu. V. Drobyshevskii, V.F. Serik, V.B. Sokolov, M.N. Tul'skii, Radiokhimiya, vol. 20, N° 2 (1978) 238 ; traduction anglaise dans Soviet radiochemistry (nov. 1978) 200.

MAGNETIC AND ELECTRIC PROPERTIES OF  $\text{Pu}_2\text{O}_2\text{Y}$  COMPOUNDS

(Y = O, S, Se, Te)

*J.M. COSTANTINI - D. DAMIEN - C. H. de NOVION (CEN Fontenay)*

*COUSSON - ABAZLI - PAGES (Labo. Curie Paris)*

*A. BLAISE (CEN Grenoble)*

*R. GUILLAUMONT (Fac. Orsay IN2P3)*

We have prepared  $\text{A} - \text{Pu}_2\text{O}_3, \text{Pu}_2\text{O}_2\text{S}, \text{Pu}_2\text{O}_2\text{Se},$  and  $\text{Pu}_2\text{O}_2\text{Te}$  and studied their magnetic and electric properties. Some isostructural compounds have already been thoroughly investigated such as the Rare Earths compounds  $\text{RE}_2\text{O}_2\text{Y}$  [1, 2, 3] and the uranium compounds  $\text{U}_2\text{N}_2\text{Y}$  [4].

Our aim was to correlate the variations of some physical properties with the expected change of covalency in the chemical bonding across that series of compounds.

I SAMPLES PREPARATION

These compounds were obtained using two different methods.

i) In the first one, plutonium dioxide and plutonium monochalcogenide ( $\text{PuY}$ ) were pressed together in stoichiometric amounts. The resulting pellet was then heated under high vacuum either in an alumina crucible (for Y = Se at about 1 550°C) or in a silica tube (for Y = Te at 800°C).

ii) In the second method plutonium hydride was reacted with stoichiometric amounts of chalcogen vapor and plutonium dioxide in a vacuum sealed silica tube (at 800°C for Y = S, Se, Te).

To obtain the sesquioxide, plutonium hydride was allowed to react with a stoichiometric amount of plutonium dioxide. This was done under vacuum in a tungsten crucible heated by an induction coil. The high temperature trigonal phase was then quenched by switching off the high frequency current.

## II STRUCTURE AND BONDING

The resulting powders were all black in colour. They were X-rayed in a Debye-Scherrer camera and were found to be pure except for some very weak lines corresponding to  $\text{PuO}_2$  ( $\text{PuO}_2$  is a weak Temperature Independent Paramagnet).

The X-ray powder patterns of the sesquioxide, oxysulfide, oxyselenide were indexed in the hexagonal system, and the oxy-telluride in the tetragonal system.

Our values are in good agreement with literature data (see table 1).

No single crystal could easily be grown partly because of the very high refractory character of these compounds.

Yet by checking the intensities of the diffraction lines of both crystal structures these compounds were found to be iso-structural with the rare earths similar compounds (see fig 1 & 2).

Both crystal structures can be described as piled up  $[\text{Pu}_2\text{O}_2]$  layers, alternating with anionic  $\text{Y}^-$  sheets. [5] (see fig 3).

These layers are made of  $\text{OPu}_4$  tetrahedra linked together by sharing of edges.

Atomic position parameters of the Rare Earths oxychalcogenides  $\text{RE}_2\text{O}_2\text{Y}$  were used to estimate the interatomic distances in these plutonium compounds.

Metal-oxygen distances in [Pu O] layers are found to be shorter than expected from ionic radii data and suggest a covalent character of the bonding within these layers.

In the oxytelluride a similar situation occurs but no definite oxycation can be isolated as the layers are made of continuous chains of alternating equispaced plutonium and oxygen atoms. (see fig. 3)

The same kind of oxycation  $(M_2O_2)^{++}$  appears in many rare-earth oxysalts [1,6]

Moreover when growing rare earth oxysulfide single-crystals, Henri at Grenoble recently observed very thin layer-shaped crystals showing the bonding anisotropy in these compounds. [7]

### III MAGNETIC SUSCEPTIBILITY MEASUREMENTS

The static magnetic susceptibilities of these compounds were measured using a Faraday balance. The applied field was 5.5 kilogauss. No field dependence was observed at room temperature. The curves  $1/X$  vs  $T$  suggest that all these compounds order antiferromagnetically at low temperature. (fig. 4)

High temperature data fit a Curie-Weiss law. The Neel points show a slight increase when going from oxygen to selenium via sulfur. Direct f.f interactions between neighbouring metallic sites are very unlikely due to geometrical reasons. Yet superexchange coupling interactions via the anionic  $Y^-$  orbitals strengthen when going from oxygen to sulfur then selenium and this could account for the observed increase of the ordering point. (see table 2)

Inside the layers superexchange coupling occurs mainly via oxygen ions with a contribution of  $Y^-$  anions but like in rare earth oxychalcogenides [1,2] this coupling is expected to be weaker than the inter-layer coupling interactions.

Furthermore an increase of the Neel point is noticed with increasing metal-metal spacing. This distance remains always higher than the Hill critical distance of 3.40 Å for appearance of magnetism.

The rare earths oxychalcogenides which have been reported to be antiferromagnets [1,2,3] exhibit much lower Neel points (below 10°K). This suggests stronger exchange coupling and then greater covalency of bonding in the plutonium compounds.

#### IV ELECTRICAL RESISTIVITIES MEASUREMENTS

The electrical resistivities were also measured using a 4 point-method. These measurements were performed on pellets annealed at about 1 250°C. These compounds were found to be highly resistive semiconductors.

The experimental intrinsic energy gaps are comparable to those encountered for plutonium dioxides. Measurements are under work to draw further conclusions.

#### CONCLUSION

To improve the discussion on the magnetic properties of these compounds neutron diffractions are needed. Yet these experiments are not straightforward for plutonium since  $^{239}\text{Pu}$  is the most available isotope.

In addition absorption spectra would certainly throw light on the problem of bonding and we particularly think of a possible nephelauxetic effect as evidenced for the rare-earths isostructural compounds[8,9].

Acknowledgements : The authors are indebted to Dr R. TROC for many helpful discussions.

Lattice parameters of  $\text{Pu}_2\text{O}_2\text{Y}$  compounds

Y=O, S, Se, Te

	a(Å)		c(Å)		c/a	
	This work	Litterature	This work	Litterature	This work	Litterature
A- $\text{Pu}_2\text{O}_3$	3.830(2)	3.841 (a)	5.997(6)	5.958	1.56	1.55
$\text{Pu}_2\text{O}_2\text{S}$	3.929(7)	3.927 (b)	6.804(2)	6.769	1.73	1.72
$\text{Pu}_2\text{O}_2\text{Se}$ {	3.962(1)	3.957 (c)	6.987(1)	6.977	1.76	1.76
	3.961(1)		6.983(1)			
$\text{Pu}_2\text{O}_2\text{Te}$ {	4.008(1)	4.03 (c)	12.659(2)	12.66	3.16	3.14
	4.008(1)		12.668(4)			

(a)D.H. Templeton- C.H Dauben UCRL 1886 (1952)

(b)W.H. Zachariasen Acta Cryst (1949) 2,60

(c)M. Allbutt-R.M. Dell-A.R. Junkinson AERE-R.5541 (1967)

TABLE 2

**Pu<sub>2</sub>O<sub>2</sub>Y      magnetic properties**

Y	O	S	Se	Te
shortest Pu-Pu(Å)	3.40	3.70	3.80	3.60
T <sub>N</sub> (°K)	26(1)	28(1)	34(1)	53(2)

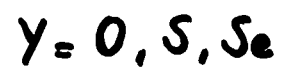
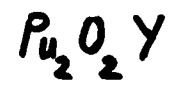
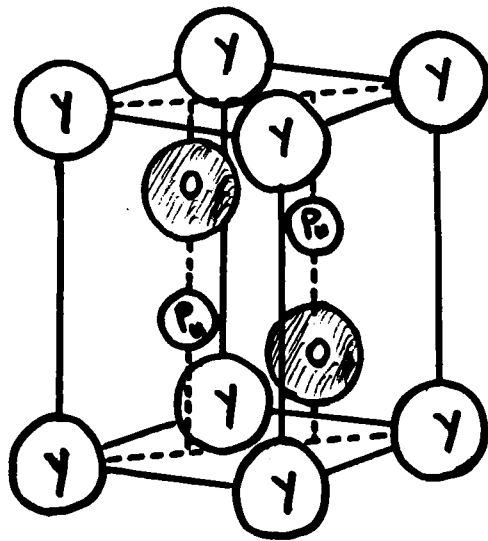


Fig 1

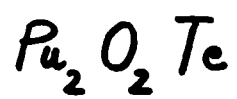
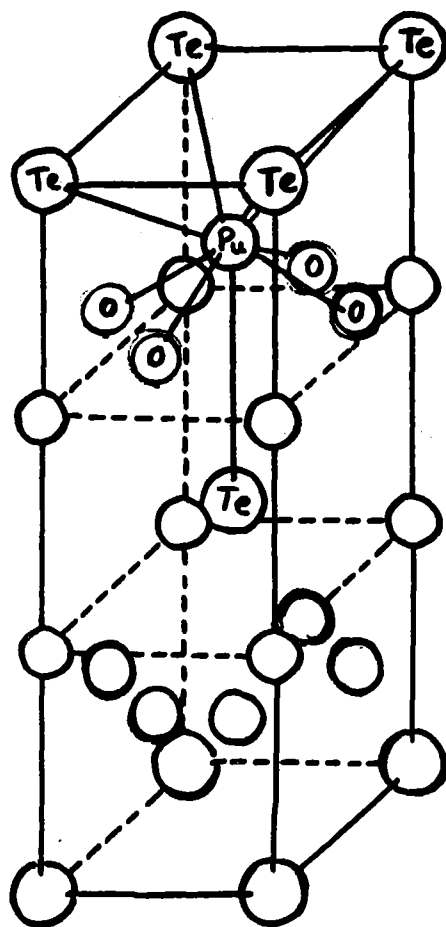
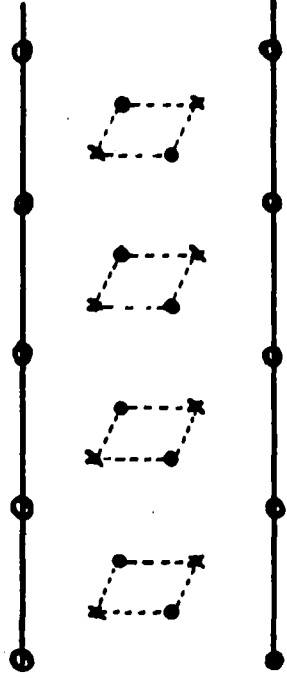


Fig 2



$\gamma = O^{\cdot-}, S^{\cdot-} \text{ or } Se^{\cdot-}$

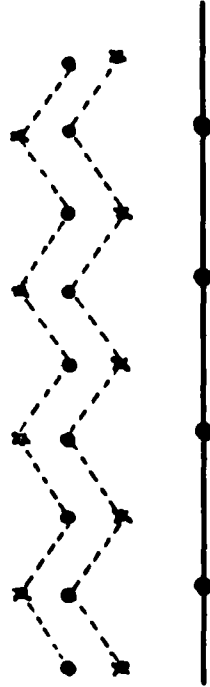
$\times Pu$   
 $\cdot O$



Hexagonal  
structure  
proj. in (100)

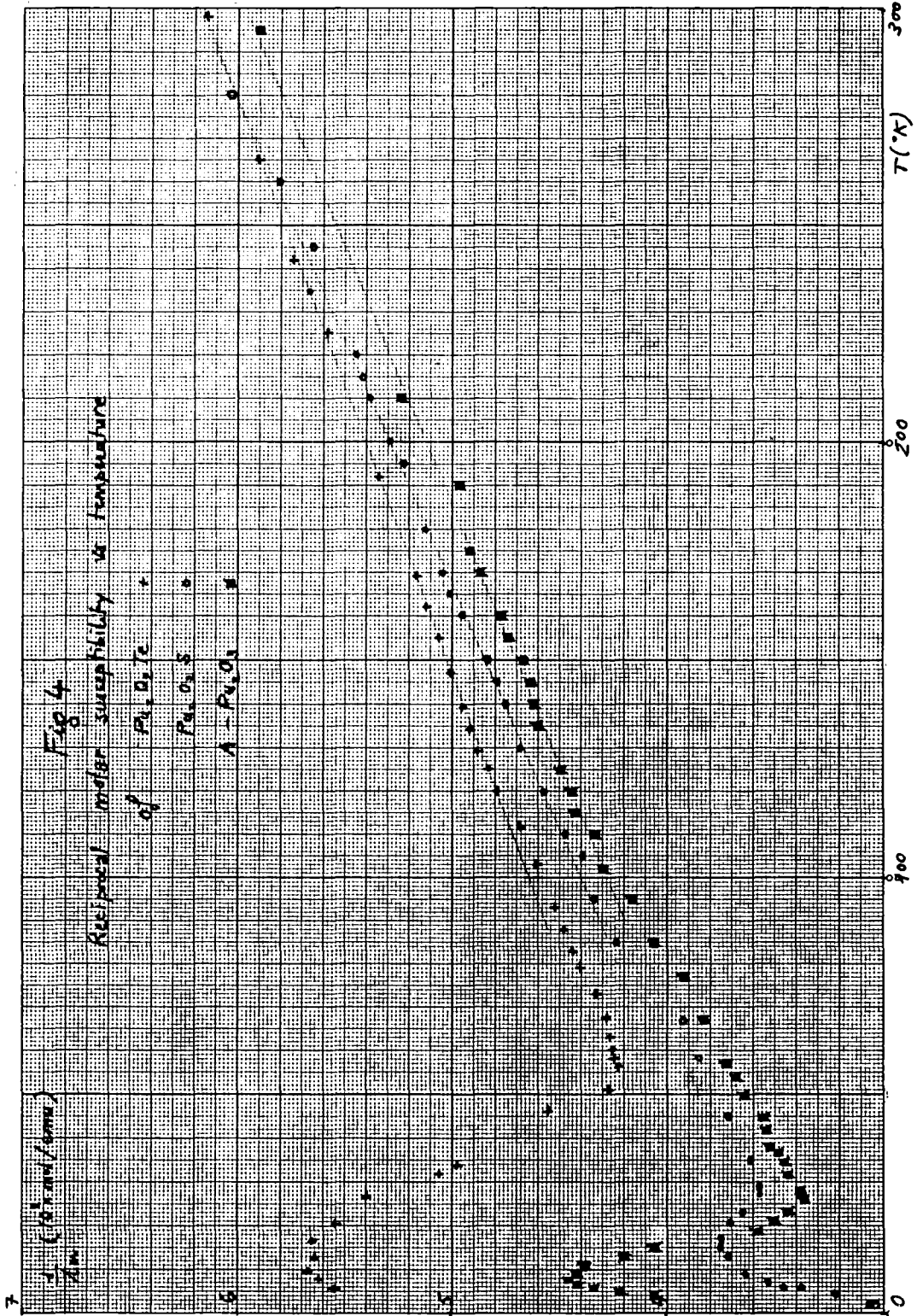
$Te^{\cdot-}$

$\times Pu$   
 $\cdot O$



Tetragonal  
structure  
proj. in (100)

Fig 3



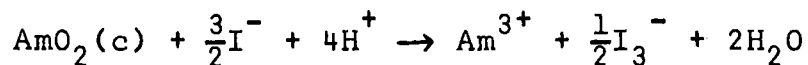
REFERENCES

1. R. BALESTRACCI - Thesis 1967 Grenoble
2. J. ROSSAT-MIGNOD - Thesis 1972 Grenoble
3. Y. ABBAS - Thesis 1976 Grenoble
4. Z. ZOLNIEREK - R. TROC. p. 589 Plutonium 75 and other actinides - Baden-Baden
5. P. CARO . J. Less Common metals 16 (1968) 367
6. P. CARO . CR Acad. Sci Paris 262, 992, série C
7. Private Communication
8. C.K. Jørgensen R. Pallalardo J Flahaut  
J. Chem. Phys. 62, (1953) 6069
9. P. CARO Bull. de la Société Chimique de France 1972  
N° 1 p. 46

ENTHALPY OF FORMATION OF AMERICIUM DIOXIDE AND  
ESTIMATE OF ENTHALPY OF FORMATION OF AQUEOUS AMERICIUM(IV) ION

L. R. Morss\* and J. Fuger  
Institute of Radiochemistry, B-16  
University of Liège, Sart Tilman  
4000 Liège, Belgium

Because there are uncertainties in the determination of  $\Delta H_f^\circ(\text{AmO}_2, c)$  reported by Eyring, Lohr, and Cunningham in 1952, we have redetermined this datum by measuring the heat of solution of  $\text{AmO}_2$  (calcined from oxalate at 500 °C) in sulfuric acid-potassium iodide media according to the following reaction:



The resultant enthalpy of formation of  $\text{AmO}_2$  has been correlated with those of lighter actinide dioxides in order to estimate the enthalpy of formation of the aqueous americium(IV) ion.

---

\*On sabbatical leave from Rutgers University, New Brunswick, New Jersey 08903.

LOW TEMPERATURE SPECIFIC HEAT OF PLUTONIUM CARBIDES

R. O. A. Hall, H. R. Haines, J. A. Lee, M. J. Mortimer (AERE Harwell)  
and D. McElroy (ORNL)

ABSTRACT

The specific heats of plutonium monocarbides of a range of stoichiometries are presented, and analysed using Debye and Einstein specific heat models. The parameters found are compared with those obtained by inelastic neutron scattering for thorium compounds. The variations in magnetic parameters with stoichiometry are noted.

## INTRODUCTION

Plutonium monocarbide crystallises in the NaCl f.c.c. structure, and is always substoichiometric with respect to carbon, the lattice parameter increasing with carbon content. It orders anti-ferromagnetically at 100K in carbon saturated PuC and  $T_N$  falls with the carbon content, as shown in neutron diffraction<sup>(1)</sup>, electrical resistivity<sup>(2)</sup> and magnetic susceptibility<sup>(2,3)</sup> measurements.

This paper is based on the results of measurements of the low temperature specific heats of 8 samples of single phase PuC ( $0.8 < x < 0.9$ ) and 2 samples of 2-phase material ( $x = 1.013$  and  $1.124$ ). No detailed discussion of the experimental methods or sample characterisation will be given here. These aspects are fully discussed in a forthcoming Harwell Internal Report, which will subsequently be published in the open literature. Copies of the report will be available in June from one of the authors (M.J.M.). That report also discusses the specific heats of  $Pu_3C_2$ ,  $Pu_2C_3$  and of two-phase mixtures with PuC.

In this report we present analysis of the data obtained, and compare it with inelastic neutron scattering data, which can give comparable parameters. We do not discuss in detail the dependence of various parameters on stoichiometry - these are given in the full report.

### Analysis

Although we do not discuss here details of errors of measurement and the reliability of sample characterisation, these are fundamental questions which must precede analysis. The justification for our analysis is based on, first, the dependence of  $C_p$  on temperature for varying stoichiometries (Figure 1). The specific heats above 150K for the 8 samples reported lie in a band

only 16% of  $C_p$  wide, and within this band order logically. This suggests that our estimated errors of  $\pm 2\%$  are pessimistic and that the sample characterisations are reliable - an overall precision of about  $\pm 0.5\%$  is indicated. Below 150K, the samples have stoichiometry-dependent Neel points, so the various specific heat excesses overlap. Below about 50K, the results again lie in order. The room temperature  $C_p$  as a function of stoichiometry also shows the small amount of random scatter in the data (Figure 2). Any analysis is therefore justified which looks at  $C_p$  variations greater than these error limits.

The experimentally determined heat capacity at constant pressure ( $C_p$ ) must first be corrected to the heat capacity at constant volume ( $C_v$ ) by subtraction of a dilation term. To determine accurately the magnitude of this correction, at all temperatures, the temperature dependencies of the expansion coefficient, density and bulk modulus are required. In the absence of this data an approximation can be made using the Nernst-Lindemann equation:

$$C_p - C_v = A C_p^2 T$$

where  $A = (9\alpha^2 K_T V) / (C_p)^2$ ,  $\alpha$  is the linear expansion coefficient,  $K_T$  is the isothermal bulk modulus,  $V$  is the molar volume and  $C_p$  is the measured heat capacity.  $A$  is independent of temperature, and so it may be calculated at any convenient reference point, in this case 298K.

No measurements on the elastic constants of plutonium monocarbide have been published, but Padel and de Novion<sup>(4)</sup> have reported measurements in the elastic constants of uranium monocarbide at room temperature. The lattice parameters, molar volume and expansion coefficients, all at 298K, of uranium and plutonium monocarbides are very similar, and it seems reasonable

to assume that the bulk moduli will also be similar. In practice a large error in this assumption would only have a small effect on the value of A, which is dominated by the value of  $\alpha^2$ . The value of A for plutonium monocarbide is  $\sim 1.4 \times 10^{-6}$  and the resulting dilation correction is less than the experimental scatter, but has been included in the calculations.

The deduced  $C_v$  may be treated as the sum of three possible contributions:

- 1) a contribution from the heat capacity of the conduction electrons. This is linear in temperature and its magnitude,  $\gamma T$ , is an indication of the density of states at the Fermi surface.  $\gamma$  is the electronic heat capacity coefficient.
- 2) the acoustic phonons from the normal lattice vibrations, producing a contribution to the heat capacity which may be analysed as a classical Debye model.
- 3) a contribution from the optical phonons which arise from the relative vibration of the light carbon atoms about the heavier plutonium atoms. Ideally, provided the carbon atoms do not interact, they will behave as simple harmonic oscillators, and can be treated as an Einstein contribution.

First of all, the magnitude of the contribution due to optical phonons was calculated from the Einstein model, taking a molar fraction equal to the carbon-plutonium ratio. This contribution, together with a linear term proportional to the electronic specific heat, was subtracted from the deduced  $C_v$ . The remainder was then analysed as one mole of plutonium in a simple Debye model. A range of possible Einstein temperatures and a range of electronic heat capacity co-efficients were tried. The best fit was determined as those values which gave the most temperature independent Debye temperature above  $\theta/2$ . Figure 3 shows a typical

curve for the variation in the Debye temperature for  $\text{PuC}_{0.825}$ , after subtraction of a dilation term and an Einstein contribution, with a  $\theta_E$  of 440K, for various possible electronic terms. In figure 3 the best fit is given by  $\gamma = 14\text{mJ.mol}^{-1}\text{K}^{-2}$ . These best values for the  $\text{PuC}_x$  samples are given in table II. It was found that the quality of the fits depended strongly on the  $\gamma$  values selected, so that the error bars for this parameter are small. The derivation of  $\theta_E$  and  $\theta_D$  was less precise since, the Debye and Einstein functions having a rather similar temperature dependence, an upwards variation in  $\theta_D$  could be to some extent compensated by a downwards variation in  $\theta_E$ . This variation is covered by the error bars shown in table II. The total lattice heat capacity  $f_D(\theta_D) + f_E(\theta_E)$ , was well defined.

This separation of the specific heat into separate terms also simplifies the extraction of the magnetic contribution to the specific heat. In Figure 3, the dashed line is a typical interpolation used to generate the Debye specific heat and hence, the total lattice specific heat, which, together with the electronic term gives the total non-magnetic contribution.

Figure 4 shows the specific heat separated into these terms.

### Discussion

The results of this analysis, as given in table II are shown graphically in Figures 5 and 6. The peak in the measured  $C_p$  at  $\text{PuC}_{0.89}$  is not seen in the lattice term ( $f_D(\theta_D) + f_E(\theta_E)$ ) but only in the electronic specific heat (Figure 5). This is presumably due to a peak in the electronic density of states with stoichiometry, and is seen also in magnetic susceptibility measurements<sup>(2,3)</sup>. The magnetic entropy does not show any such peaking, rising by a factor of two across the series of plutonium carbides studied. These properties are discussed in detail in the

full report.

The Einstein temperature derived here may be compared with that derivable from the neutron time-of-flight spectrum due to inelastic scattering. In cases where the ratio of the Actinide-ion anion mass is high, and the anion-anion interactions are negligible, the optical phonons have an almost constant frequency, which can be derived from the position of the optical phonon t.o.f. peak. On the same assumptions the specific heat of the carbon atoms is represented by a simple harmonic oscillator, and gives the Einstein specific heat already discussed.

This procedure has already been applied by Wedgwood<sup>(5)</sup> to some thorium compounds<sup>(5,6,7)</sup>. Given below are the values derived

<u>Thorium carbide</u>	<u>Table I</u>		
	$\theta_E$	$\theta_D$	$\gamma$
Danan ( $C_p$ )	467 ± 5	262 ± 2	1 ± 1
Neutron scattering	446 ± 9		
Present calculations of Danan's $C_p$	465 ± 15	280 ± 50	1 ± 1
<u>Thorium nitride</u>			
Danan ( $C_p$ )	495	284 ± 2	3.12
Neutron scattering	494 ± 4		
Present calculations of Danan's data	485 ± 15	290 ± 30	2 ± 1

by Danan, using the same model as ourselves, but arriving at the parameters by a different route. (The values we derive from his data are also given). These are compared with the inelastic neutron scattering results. All the results agree to within the estimated errors, and give confidence to the analysis. In the case of PuC, which, unlike the thorium compounds, orders magnetically, the analysis is only possible because  $T_N$  is lower than  $\frac{\theta_D}{2}$  and does not interfere with the extraction of the terms.

The Einstein temperatures calculated here for PuC vary with stoichiometry from 370K to 440K, although this may not be a significant variation, since it is only just greater than experiment error. For a middle of the range value,  $\theta_E = 400\text{K}$ , the optical phonon peak would be expected at 8.3 THz. Measurement of the inelastic neutron scattering from the optical phonons in PuC would be interesting, as a check on the quality both of the data and of the analysis.

TABLE II Derived parameters for  $\text{PuC}_x$  ( $0.8 < x < 1.12$ )

Composition	Einstein Temperature K	Debye Temperature K	Electronic Coefficient $\text{mJ}\cdot\text{mol}^{-1}\text{K}^{-2}$	Magnetic Entropy $\text{J}\cdot\text{mol}^{-1}\text{K}^{-1}$	Néel Temperature K
$\text{PuC}_{0.80}$	$440 \pm 10$	$200 \pm 20$	$14 \pm 1$	1.78	45
$\text{PuC}_{0.825}$	$410 \pm 10$	$250 \pm 30$	$14 \pm 1$	1.82	50
$\text{PuC}_{0.85}$	$390 \pm 10$	$290 \pm 25$	$19 \pm 1$	2.58	60
$\text{PuC}_{0.865}$	$370 \pm 10$	$285 \pm 20$	$19 \pm 1$	3.35	70
$\text{PuC}_{0.89}$	$400 \pm 30$	$250 \pm 20$	$20 \pm 1$	2.48	85
$\text{PuC}_{0.90}$	$440 \pm 20$	$200 \pm 20$	$13 \pm 1$	3.34	85
$\text{PuC}_{1.01}$	$400 \pm 20$	$270 \pm 15$	$14 \pm 1$	2.912	111
$\text{PuC}_{1.12}$	$420 \pm 10$	$280 \pm 10$	$9 \pm 1$	2.399	118

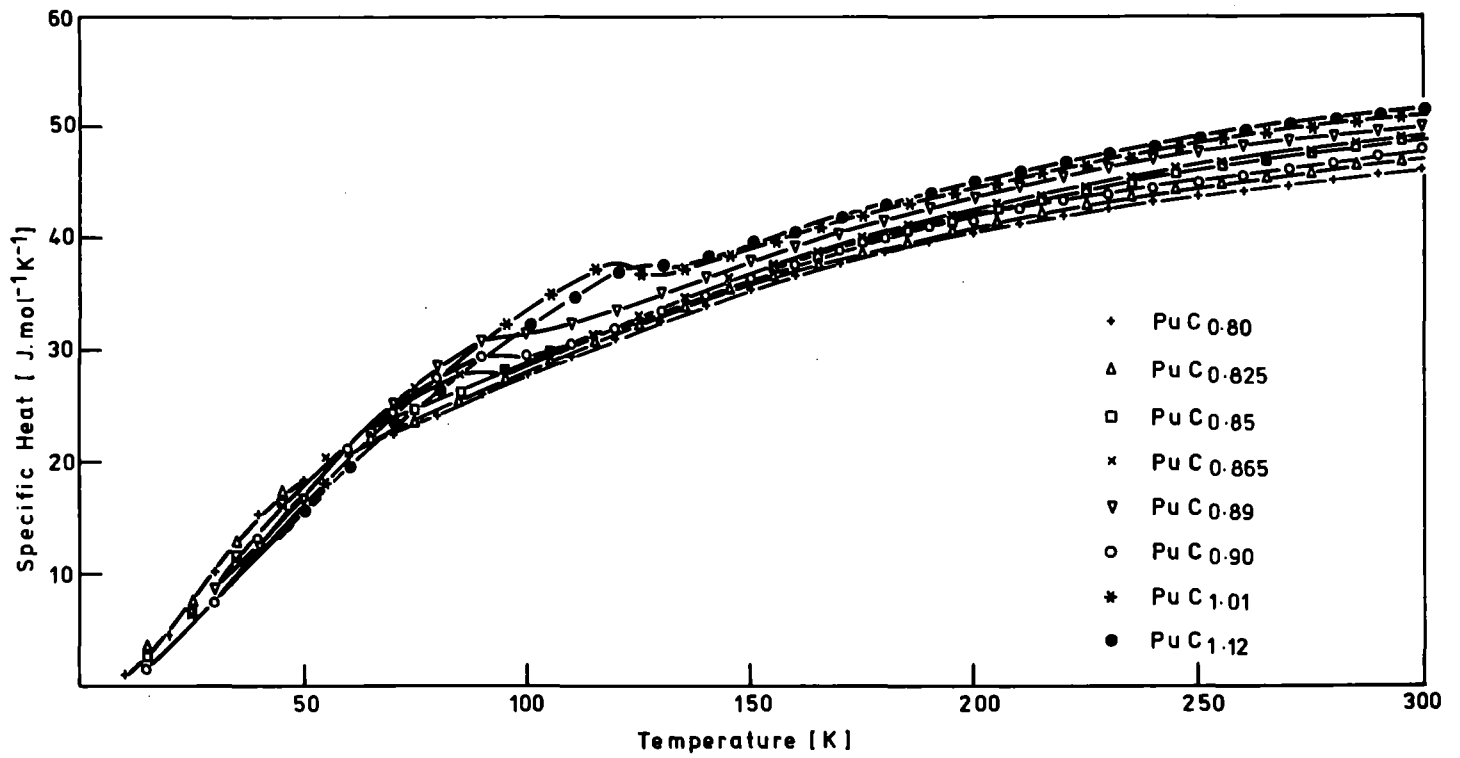


Figure 1 Heat Capacities of PuC<sub>x</sub> (0.80 < x < 1.12)

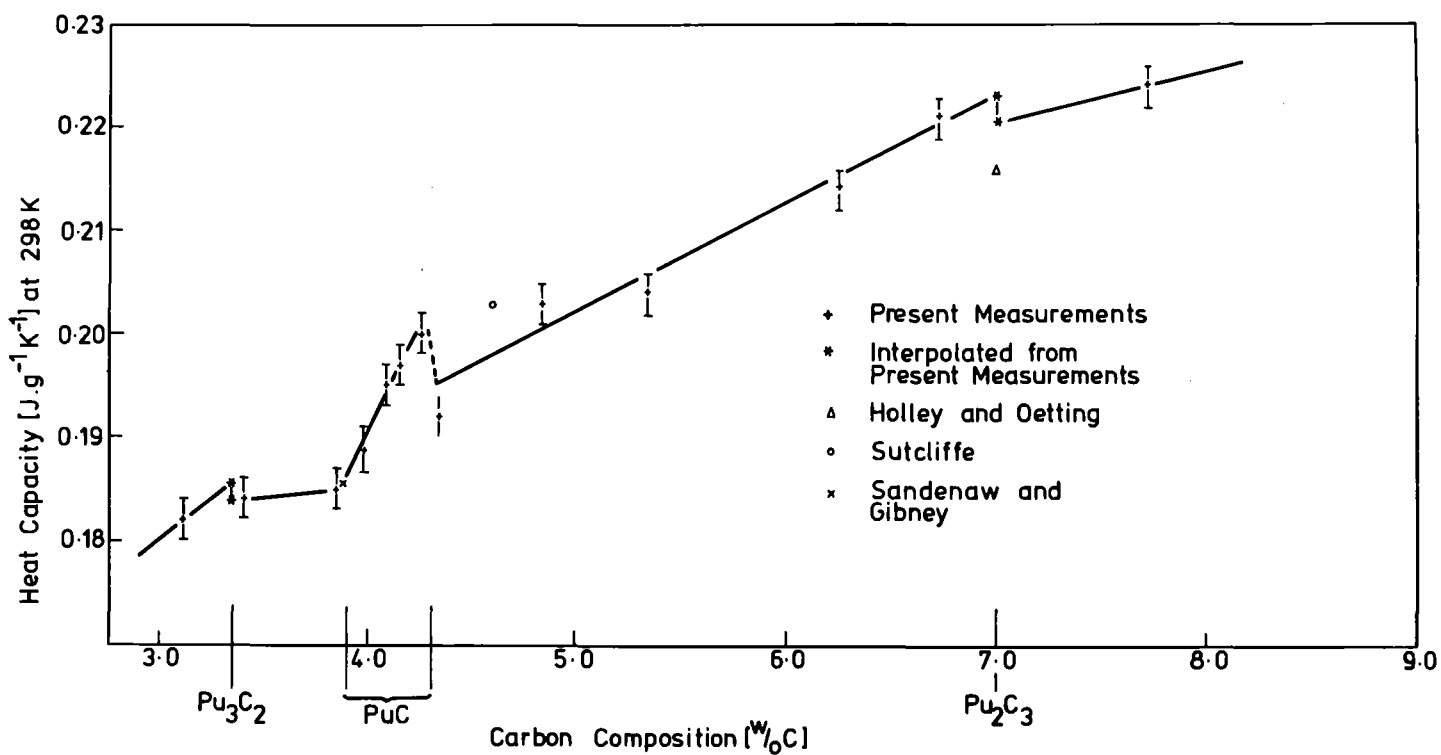


Figure 2 Heat capacities at room temperature ( $C_{p298}$ ) as a function of carbon content

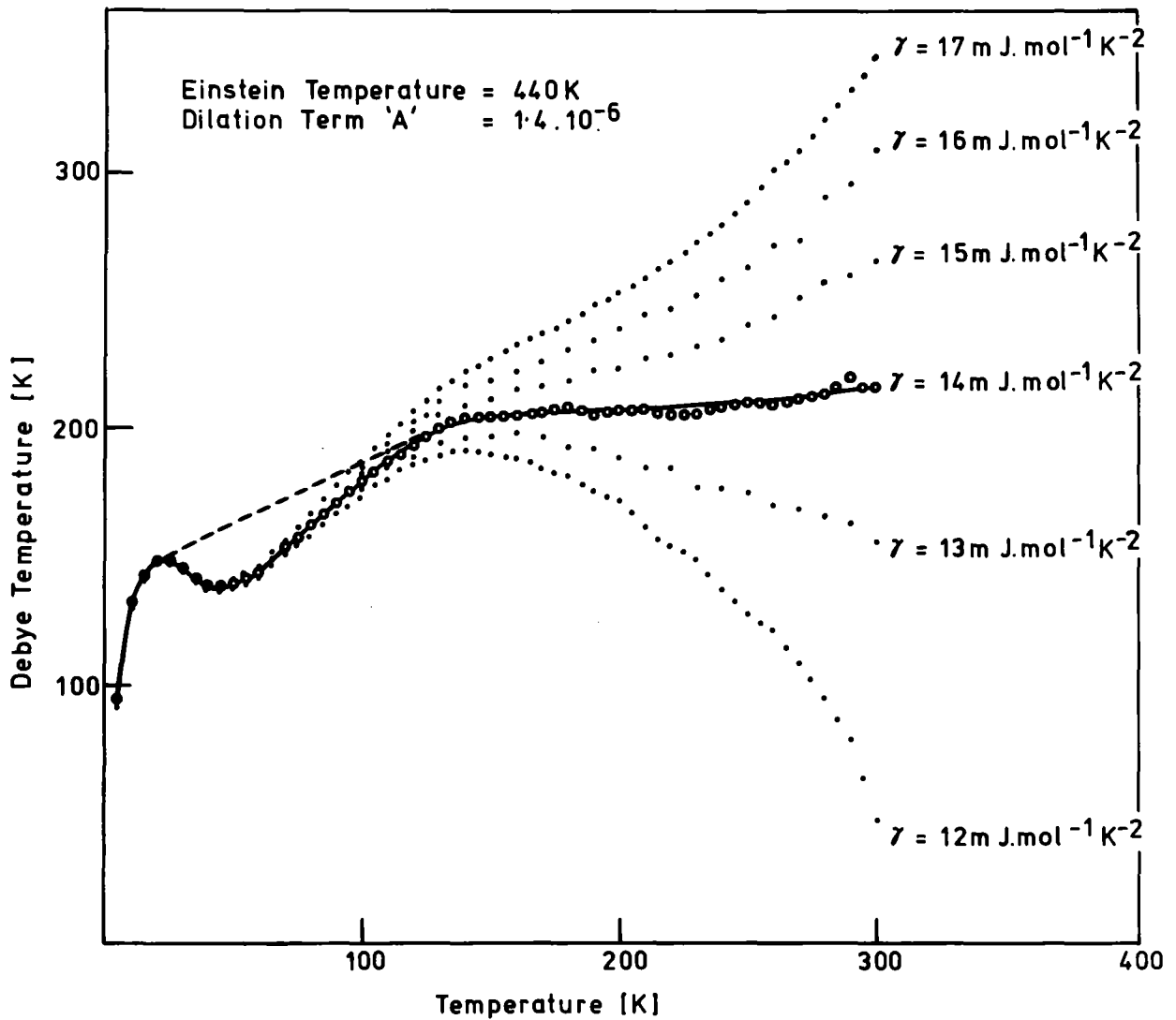


Figure 3 Derivation of the electronic heat capacity coefficient for  $\text{PuC}_{0.825}$

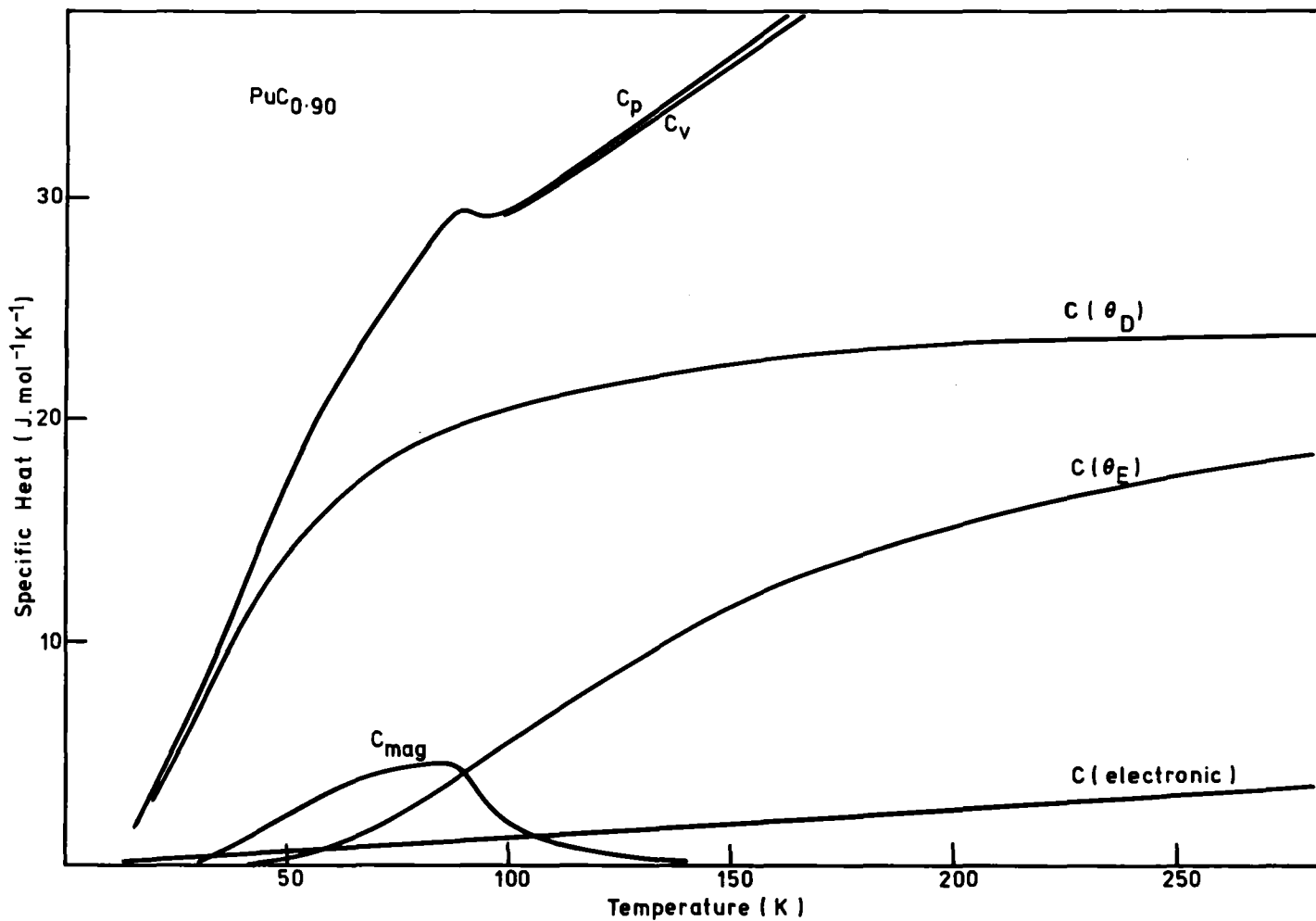


Figure 4 Separation of contributions to the heat capacity of  $\text{PuC}_{0.90}$

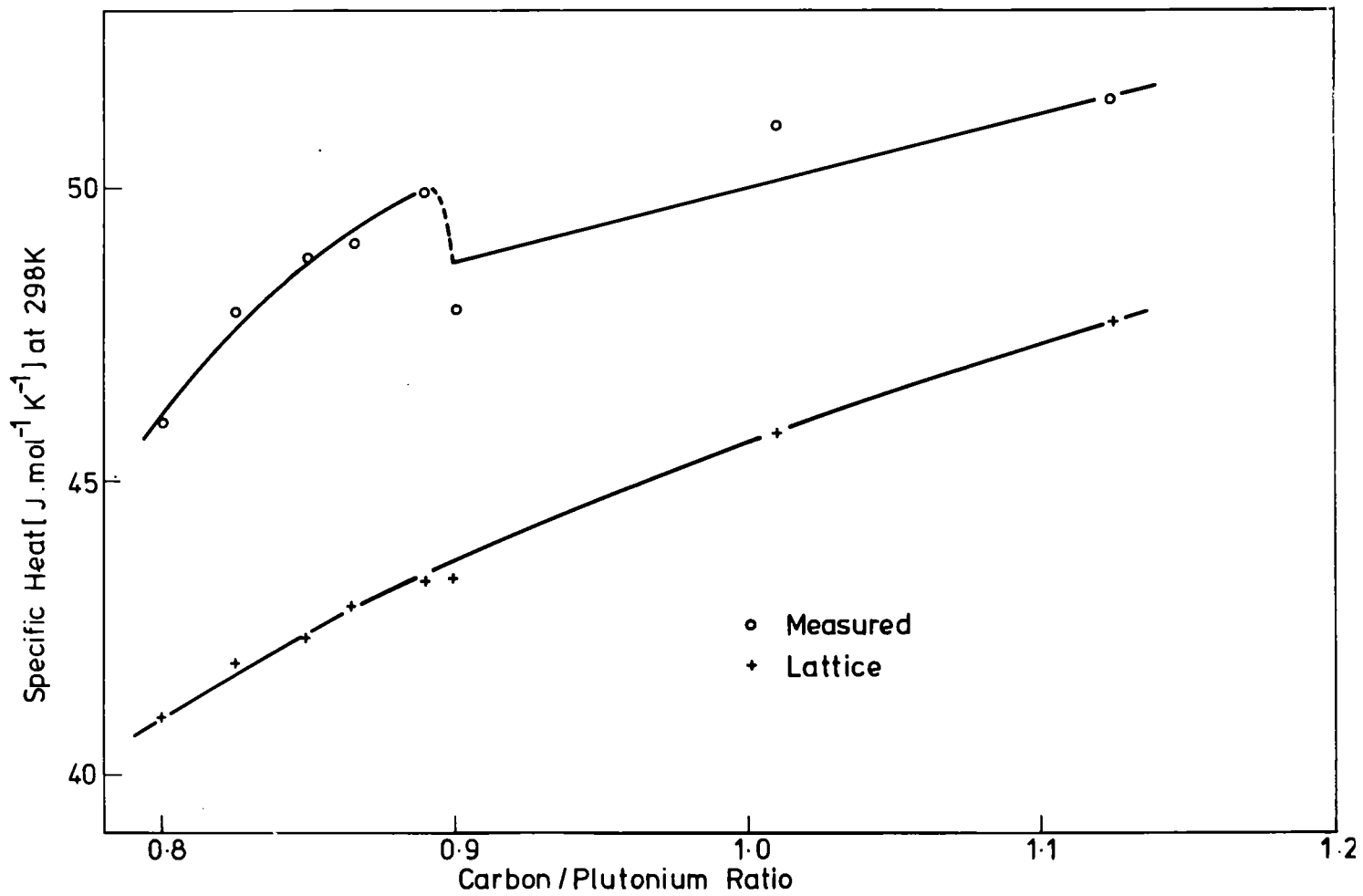


Figure 5 Comparison of measured heat capacity and calculated lattice heat capacity for  $\text{PuC}_x$

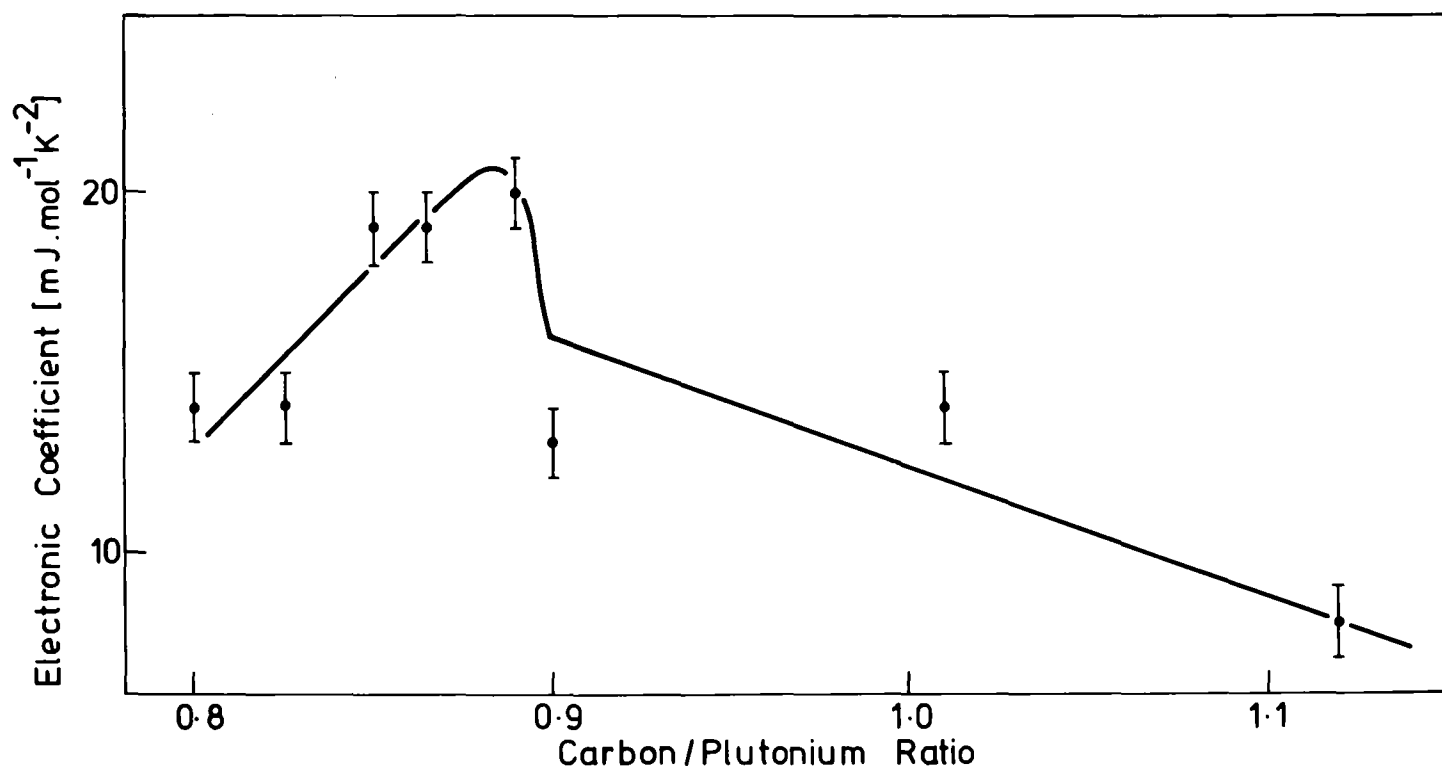


Figure 6 Electronic heat capacity coefficient for  $\text{PuC}_x$

REFERENCES

1. Green, J.L., Arnold, G.P., Leary, J.A. and Mereson, R.G. J.Nuc.Mat. 1970, 34, 281
2. Lallement, R., Costa, P. and Pascard, R. J.Phys.Chem.Solids 1965, 26, 1255
3. Lam, D.J., Nevitt, M.V., Ross, J.W. and Mitchell, A.W. Plutonium 1965 (A.G.Kay and M.B.Waldron eds.) Chapman and Hall, London, p.274.
4. Padel, A. and de Novion, Ch.J.Nuc.Mat.1969, 33, 40
5. Wedgwood, F.A. J.Phys.C. Solid State Physics 1974, 7, 3203.
6. Danan, J. J.Nuc.Mat. 1975, 57, 280
7. Danan, J., De Novion C. and Delaporte, A. Solid State Comm. 1972, 10, 775.

NEWS FROM THE URANIUM-SULFUR SYSTEM: ON THE SYNTHESIS AND THE MAGNETIC PROPERTIES OF THE URANIUM POLYSULFIDE  $U_2S_5$ .

---

Henri NOËL

Université de Rennes

Laboratoire de Chimie Minérale B, Associé au C.N.R.S. ( n°254 )

Avenue du General Leclerc. 35042 RENNES.

Uranium forms with sulfur a large variety of binary compounds, with sulfur to uranium ratio ranging from 1 to 3 <sup>(1)</sup>. The existence of a diuranium pentasulfide,  $U_2S_5$ , was mentioned only by one author <sup>(2)</sup> a decade ago, and little is known about this compound. We have precised the conditions of its existence and measured its magnetic susceptibility in the temperature range 4.2–300 K. Furthermore, the resolution of this new crystallographic type has been performed from single crystal X-ray diffraction studies of the isomorphous thorium polysulfide  $Th_2S_5$  <sup>(3)</sup>.

(1) R.M. DELL, "Comprehensive Inorganic Chemistry", 5 (1973) 319 (Pergamon Press).

(2) J.P. MARCON, Thesis, PARIS, 1969.

(3) H. NOËL, M. POTEL, to be published.

MAGNETIC PROPERTIES OF  $\text{NpAs}_2$ \*

M. Bogé, J. Chappert  
Centre d'Études Nucléaires,  
D.R.F./Laboratoire d'Interactions Hyperfines - Grenoble, France

A. Blaise, J.M. Fournier  
Centre d'Études Nucléaires,  
D.R.F./Section de Physique du Solide - Grenoble, France

D. Damien  
Département de Génie Radioactif - C.E.N./Fontenay-aux-Roses

J. Rebizant, J.C. Spirlet  
European Institute for Transuranien Elements,  
D-7500 Karlsruhe, Germany

Magnetic properties of  $\text{NpAs}_2$  were studied by susceptibility measurements a few years ago by J.M. Fournier et al. (1). These authors showed that this compound which crystallizes with the tetragonal structure, has interesting by complex magnetic properties. Below 22 K, it is ferromagnetic, and the susceptibility curve  $1/\chi(T)$  shows two minima between 22 and 180 K. On the other hand, the valence state was thought to be  $\text{Np}^{4+}$ .

We have used the Mössbauer technique on  $^{237}\text{Np}$  in order to investigate these magnetic properties. The 59.6 keV  $\gamma$ -ray was provided by source of metallic  $^{241}\text{Am}$  with an activity of 30 millicuries. At 4.2 K the measured isomer shift (9.5 mm/sec with respect to  $\text{NpO}_2$ ) conforms the  $4^+$  valence state ( $5f^3$  configuration). The magnetic hyperfine field is about 2 900 kG and the quadrupole interaction  $e^2qQ$  is about 24 mm/sec. The temperature dependence of these parameters between 4.2 K and 77 K will be discussed.

- (1) J.M. Fournier, A. Blaise and P. Salmon,  
Intern. Conf. on Magnetism, Moscow, vol. IV, p. 65 (1973).

\* Published at the International Conference on the Mössbauer Effect (Portoroz, 10-14 September 1979).

MAGNETIC SUSCEPTIBILITY OF PENTAVALENT URANIUM OXYHALIDES.

---

Jean-Claude LEVET, Henri NOËL

Université de Rennes

Laboratoire de Chimie Minérale B, Associé au C.N.R.S. (n°254)

Avenue du Général Leclerc. 35042 RENNES.

Pentavalent uranium compounds are potentially interesting, from spectroscopic and magnetic points of view, because of the  $5f^1$  electronic state of the uranium ion. We have prepared the following oxyhalides:  $UOCl_3$ ,  $UO_2Cl$ ,  $UOBr_3$ ,  $UO_2Br$  (1) and measured their magnetic susceptibility in the temperature range 4.2–300 K.

(1) J.C. LEVET, Thesis, RENNES, 1978.

EPR of Gd<sup>3+</sup> in actinide compounds.

G. Amoretti, D.C. Giori, V. Varacca

Istituto di Fisica dell'Università, Via D'Azeglio, 85

and

Groppo Nazionale di Struttura della Materia del CNR

43100 PARMA , Italy

The paramagnetic resonance study of S-state ions in host crystals has its main application in the determination of site symmetry and orientations, in the investigation of electronic and magnetic properties and in the study of phase transitions.

Although a detailed characterization of the crystal field acting on the impurity ions is usually possible in terms of spin-hamiltonian parameters, very little progress has been made in understanding the physical processes which govern the zero-field splittings of the ground state and account for the magnitude of these parameters. In this regard, it has been shown that a pure ionic model is inadequate to explain the experimental results and that a certain amount of covalency with the ligands, induced by spin-orbit coupling, must be considered<sup>(1)</sup>.

We are dealing principally with the determination of site symmetry and crystal field parameters for S-state ions in actinide compounds, such as oxides, oxisulfides, sulfides, selenides and so on. We have in mind a systematic study both of isoelectronic ions in the same crystal environment and of a particular ion on sites with the same pointgroup in different compounds. We hope that such a study, besides giving informations on the structural and electronic properties of the quoted compounds, can also contribute to a better understanding of the zero-field splitting mechanism.

We have started with the study of the EPR spectra of  $Gd^{3+}$  in  $ThOS$ <sup>(2)</sup>. The sample, a single crystal of thorium oxisulfide with about 10 p.p.m. of  $Gd^{3+}$  doping ions, was grown at the European Institute for Transuranium Elements, Euratom, Karlsruhe (BRD), with the method of chemical transport reaction using iodine as transporting agent<sup>(3)</sup>.

We have observed that the trivalent ion enters substitutionally and that the related charge compensation lies far enough to preserve the local symmetry. In fact, the angular variation of the spectra reproduce the tetragonal symmetry of the  $\text{Th}^{4+}$  crystal site (point group  $C_{4v}$ ).

The resonance field positions for the lines of the EPR spectra have been measured by means of a modified X-band 9E-line spectrometer<sup>(4)</sup>, so that a sensitivity better than 0.1 gauss for lines about 15 gauss wide was obtained. The measurement procedure was made easier by the fact that no hyperfine structure was observed.

The field positions for the static field  $H$  along the tetragonal  $z$  axis, for which the spectrum shows the maximum overall splitting, and along the  $x$  axis, that is the direction of maximum splitting in a plane perpendicular to  $z$ , have been fitted very accurately in order to determine the spin-hamiltonian parameters. This was performed by means of an iterative procedure on the third order perturbation expressions for the field positions. The values of the parameters obtained in this way were then used as starting values for a trial and error procedure, in which the energy matrix for the spin-hamiltonian was exactly diagonalized.

The final values of the parameters are shown in Tab. 1, while in Tab. 2 we report, for comparison, the experimental and calculated values of the fields (obtained with the parameters of Tab. 1) for the parallel and perpendicular spectra. The precision of the fitting, for both the chosen directions, is evident from Tab. 2, taking into account that the uncertainty on the values of the measured field positions can be estimated, considering all the possible error sources, about 0.4 gauss.

From Tab. 1 we observe that the  $g$ -factor is practically isotropic and its value is smaller than the calculated  $1.9928^{(1,5)}$ , showing the possible presence of a certain amount of covalency. This is also consistent with the relatively low absolute value of  $b_2^0$  (one of the smallest for tetragonal symmetry<sup>(6)</sup>).

At present, we are dealing with  $Gd^{3+}$  doped  $ThS_2$ , grown at the European Institute for Transuranium Elements in Karlsruhe. This case is particularly interesting and much more complicated than the preceding one. This fact gives us the opportunity to set up a general procedure to solve the problem of the determination of the spin hamiltonian parameters in the case of low symmetry and great zero-field splitting.

The preliminary X-band measurements of the resonance field positions, when the static field  $H$  lies in the crystallographic  $bc$  plane (Fig. 1), show that two magnetically nonequivalent sites are present in the unit cell. In fact, we have two families of curves, corresponding to the  $\Delta M = 1$  transitions. The curves of a family may be obtained from those of the other family by a reflection through the  $b$  or  $c$  axis, which are characterized by the coincidence of the spectra of the nonequivalent sites. This is consistent with the assumption that  $Gd^{3+}$  enters in the  $ThS_2$  lattice substitutionally for  $Th^{4+}$ , and moreover that the charge compensation does not affect the local symmetry.

The crystal structure of  $ThS_2$  is of the  $PbCl_2$  type<sup>(7)</sup>, so that the point symmetry is monoclinic  $C_s$ , with the  $bc$  plane as the reflection plane. If we choose the  $z$  and  $x$  axis in this plane and the  $y$  axis along the crystallographic  $a$  axis, the spin hamiltonian may be written as

Figure and Table captions

Fig. 1 - Angular dependence in the bc plane of the experimental resonance fields for the two magnetically unequivalent sites of  $Gd^{3+}$  in  $ThS_2$  .

Fig. 2 - Angular dependence in the bc plane of the experimental resonance fields for one of the two magnetically unequivalent sites of  $Gd^{3+}$  in  $ThS_2$  .

Tab. 1 - g values and crystal field parameters (in units of  $10^{-4} \text{ cm}^{-1}$ ) for  $Gd^{3+}$  in  $ThOS$ .

Tab. 2 - Fitting of the field positions (in gauss) of the lines, for the parallel and perpendicular spectra, obtained with the parameters of Tab. 1 .

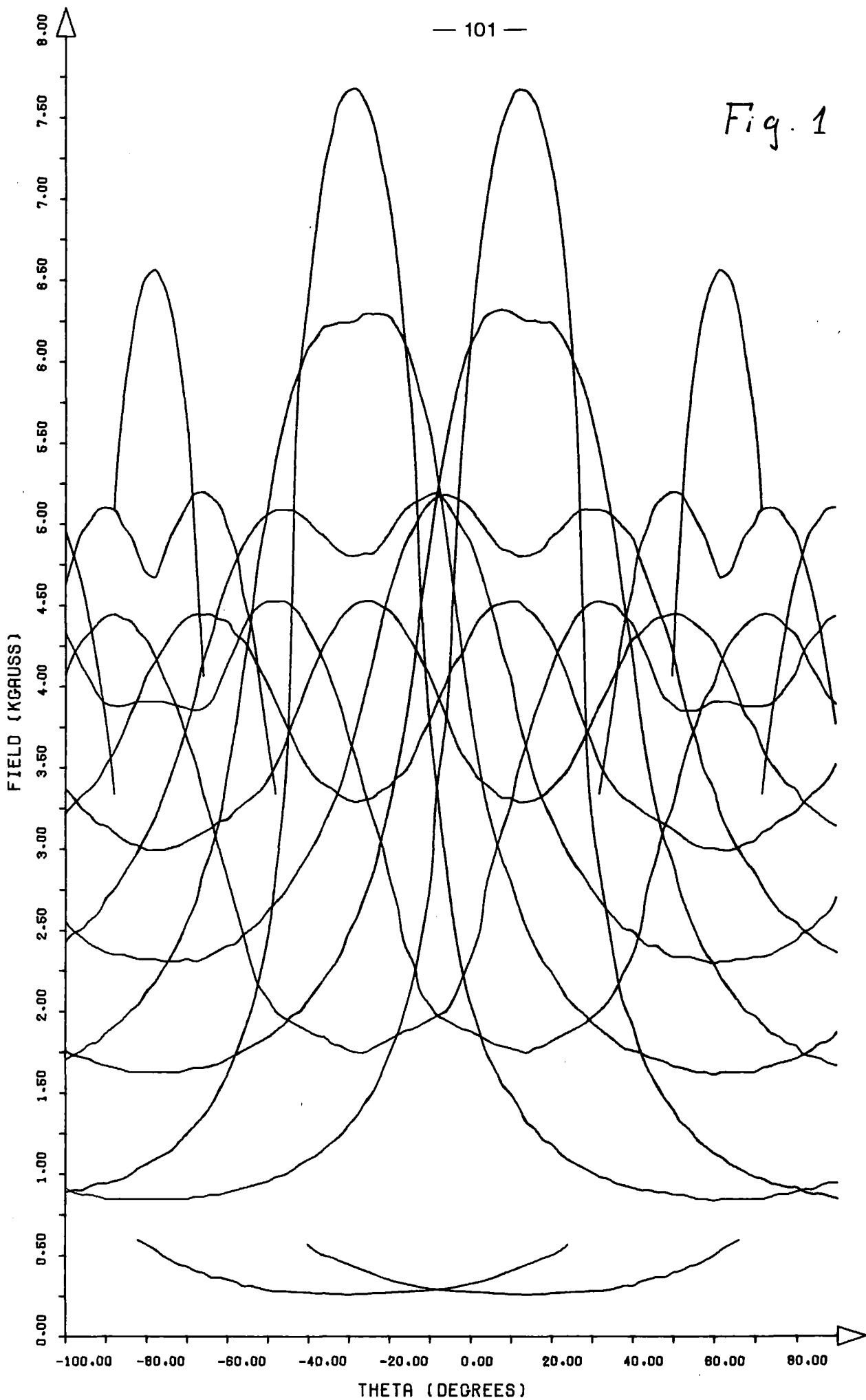
Tab. 1

$g_{  }$	$g_{\perp}$	$b_2^0$	$b_4^0$	$b_6^0$	$b_4^4$	$b_6^4$
1.9915+0.0003	1.9911+0.0003	-183.33+0.02	1.704+0.006	-0.591+0.008	28.30+0.05	-4.76+0.13

Tab. 2

H // z		H // z	
$H_{exp.}$	$H_{calc.}$	$H_{exp.}$	$H_{calc.}$
2076.1	2076.7	2588.0	2587.9
2428.2	2428.6	2890.8	2890.4
2801.4	2801.2	3040.9	3040.5
3227.1	3226.5	3171.3	3171.0
3652.0	3651.8	3336.1	3336.3
4024.7	4024.8	3560.3	3560.8
4376.8	4377.0	3941.5	3942.1

Fig. 1



$$\mathcal{H} = \mu_B (g_x H_x S_x + g_y H_y S_y + g_z H_z S_z) + \sum_{\substack{l=2 \\ \text{even}}}^6 \sum_{m=0}^l B_l^m O_l^m ,$$

if we assume, on account of the small  $\underline{g}$  anisotropy, that its principal axes coincides with those of the fine structure. The number of parameters to be determined is then very high (fifteen crystal field parameters and three  $g$  values).

It may be noted from Fig. 2, where a single family of curves in the  $bc$  plane is presented, that the maximum splitting is much greater than in the case of  $\text{ThOS}$  and about twice the maximum splitting for  $\text{Gd}^{3+}$  or  $\text{Eu}^{2+}$  in compounds with the same structure of  $\text{ThS}_2$  (8,9,10). In this situation the fine structure term in the hamiltonian becomes of the same order of magnitude of the Zeeman term (in the X-band) and perturbation theory fails, so that computer diagonalization methods must be extensively used (11,12).

We are dealing with this problem, in order to obtain a general method to fit the angular variation of the resonance fields.

At the same time, we are performing accurate measurements of the field positions, with the direction of  $\underline{H}$  varying in the three crystallographic principal planes, in order to test the consistency of the model.

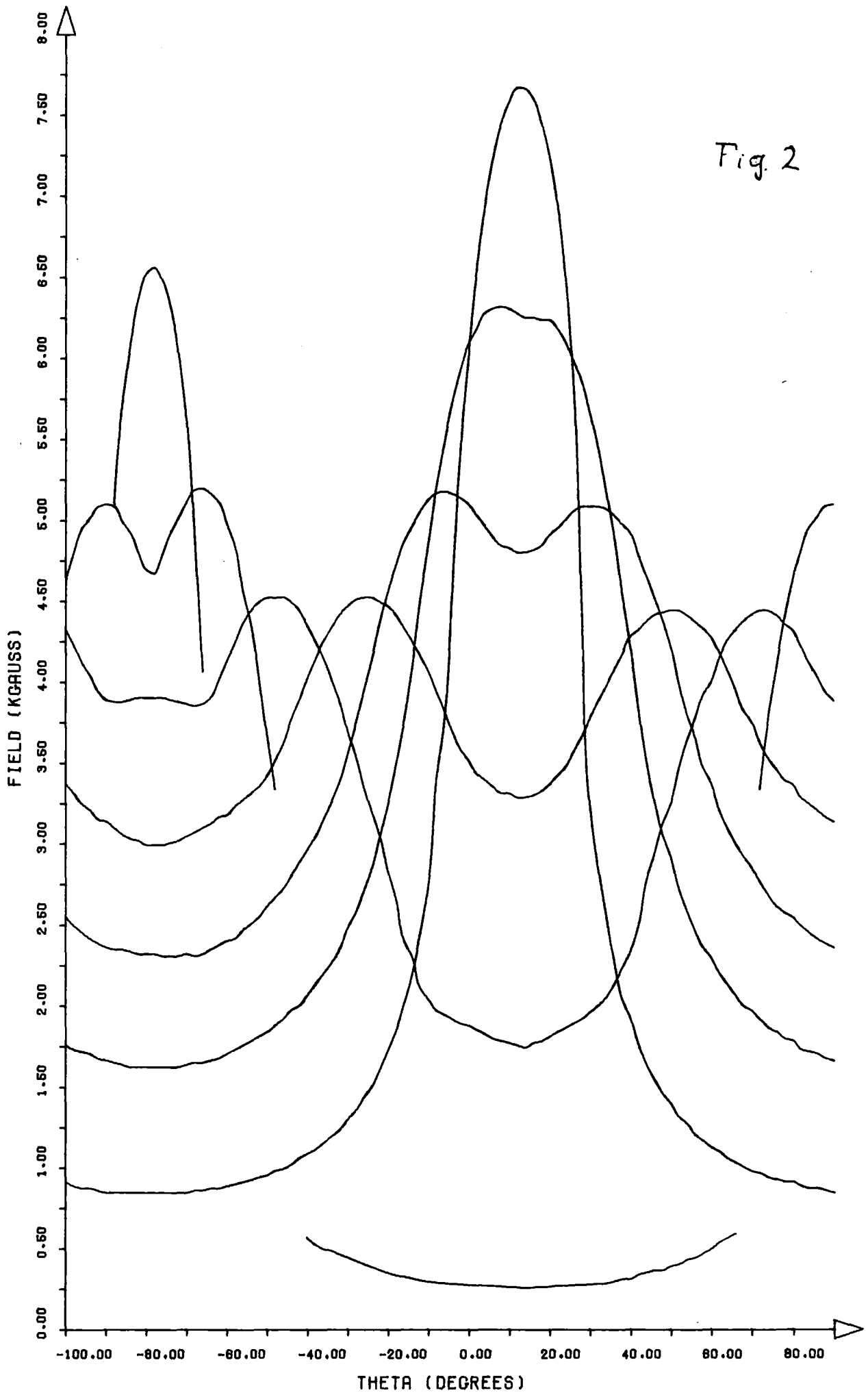


Fig. 2

References

- 1) D.J.Newman, W.Urban, Advances in Phys. 24, 793 (1975).
- 2) G.Amoretti, D.C.Giori, V.Varacca and J.C.Spirlet, J.Rebizant, Phys. Rev. B, in press.
- 3) J.C.Spirlet, III Int. Conf. on Electr. Struct. of Actinides, Grenoble (1978), J. de Physique, in press.
- 4) D.C.Giori,U.Pozzi, G.Ruggeri, to be published.
- 5) B.G.Wybourne, Phys. Rev. 148, 317 (1966).
- 6) H.A.Buckmaster, Y.H.Shing, phys. stat. sol.(a) 12, 325 (1972).
- 7) W.H.Zachariasen, Acta Cryst. 2, 291 (1949).
- 8) Q.H.F.Vrehen, J.Volger, Physica 31, 845 (1965).
- 9) H.C.W.Beijerinck, B. Willemsen, Physica 47, 515 (1970).
- 10) B. Willemsen, W.C.Hommels, phys. stat. sol.(a) 10, 183 (1972).
- 11) S.K.Misra, G.R.Sharp, J. Magn. Res. 23, 191 (1976).
- 12) S.K.Misra, J. Magn. Res. 23, 403 (1976).

Classification  
 Physics Abstracts  
 61.12

## Neutron diffraction study of $^{243}\text{AmO}_2$

A. Bœuf (\*), J. M. Fournier (\*\*), J. F. Gueugnon (\*\*\*), L. Manes (\*\*\*),  
 J. Rebizant (\*\*\*), and F. Rustichelli (\*)

(\*) Commission of the European Communities, Joint Research Centre, Ispra Establishment,  
 Physics Division Group at Institut Laue-Langevin, Grenoble, France

(\*\*) DRF/PHS, C.E.N., Grenoble, France

(\*\*\*) Commission of the European Communities, Joint Research Centre, Karlsruhe Establishment,  
 Postfach 2266, D-7500 Karlsruhe, R.F.A.

(Reçu le 20 avril 1979, accepté le 30 mai 1979)

**Résumé.** — L'oxyde d'américium  $\text{AmO}_2$  a été étudié par diffraction neutronique à différentes températures afin de vérifier l'apparition d'une phase antiferromagnétique en dessous de 8,5 K que des mesures de susceptibilité magnétique avaient prévue. Aucun ordre antiferromagnétique n'a été observé en accord avec des expériences Mössbauer. De plus, la longueur de Fermi de l'américium et les facteurs de température de l'américium et de l'oxygène ont été déterminés.

**Abstract.** — The actinide compound  $\text{AmO}_2$  was studied by neutron diffraction at different temperatures in order to check the occurrence of antiferromagnetism below 8.5 K as predicted by magnetic susceptibility measurements. No antiferromagnetic order was observed in agreement with Mössbauer results. Furthermore, the coherent neutron scattering length of Am and the Debye-Waller factors for Am and O were determined.

1. **Introduction.** — Actinide dioxides ( $\text{AnO}_2$  with  $\text{An} \equiv \text{Th, Pa, U, Np, Am, Cm}$ ) form an interesting family characterized by the filling of the well localized 5f levels.  $\text{UO}_2$  undergoes an antiferromagnetic transition at 31 K associated with a distortion of the oxygen sublattice [1].  $\text{NpO}_2$  undergoes a cooperative transition at 25 K observed by specific heat [2] and magnetic susceptibility [3] measurements. However, no magnetic moment has so far been detected by neutron diffraction [4, 5] (upper limit  $0.5 \mu_B$ ). A moment of only  $0.01 \mu_B$  can be associated with the magnetic hyperfine field observed by Mössbauer effect measurement [6]. In the case of  $\text{AmO}_2$ , an antiferromagnetic transition was reported to occur at 8.5 K on the basis of susceptibility measurements [7] whereas no magnetic hyperfine field was detected by the Mössbauer effect [8]. In this paper we present the results of our investigation of this transition by neutron scattering measurements. Furthermore, the coherent neutron scattering length and the temperature factors for Am and O were obtained. The high radioactivity of the sample (150 rem/h at 1 cm) made the experiment particularly delicate.

2. **Experimental details.** — The purified  $^{243}\text{AmO}_2$  [9] was refired at 900 °C under oxygen atmosphere. The isotopic composition of the actinide was 99.80 %  $^{243}\text{Am}$ , 0.20 %  $^{241}\text{Am}$  and trace amounts of Cm. Spark source mass spectrometry examination revealed the following impurities : 1 000 ppm Al, 300 ppm Cr, 700 ppm Cu, 300 ppm Fe, < 50 ppm Mn, 300 ppm Ni, < 100 ppm P, < 100 ppm Pb,  $\lesssim$  600 ppm Zn, 1 000 ppm  $^{244}\text{Cm}$ .

The sample weighed 730 mg. Due to the high radioactivity and to the contamination hazard the sample was loaded into a double wall aluminium container welded by electron beam. Inside the first wall the sample was kept under helium atmosphere to insure a good thermal contact with the container (the self-heating of the sample was 5 mW). The cryostat used for the experiment was modified to allow detection of  $\alpha$ -radiation during the experiment. The measurements were done at different temperatures, 293 K, 20 K and 6.5 K. Due to the self-heating 6.5 K was the lowest obtainable temperature. It was reached by pumping on the helium bath (helium temperature 1.5 K). The radiation level was 2 rem/h ( $\gamma$ ) and 6 mrem/h (neutrons) at the outer wall of the

sample container. It dropped to 500 mrem/h ( $\gamma$ ) at the outer wall of the cryostat.

Powder neutron diffraction data were obtained on the D2 diffractometer of the High Flux Reactor of the Institut Laue-Langevin (Grenoble). The neutron wavelength was 1.22 Å. The runs were done with 60' collimation in pile, 60' collimation between the monochromator and the sample and 10' collimation between the sample and the counter.

3. Results. — 3.1 LOW TEMPERATURE TRANSITION.

— In order to investigate the possible existence of an antiferromagnetic transition at 8.5 K [7] neutron diffraction patterns were recorded at both a higher temperature (20 K) and at a lower temperature (6.5 K). No variations were detected, within experimental uncertainties, in the neutron diffraction patterns at the two temperatures. In particular, figure 1 shows the low angle region of the neutron diffraction patterns where the (100) and (110) magnetic reflections should be observed at 6.5 K in the case of a type I antiferromagnetic ordering. Assuming this kind of magnetic ordering an upper limit of the ordered moment ( $\mu_{ord}$ ) can be obtained by comparing the minimum detectable (100) peak intensity  $I_{min}$  to the (111) peak intensity  $I_{(111)}$ . By taking  $I_{min}$  equal to the statistical error, as is usually done, one obtains  $I_{min}/I_{(111)} = 1/200$  corresponding to  $\mu_{ord} = 0.3 \mu_B$ . However, we believe it is more realistic to take a value four times higher for  $I_{min}$  which corresponds to  $\mu_{ord} = 0.6 \mu_B$ .

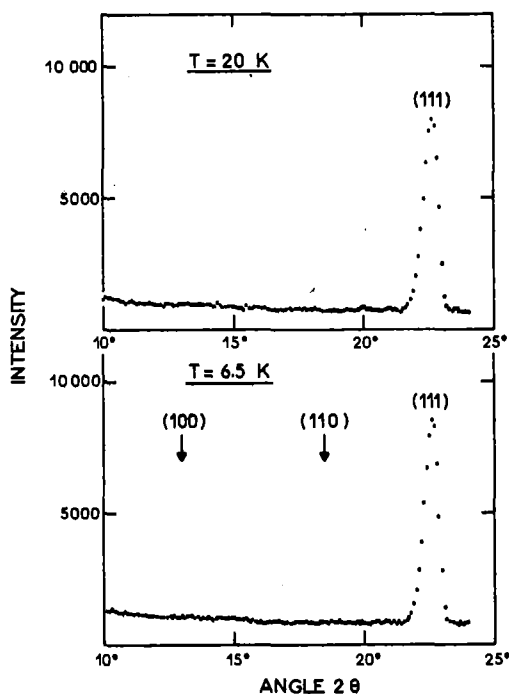


Fig. 1. — Low angle neutron diffraction patterns of AmO<sub>2</sub> at temperature higher and lower than at 8.5 K at which antiferromagnetic ordering is supposed to occur.

3.2 NEUTRON COHERENT SCATTERING LENGTH AND TEMPERATURE FACTORS. — The neutron coherent scattering length of americium has only been determined once previously by Mueller *et al.* [10]. They found  $b_{Am} = 0.76(1) \times 10^{-12}$  cm and temperature factors

$$B_{Am} = 0.79(6) \text{ \AA}^2 \quad \text{and} \quad B_O = 1.65(13) \text{ \AA}^2.$$

However, it is not clear from the publication if the temperature factors refer to 80 K or room temperature.

Our neutron diffraction data at 293 K, 20 K and 6.5 K were refined using a Busing-Levy Least Square Structure Factor Program in order to obtain  $b_{Am}$ ,  $B_{Am}$  and  $B_O$  at the three temperatures. The results are shown in table I. In addition, a value for the lattice parameter equal to  $5.380 \text{ \AA} \pm 0.002 \text{ \AA}$  at room temperature was obtained in agreement with previous values [10]. No temperature variation of this quantity was observed within the experimental errors. Table II presents the observed and calculated neutron intensity for the different Bragg reflections at one temperature, namely 20 K. The neutron coherent scattering length of oxygen was assumed to be  $b_O = 0.580 \times 10^{-12}$  cm [11]. An absorption correction was applied to the observed intensities. The agreement between the observed and calculated intensities is expressed by the weighted residual  $R$  which takes the values  $R=1.5\%$  at 293 K,  $R=0.5\%$  at 20 K and  $R=1\%$  at 6.5 K.

The coherent neutron scattering length,

$$b_{Am} = 0.83(3) \times 10^{-12} \text{ cm},$$

was obtained assuming that the oxide was stoichiometric, i.e. O/Am ratio of 2. In fact, while a ratio

Table I. — Coherent neutron scattering lengths and temperature factors of AmO<sub>2</sub>.

Temperature	$b \times 10^{12}$ (cm)	$B_{Am}$ (Å <sup>2</sup> )	$B_O$ (Å <sup>2</sup> )
293 K	$0.83 \pm 0.04$	$0.64 \pm 0.38$	$0.56 \pm 0.27$
20 K	$0.83 \pm 0.02$	$0.59 \pm 0.17$	$0.42 \pm 0.10$
6.5 K	$0.83 \pm 0.02$	$0.50 \pm 0.17$	$0.49 \pm 0.13$

Table II. — Observed and calculated intensities of AmO<sub>2</sub> Bragg reflections.

$hkl$	$I_{obs}$	$I_{calc}$
111	50 877	51 960
200	4 744	5 173
220	165 161	164 219
311	41 635	42 160
400	42 637	42 995
422	103 163	102 203
333,511	20 097	20 089

greater than 2 cannot be obtained with americium, a two phase region has been reported where the O/Am ratio is reduced slightly below 2 [12]. No extra peak was detected either by X-ray or neutron diffraction in our sample. This excludes the presence of a second phase within the detection limit. Moreover, the scattering length was also calculated by using only the odd Bragg peaks which have contribution from Am only and hence are independent of oxygen concentration. The scale factor used in this calculation was the same as that determined previously, thus  $b_{\text{Am}}$  is again scaled by  $b_{\text{O}}$ . The obtained value

$$b_{\text{Am}} = 0.835(30) \times 10^{-12} \text{ cm}$$

shows that deviation from stoichiometry is less than 0.5% and has negligible influence on the given coherent scattering length.

**4. Discussion.** — The neutron investigation of the low temperature magnetic transition on  $\text{AmO}_2$  shows that no antiferromagnetic order occurs below 8.5 K within the experimental limits indicated above. This confirms the results obtained by Mössbauer measurements. As a consequence of our results and according to the susceptibility measurements [7] which are unfortunately the only evidence up to now for a cooperative transition at 8.5 K, the transition in  $\text{AmO}_2$  is apparently very similar to the transition in  $\text{NpO}_2$ .

It has been found in  $\text{UO}_2$  that a distortion of the oxygen sublattice is associated with a first order magnetic transition [1]. In the case of  $\text{NpO}_2$  and  $\text{AmO}_2$  where no magnetic ordering is found, the transition might be only due to a lattice distortion associated with a cooperative Jahn-Teller transition.

At this point it is useful to recall the crystal field 5f ground states of the actinide dioxides.

$\text{UO}_2$	: $\Gamma_5$ (triplet)	[1]
$\text{NpO}_2$	: $\Gamma_8$ (quadruplet)	[13]
$\text{PuO}_2$	: $\Gamma_1$ (singlet)	[13]
$\text{AmO}_2$	: $\Gamma_7$ (doublet)	[7]
$\text{CmO}_2$	: $\Gamma_1$ (singlet)	[13].

In  $\text{PuO}_2$  and  $\text{CmO}_2$ , no transition is expected and in fact, none is found [14, 15]. In  $\text{UO}_2$  the transition is magnetic and crystallographic. In  $\text{NpO}_2$ , the transition is apparently only crystallographic (there could be a magnetic ordering at very low temperature). In  $\text{AmO}_2$ , if the degeneracy of the  $\Gamma_7$  doublet is lifted no magnetic ordering can occur (the first excited level  $\Gamma_8$  is about  $35 \text{ cm}^{-1}$  above the ground state [7]). Since  $\text{NpO}_2$  and  $\text{AmO}_2$  keep the fluorite structure, the only possible lattice distortion is the distortion of the oxygen sublattice, as in the case of  $\text{UO}_2$ . A single crystal diffraction study of  $\text{NpO}_2$  is underway to try to detect such a distortion. A similar study would be very interesting in the case of  $\text{AmO}_2$  as well as a confirmation of the 8.5 K transition.

The value of the coherent scattering length of  $^{243}\text{Am}$ ,  $b_{\text{Am}} = 0.83(2) \times 10^{-12} \text{ cm}$  is slightly higher than the value found by Mueller *et al.* [9] but nevertheless the difference is less than 10%. The temperature factors presented in this paper are  $B_{\text{Am}} = 0.64$  and  $B_{\text{O}} = 0.56$  at 293 K; they are much lower than the values given in ref. [9] ( $B_{\text{Am}} = 0.79$ ;  $B_{\text{O}} = 1.65$ ) and are comparable with values obtained for other actinide dioxides.

Neutron coherent scattering lengths of actinides have been determined up to curium, we thought it useful to collect them in table III.

Table III. — Coherent neutron scattering lengths of some actinides.

Isotope	$b(\times 10^{12})$ cm <sup>(1)</sup>	Reference
$^{232}\text{Th}$	1.000 (9)	WILLIS, B. T. M., <i>Proc. R. Soc. (London) A</i> <b>274</b> (1963) 122
$^{231}\text{Pa}$	1.3 (2)	WEDGWOOD, F. A., BURLET, P., unpublished (1973) from $\text{PaO}_2$
	0.91 (3)	WEDGWOOD, F. A., BURLET, P., unpublished (1973) from $\text{PaC}$
$^{235}\text{U}$	0.98 (6)	WILLIS, B. T. M., <i>Proc. R. Soc. (London) A</i> <b>274</b> (1963) 122
$^{238}\text{U}$	0.855 (6)	WILLIS, B. T. M., <i>Proc. R. Soc. (London) A</i> <b>274</b> (1963) 122
$^{237}\text{Np}$	1.05 (1)	HEATON, L., MUELLER, M. H., WILLIAMS, J. M., <i>J. Phys. Chem. Solids</i> <b>28</b> (1967) 1651
	1.054 (15)	COX, D. E., FRAZER, B. C., <i>J. Phys. Chem. Solids</i> <b>28</b> (1967) 1649
$^{240}\text{Pu}$	0.35 (1)	LANDER, G. H., MUELLER, M. H., <i>Acta Crystallogr.</i> <b>B</b> <b>27</b> (1971) 2284
$^{242}\text{Pu}$	0.81 (1)	LANDER, G. H., MUELLER, M. H., <i>Acta Crystallogr.</i> <b>B</b> <b>27</b> (1971) 2284
$^{243}\text{Am}$	0.76 (1)	MUELLER, M. H., LANDER, G. H., REDDY, J. F., <i>Acta Crystallogr.</i> <b>A</b> <b>30</b> (1974) 667
	0.83 (2)	This paper
$^{244}\text{Cm}$	0.95 (3)	FOURNIER, J. M., BLAISE, A., MUELLER, W., SPIRLET, J. C., <i>Physica</i> <b>86-88B</b> (1977) 30

(1) With the assumption that  $b_{\text{O}} = 0.580 \times 10^{-12} \text{ cm}$ .

**Acknowledgments.**— It is a pleasure to thank Mr. R. Chagnon for valuable technical assistance and M. G. Lelan and R. Mathieu and all the radio-protection service of the Institut Laue-Langevin for active cooperation in solving the problems connected with the high radioactivity of the sample.

#### References

- [1] FABER, J., LANDER, G. H., COOPER, B. R., *Phys. Rev. Lett.* **25** (1975) 1770.
- [2] WESTRUM, E. F., HATCHER, J. B., OSBORNE, D. W., *J. Chem. Phys.* **21** (1953) 419.
- [3] ROSS, J. W., LAM, D. J., *J. Appl. Phys.* **38** (1967) 1451.
- [4] HEATON, L., MUELLER, M. H., WILLIAMS, J. M., *J. Phys. Chem. Solids* **28** (1967) 1651.
- [5] COX, D. E., FRAZER, B. C., *J. Phys. Chem. Solids* **28** (1967) 1649.
- [6] DUNLAP, B. D., KALVIUS, G. M., LAM, D. J. and BRODSKY, M. B., *J. Phys. Chem. Solids* **29** (1968) 1365.
- [7] KARRAKER, D. G., *J. Chem. Phys.* **63** (1975) 3174.
- [8] FRIEDT, J. M., POINSOT, R., REBIZANT, J., to be published.
- [9] BUIJS, K., MAINO, F., MUELLER, W., REUL, J., TOUSSAINT, J. C., *J. Inorg. Nucl. Chem. Suppl.* (1976) 209.
- [10] MUELLER, M. H., LANDER, G. H., REDDY, J. F., *Acta Crystallogr. A* **30** (1974) 667.
- [11] BACON, G. E., *Acta Crystallogr. A* **28** (1972) 357.
- [12] CHIKALINA, I. D., EYRING, L., *J. Inorg. Nucl. Chem.* **30** (1968) 133.
- [13] CHAN, S. K., LAM, D. J., *The actinide electronic structure and related properties*, edited by A. J. Freeman, J. B. Darby (Academic Press) **1** (1974).
- [14] RAPHAEL, G., LALLEMENT, R., *Solid State Commun.* **6** (1968) 383.
- [15] FOURNIER, J. M., BLAISE, A., MULLER, W., SPIRLET, J. L., *Physica* **86-88B** (1977) 30.

E.S.C.A. STUDY OF URANIUM (IV) HALIDES

Elisabeth THIBAUT, Jean-Pol BOUTIQUE, Jacques VERBIST  
Facultés Universitaires Notre-Dame de la Paix  
Laboratoire de Spectroscopie Electronique  
Rue de Bruxelles, 61, 5000-Namur (Belgique)

and

Henri NOËL, Jean-Claude LEVET  
Université de Rennes  
Laboratoire de Chimie Minérale B,  
associé au C.N.R.S. (n°254)  
Avenue du Général Leclerc, F-35042-Rennes (France)

During the recent years, we have been interested in the characterization by E.S.C.A. of uranium ions in different oxidation states, and bound to different anions : oxygen, sulfur, nitrogen and phosphorous (1-2-3). Here, we report some recent results obtained on the tetravalent uranium halides  $UF_4$ ,  $UCl_4$ ,  $UBr_4$ .

It is well known that most of these compounds are very sensitive to atmospheric oxygen and/or water, so that drastic conditions must be observed during their synthesis and handling. In spite of the use of a dry nitrogen-conditioned glove box, we still met severe difficulties in obtaining non-contaminated samples.  $UCl_4$  and  $UBr_4$  are particularly hygroscopic ; however, thanks to many precautions, their spectra are little affected by the oxygen contribution.

The experimental data were obtained on a HP 5950 A spectrometer, using mono-chromatized  $AlK_{\alpha}$  radiation ( $h\nu = 1486.7$  eV). They have been calibrated by the gold decoration technique ( $Au 4f_{7/2} = 83.8$  eV), ensuring a common zero for our binding energy scales.

Different characteristics of the E.S.C.A. spectra are relevant to the electronic structure studies :

- a) Core levels , where we can examine the influence of the electronegativity of the anions on the  $U4f$  binding energy chemical shifts, knowing here that uranium is in a constant formal oxidation state.

The spectra (Fig. 1) show clearly that the binding energy increases as the electronegativity of the anion rises. This indicates that the charge separation increases as we go from bromine to chlorine to fluorine. Consequently, the cation core electrons are more tightly bound in the last case (table 1).

- b) The shake-up satellites which are observed on the high binding energy side of the core level peaks (fig.1) correspond to a valence excitation simultaneous to U4f photoemission.

Here, we can examine the influence of the anion on two values ; firstly, the satellite-to-mean peak separation and secondary, their intensity ratio.

In table 2, we note that the peak separation increases with the electronegativity of the anion, but the shake-up probability is reduced in the more ionic compound.

We will come back on the interpretation of these electronic excitations.

- c) The valence levels

Fig.2 shows that the whole valence spectrum shifts to the left (i.e. to higher binding energies) for more ionic compounds.

But the most relevant detail is a significant decrease in intensity of the sharp U5f peak (A, close to the Fermi level) for less ionic compounds (table 3). Simultaneously, it becomes closer to the U-X band, going through the  $UF_4$ - $UCl_4$ - $UBr_4$  series.

We suggest the following explanation ; in tetravalent uranium compounds, there are formally two non-bonding 5 f electrons. These are only in fact localized (peak A), the remainder being mixed with the 6d and 7s orbitals to build the band of the U-X bond (B). This happens the more as the electronegativity of the anion is lower meaning that the compound becomes more covalent.

Indeed, if we replace fluorine by chlorine, the 5f electrons becomes less tightly bound, but take a larger part in the bond, thereby minimizing the system's total energy.

Let us come back to the shake-up satellites, to identify which valence levels are concerned in this electronic jump :

By comparison, with a detailed study on  $UO_2^{(4)}$ , the starting level of the transition should be in the U-X band (B). The electrons should be excited, obeying the monopole selection rule , in the  $U5f_{7/2}$  level just above the

Fermi level.

There is one more relation, between the position of the U-X band (B) and the relative satellite position. The deeper the band below Fermi level, the farther is the satellite from mean peak.

This is of course only a first interpretation, which should be verified by considering additional possibilities ; but this requires detailed theoretical models or other types of experimental data (such as luminescence).

A last encouraging point is the first successful study of clean  $\text{UBr}_4$ . For the first time, a very hygroscopic sample was found without any contamination, it was a platelet-like single crystal.

It is interesting to compare the results obtained with and without the unwanted oxygen, and to evaluate the consequences of contamination.

For this purpose, we will focus on a highly sensitive spectra detail , i.e. the valence levels.

These provide a direct view of the levels involved in the bond. They are quite different (fig.3): the U5f peak is not resolved from the U-X band in clean  $\text{UBr}_4$ , in spite of better resolution (see other peaks). This observation is consistent with that reported for the  $\text{UX}_4$  series.

On the other hand, the levels located in the 10-20 eV region are better separated (Br4s and  $\text{U}6p_{3/2}$  levels).

This is a first approach to the nature of the bond in the  $\text{UX}_4$  series (X = F, Cl, Br). Deeper studies of the U-X band, considering the atomic orbital cross sections will be the next step forward in the more general understanding of the bond character in uranium compounds.

Table 1 : core levels binding energies (eV) in some halides and oxides of uranium.

Compound	U4f <sub>5/2</sub> Binding Energy (eV)	U4f <sub>7/2</sub> Binding Energy (eV)	Pauling E.N. of the Halogen	% ionic character of the U-X band (Pauling)(X=halogen)
UF <sub>4</sub>	392.8	382.0	4.0	73
UCl <sub>4</sub>	390.9	380.0	3.0	34
UBr <sub>4</sub>	390.7	379.7	2.8	26
UO <sub>2</sub>	390.4	379.6		
UO <sub>3</sub>	391.4	380.7		

Table 2 : description of the shake-up satellites of the U4f core levels in UF<sub>4</sub>, UCl<sub>4</sub>, UBr<sub>4</sub>.

Compound	Satellite-to-main peak separation (eV)	$\frac{\text{Satellite intensity}}{\text{U4f}_{7/2} \text{ intensity}}$
UF <sub>4</sub>	7.3	0.14
UCl <sub>4</sub>	6.1	0.26
UBr <sub>4</sub>	5.5	0.67

Table 3 : description of the U5f level and the U-X band (X=F,Cl,Br) in UX<sub>4</sub> compounds.

	UF <sub>4</sub>	UCl <sub>4</sub>	UBr <sub>4</sub>
$\frac{I(\text{U5f})}{I(\text{U6p}_{3/2})}$	1.42	1.10	0.87
$\Delta E$ U-X band to U5f(eV)	4.2	2.8	2.3

Table 4 : description of the U5f level and the U-X band of contaminated and clean UBr<sub>4</sub>.

	Contaminated UBr <sub>4</sub>	Clean UBr <sub>4</sub>
$\frac{I(\text{U5f})}{I(\text{U6p}_{3/2})}$	0.87	0.79
$\Delta E$ U-X band to U5f (eV)	2.3	1.9

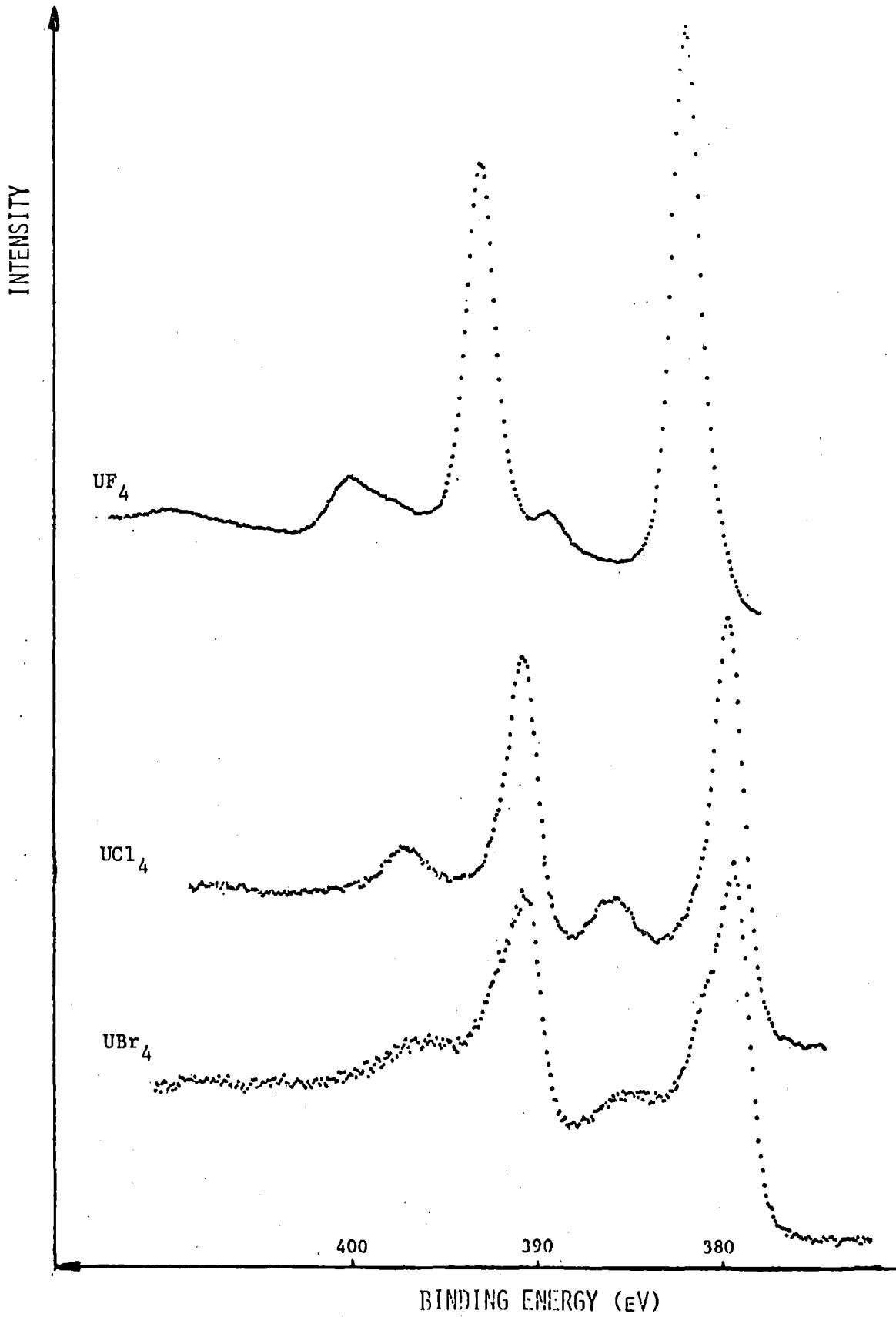


Fig.1 E.S.C.A. spectra of the U4f core levels and their shake-up satellites in UF<sub>4</sub>, UCl<sub>4</sub>, UBr<sub>4</sub>.

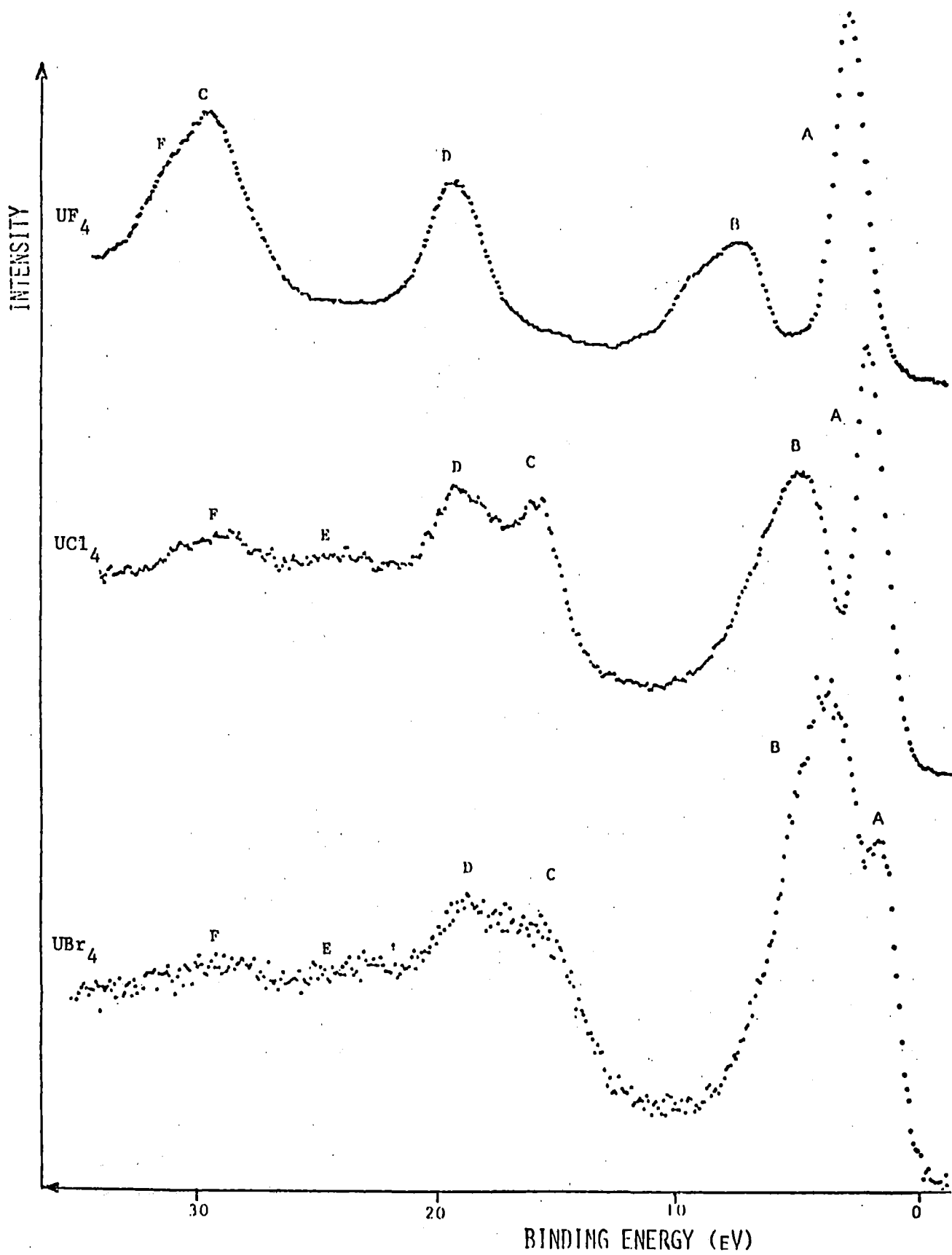


Fig.2 E.S.C.A. spectra of the valence levels in  $UF_4$ ,  $UCl_4$ ,  $UBr_4$ .

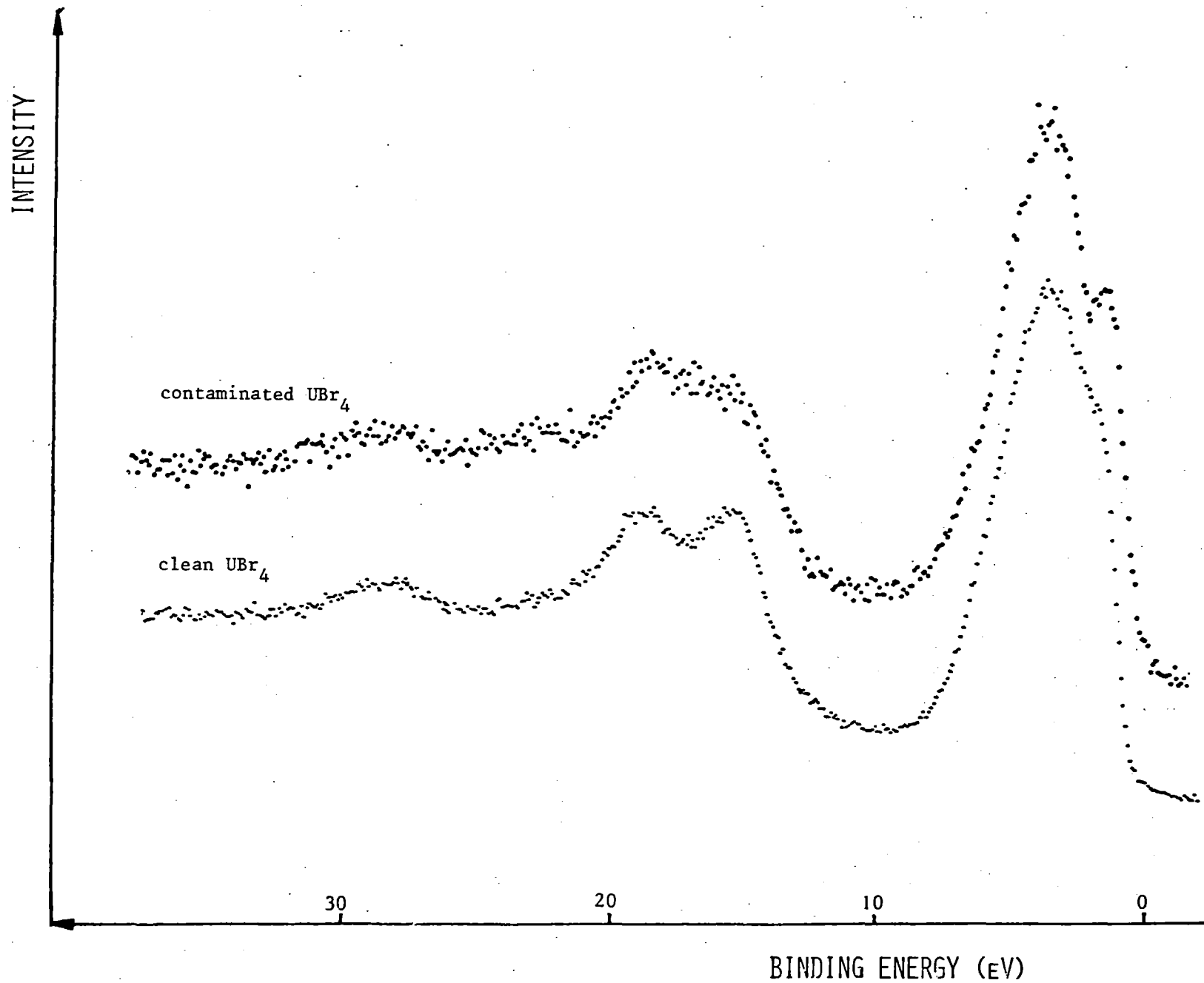


Fig.3 E.S.C.A. spectra of the valence levels in contaminated and clean UBr<sub>4</sub>.

REFERENCES

- (1) J.J. Verbist, J. Riga, C. Tenret-Noël, J.J. Pireaux, G. D'Ursel, R. Caudano, E.G. Derouane, in *Plutonium 1975 and other actinides*, eds. H. Blank and R. Lindner (North-Holland, Amsterdam, 1976) p. 409.
- (2) E. Thibaut, J.J. Pireaux, J. Riga, C. Tenret-Noël, R. Caudano, E.G. Derouane, J. Verbist, *Proc. 2nd. Int. Conf. Electr. Struct. Actinides*, Wroclaw, Poland, 1976. Eds. J. Mulak, W. Suski, R. Troc, (Ossolineum, Wroclaw, 1977) p. 139.
- (3) E. Thibaut, J. Verbist, R. Troc, *J. Physique C4* (1979) 77.
- (4) J.J. Pireaux, J. Riga, C. Tenret-Noel, E. Thibaut, R. Caudano, J. Verbist, *Chem. Phys.*, 22 (1977) 113.

Surface Studies by Photoemission of the Laves Phases  $UAl_2$  and  $UCo_2$ <sup>x)</sup>

J.R. Naegele, L. Manes and N. Nolte

Commission of the European Communities  
Joint Research Centre  
Karlsruhe Establishment  
European Institute for Transuranium Elements  
Postfach 2266  
D-7500 Karlsruhe  
Federal Republic of Germany

and

J.M. Fournier

Centre d'Etudes Nucléaires de Grenoble  
DRF-PHS  
85X  
38041 Grenoble Cédex  
France

Abstract

Photoemission studies on Laves phases  $UAl_2$  and  $UCo_2$  have been performed. Different in-situ surface preparation techniques like scraping, sputtering and annealing have been used showing that sputtering changes essentially the surface composition of  $UAl_2$ ; the same effect, but not as pronounced is found for  $UCo_2$ . Annealing restores the initial composition but induced a strong increase of oxygen surface contamination even under UHV-conditions. Scraping in combination with sputtering has proven to be the best surface cleaning procedure. The influence of oxygen surface contamination has been investigated by examining U, Al, Co, O and C core levels (XPS) and the valence band region (UPS). For  $UAl_2$  the U4f doublet shows for clean scraped material a satellite doublet which is interpreted in terms of a shake-up process. The UPS valence spectra show a superimposition of a spectrum which is very similar to  $UO_2$  spectra and the bulk intermetallic spectrum. An energy shift of the oxide spectrum is explained by the type of electronic conduction of the basis material. The electronic structure is discussed.

## 1. Introduction

Photoemission measurements of intermetallic actinide compounds have not been performed up to now although the electronic properties of these compounds are known to be peculiar /1/. More recently these compounds have received considerable attention as catalysts and media for hydrogen storage /2/.

Among the intermetallic actinide compounds  $UA1_2$  and  $UCo_2$  have been chosen since they belong to the Laves phases which crystallize in the simple cubic  $MgCu_2$ -type structure.  $UA1_2$  has been considered to be representative of a spin fluctuation system /3,4/ for which a narrow 5f band is expected at the Fermi level. A narrow 5f state pinned at  $E_F$  and overlapping a broad conduction band is also an essential condition for valence fluctuations /5/. The actinide-actinide separation for  $UA1_2$  and  $UCo_2$  is 3.38 and 3.04 Å, respectively, and thus below the 3.4 Å proposed by Hill /6/ as a cut-off for localization of 5f electrons.

Originally, we undertook photoemission measurements to elucidate further the density of states and electronic structure of  $UA1_2$  and  $UCo_2$ . Due to the small information depth for photoemission measurements and the very easy oxidation of  $UA1_2$  and  $UCo_2$  a more detailed investigation of the surface became necessary.

## 2. Experimental

The  $UA1_2$  sample was prepared by induction heating of the formula amount of the pure metals (99.999 % pure Al, 99.99 % pure U) under an argon atmosphere. A thin slide of the sample was glued onto a copper sample holder by a silver filled conductive epoxy resin.

The  $\text{UCo}_2$  sample was prepared by electron beam heating of the formula amount of the pure metals (99.999 % pure Co, 99.9 % pure U) under high vacuum conditions ( $10^{-5}$  Pa). The sample was fixed by Ta wires together with an underlying Ta sheet onto a high temperature sample rod which allowed temperatures as high as 2000 K to be achieved by electron heating. Before introduction into the spectrometer the samples were transferred to a dry argon glove box attached to the spectrometer. The samples were ground to remove the gross surface oxide layer and then immediately introduced into the spectrometer.

The photoemission spectra were obtained with a Leybold spectrometer using a nonmonochromatized aluminium X-ray source (XPS) and a windowless UV helium discharge source (UPS) with a resolution of 1.1 and 0.15 eV, respectively, as determined by the width of the Fermi edge of gold. The vacuum in the measuring chamber was  $5.5 \cdot 10^{-9}$  Pa which dropped to  $6.5 \cdot 10^{-8}$  Pa due to helium leakage during UPS work ; a residual gas analysis indicated that no ingress of other gases occurred.

$\text{UAl}_2$  was cleaned in-situ in the preparation chamber of the spectrometer ( base pressure  $8 \cdot 10^{-8}$  Pa) by argon ion sputtering and in the measuring chamber by scraping with an  $\text{Al}_2\text{O}_3$  file.  $\text{UCo}_2$  was cleaned in-situ by argon ion sputtering, too, and annealing.

### 3. Results

$\text{UAl}_2$  and  $\text{UCo}_2$  core level spectra have been recorded for differently prepared surfaces. The surface cleanness was controlled by recording the oxygen and carbon 1s core levels. Fig. 1 shows the variation of the oxygen and carbon surface contamination with the sputter time for  $\text{UAl}_2$ . Carbon is easily removed whereas the removal of surface oxide needs up to two days. The increase of the O1s signal at the beginning of sputtering is explained by the removal of the carbon contamination from the surface oxide.

Sputtering is known to change the surface composition of compounds . As shown in Fig. 1 this effect is extremely pronounced for  $UAl_2$ . As calculated from the ratio of peak areas below the U4f and Al 2s levels the 8.8 times lighter aluminium is very preferentially sputtered ; a saturation is found at an aluminium content less than 1/3 of that found for scraped  $UAl_2$ .

Since in  $UCo_2$  the mass ratio  $m_U/m_{Co}$  is reduced to about 3.9 the preferential sputtering is not as pronounced. For long sputtering the cobalt content saturates at about 1/2 of that found for  $UCo$  the stoichiometry of which has been restored by annealing. Unfortunately, annealing induced a serious increase of the oxygen signal even under UHV-conditions. Therefore, it can be assumed that by annealing bulk oxygen introduced during the  $UCo_2$  preparation diffuses from the bulk to the surface.

Fig. 2 shows the U4f signals for different oxygen surface contamination. Oxygen induced satellites are found on the high binding energy side at 392.2 and 381.4 eV for  $UAl_2$  and at 391.2 and 380.3 eV for  $UCo_2$ . For  $UO_2$  the U4f levels are found at binding energies of 390.5 and 379.6 eV /7/. Assuming that uranium is (as in  $UO_2$ ) in a tetravalent state in oxidized  $UAl_2$  and  $UCo_2$ , the shift of 1.7 and 0.7 eV to higher binding energies for  $UAl_2$  and  $UCo_2$ , respectively, can be explained by the p-type electronic conduction. This implies that the Fermi level is shifted from about the middle of the forbidden band gap downwards towards the highest occupied levels (U5f levels for  $UO_2$ ). Similar effects have been observed by Veal and Lam /8/. The metallic states are found at 388.3 eV and 377.5eV for  $UAl_2$  and 388.8 and 378.0 eV for  $UCo_2$ . For uranium metal binding energies of about 388.0 and 377.0 eV have been reported /7/. At the time a clear identification of the valence state of uranium in  $UAl_2$  and  $UCo_2$  was not possible.

Fig. 2 shows the typical asymmetric U4f doublet for sputtered oxygen free  $UAl_2$  (curve c). Scraping induces on the high binding energy side a satellite doublet shifted by about 7eV. Generally, this is due to plasmon excitations, a fluctuating valence state and shake-up excitations. Since no higher satellites have been observed an explanation in terms of plasmon excitations seems unlikely. A valence fluctuation seems also unlikely because one would have to assume a fluctuation of the uranium atom between a valence found in a metal (clearly less than 4) and a valence larger than that for tetravalent uranium in  $UO_2$ . Valence is normally found to change from one state to the next higher state /9/. Apart from the fact that XPS studies with higher energy resolution than reported here are necessary, the shake-up process involving the low lying aluminium 3s valence band is favoured to explain the satellite structure.

Fig. 3 shows the UPS data for different oxygen surface contamination. The oxygen contamination is indicated by a strong peak at 6eV ; a very close similarity to the  $UO_2$  spectrum is found /10/. A shift similar to that found for the core levels is also found here, as determined from the U5f levels at 2.8 and 1.7 eV for  $UAl_2$  and  $UCo_2$  respectively. The removal of surface oxide removes the overlapping  $UO_x$  spectrum and increases dramatically the emission intensity at the Fermi level. Fig. 4 shows the high surface sensitivity of  $UAl_2$  as measured with HeII excitation. Each run lasted only 3 minutes ; 45 minutes while under a base pressure of about  $6 \cdot 10^{-9}$  Pa results in a considerable increase in the oxygen induced signals. A difference spectrum between curves b and c of Fig. 4 is shown in Fig.5. The charge transfer of electrons at  $E_F$  to the oxygen band at 6 eV is clearly indicated.

A comparison of UPS-data for  $UAl_2$  and  $UCo_2$  recorded for different excitation energies is presented in Fig. 6.

For He I excitation  $UAl_2$  shows at about 7.5 eV a structure which is missing for higher excitation energies and also missing in  $UCo_2$ . Taking into account cross section effects [11]

and photoemission data on aluminium /12/, this peak is explained by emission from Al 3s states. A very high density of states is found at  $E_F$  increasing with excitation energy. That clearly implies a rather narrow U5f band as proposed as an explanation of the physical properties of  $UA1_2$  /3,4/. The shoulder at about 2eV is due to overlapping U 6d, 7s and Al 3s bands.

$UCo_2$  shows a quite different behaviour. The occupied valence states are only extended by about 5 eV. A pronounced peak is found at 0.8 eV for He I excitation. This peak decreases with increasing excitation energy whereas a very narrow peak develops at  $E_F$ . Considering the additional Co 3d electrons, cross section effects /11/ and photoemission data on cobalt /13/, the 3d electrons are identified in a relative narrow band at 0.8 eV. The peak at  $E_F$  is due to U5f states the occupation of which is smaller compared with those in  $UA1_2$ .

#### 4. Conclusions

Argon ion sputter cleaning changes significantly the surface composition of  $UA1_2$ ; the aluminium content is decreased to about 1/3 of its stoichiometric value. The preferential sputtering of Co is not as pronounced.

Sputtering in combination with scraping gave clean and stoichiometric  $UA1_2$  surfaces; annealing of clean sputtered  $UCo_2$  restored the stoichiometric composition but enhanced considerably the surface oxide contamination.

U4f core level photoemission spectra of oxidized  $UA1_2$  and  $UCo_2$  showed a shift to higher binding energies in comparison to  $UO_2$  due to p-type electronic conduction in  $UO_2$ . Satellites which appear for clean scraped  $UA1_2$  are explained by a shake-up process from Al 3s states to empty conduction band states.

Valence spectra (UPS) for oxidized surfaces of  $UAl_2$  and  $UCo_2$  revealed similar shifts to those found for the U4f core level spectra (XPS).

The U5f states were found as narrow bands at the Fermi level. Co 3d electrons were found at 0.8 eV. The emission at 7.5 eV for  $UAl_2$  was only seen for He I-excitation and is believed to be due to Al 3s states.

---

x) This text has been presented at the Symposium on Applied Surface Analysis, Dayton (Ohio, USA), June 13 - 15, 1979; it will appear in a Special Issue of: Applications of Surface Science.

### Figure Captions

Fig. 1 Variation of the surface composition of  $UAl_2$  with sputter time ; above : oxygen and carbon 1s photoemission signals ; below : uranium / aluminium ratio.

Fig. 2 U4f photoemission signals (XPS)

$UAl_2$  : a) immediately after sample introduction  
b), c) after sputtering 25 minutes (01s signal reduced to 62 %) and 40 hours (01s signal not detectable), respectively.  
d) scraped (01s signal not detectable).

$UCo_2$  : a) immediately after sample introduction  
b) after annealing 30 minutes at 800 K (01s signal reduced to 58 %)  
c) after sputtering 40 hours (01s signal not detectable).

Fig. 3 Valence band photoemission signals (UPS ; He I-excitation : 21.2 eV, He II-excitation : 40.8 eV).

$UAl_2$  : a) immediately after sample introduction  
b) sputtered (01s signal reduced to 20 %)  
c) sputtered (01s signal not detectable)  
d) scraped (01s signal not detectable)

$UCo_2$  : a) immediately after sample introduction  
b) after annealing 30 minutes at 800 K (01s signal reduced to 58 %)  
c) sputtered (01s signal not detectable)

Fig. 4 Time dependent valence band photoemission signals of  $UAl_2$  (UPS ; He II-excitation 40.8 eV).

a) immediately after scraping for 10 minutes  
b), c), d) 45 minutes, 1.5 and 16 h after scraping, respectively.

Fig. 5  $UAl_2$  valence band photoemission difference spectrum of curves b and c of Fig. 4.

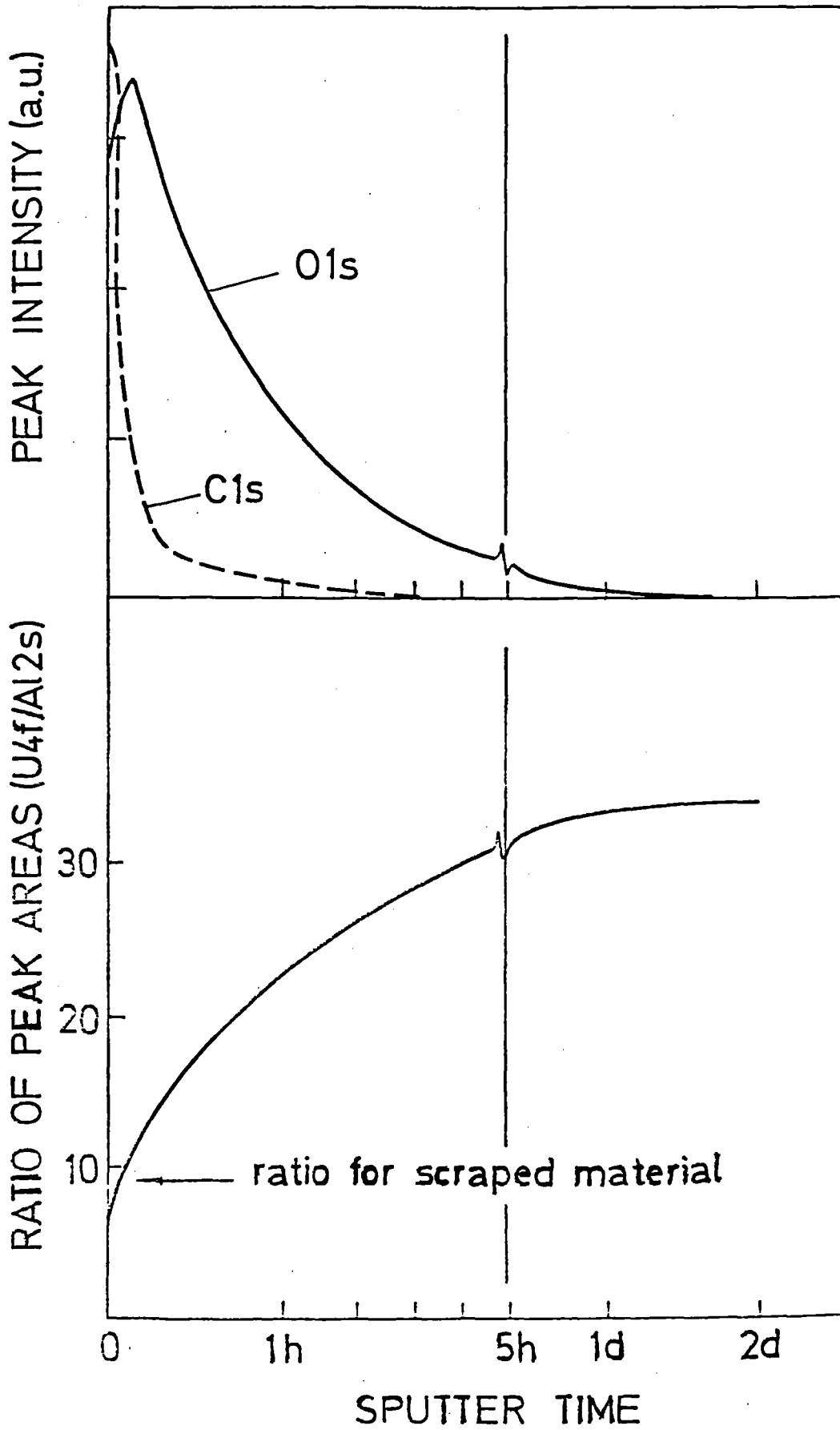
Fig. 6 Valence photoemission signals of  $UAl_2$  and  $UCo_2$  (sputtered, 01s signal not detectable)

a) He I-excitation : 21.2 eV

b) He II $_{\alpha}$  -excitation : 40.8 eV

c) He II $_{\beta}$  -excitation : 48.4 eV.

Fig. 1



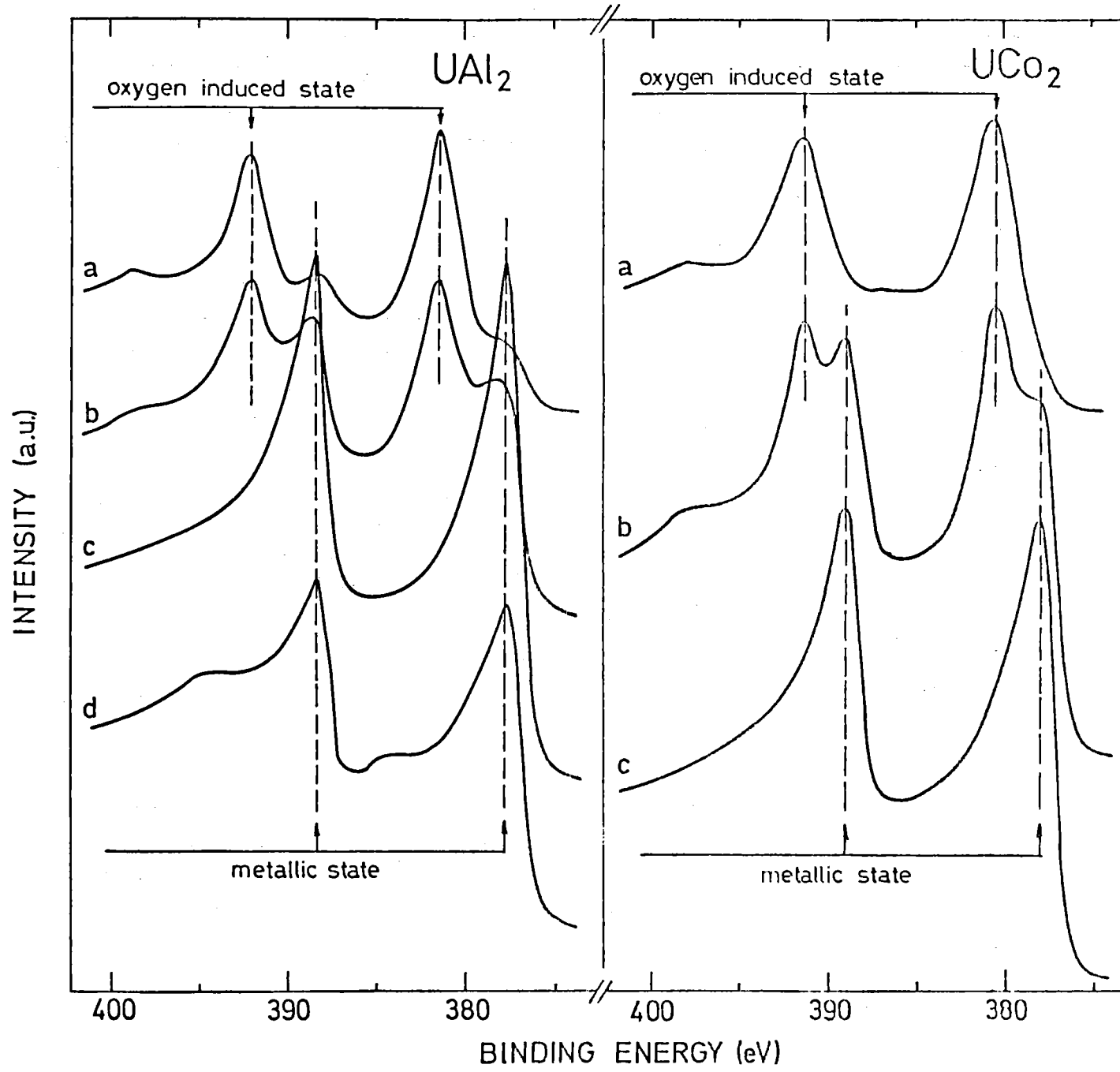


Fig. 2

Fig.3

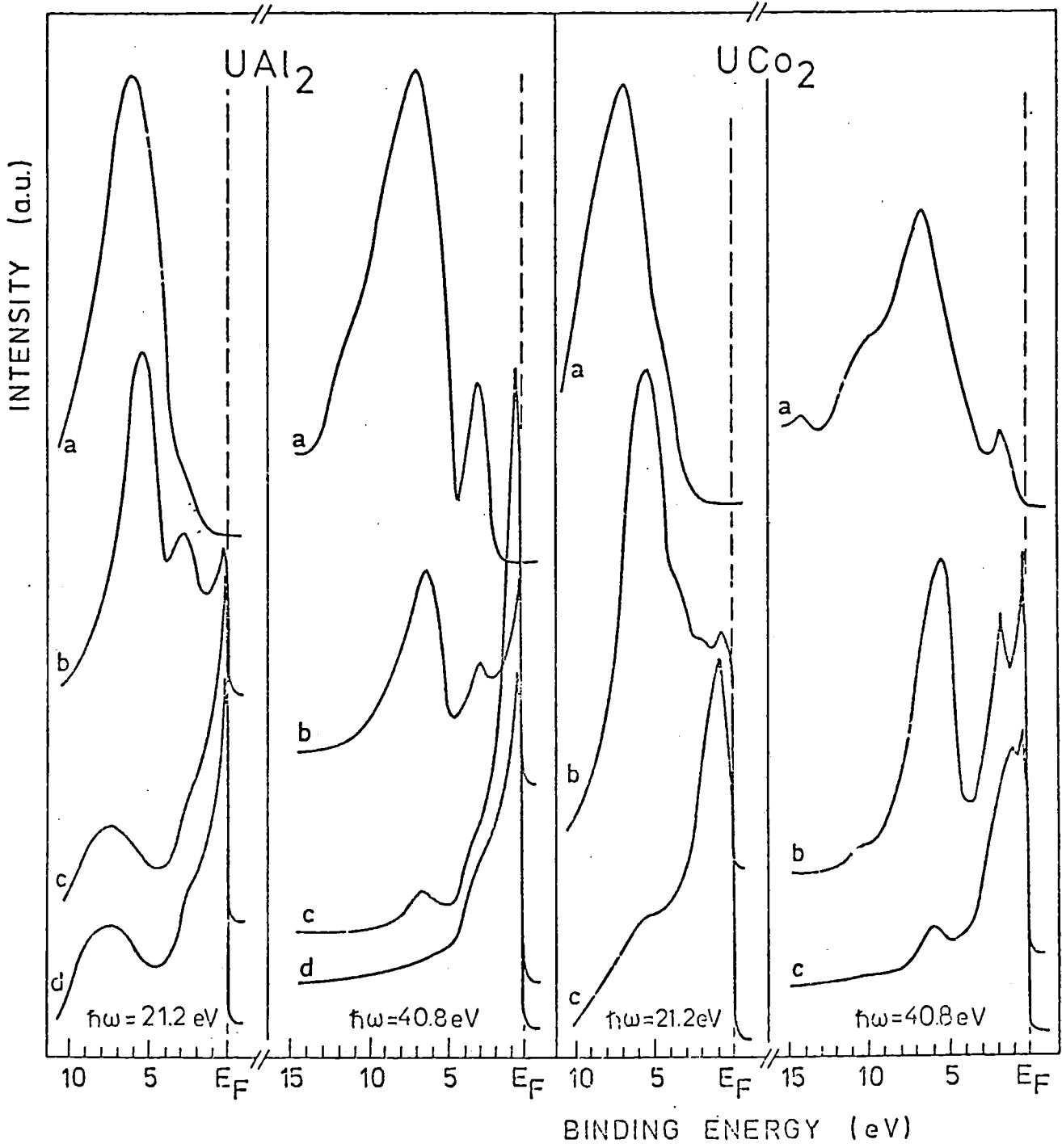


Fig.4

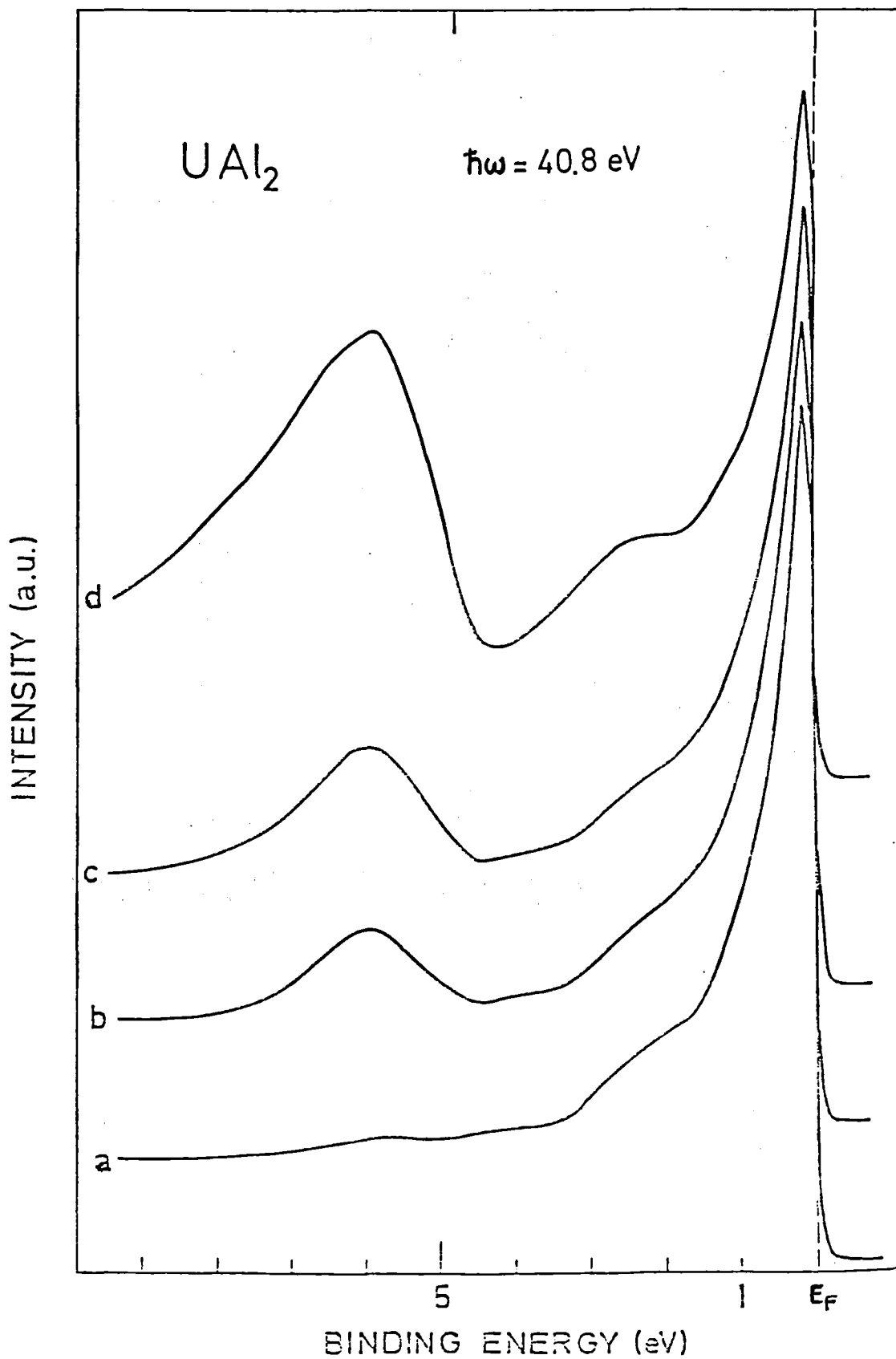


Fig.5

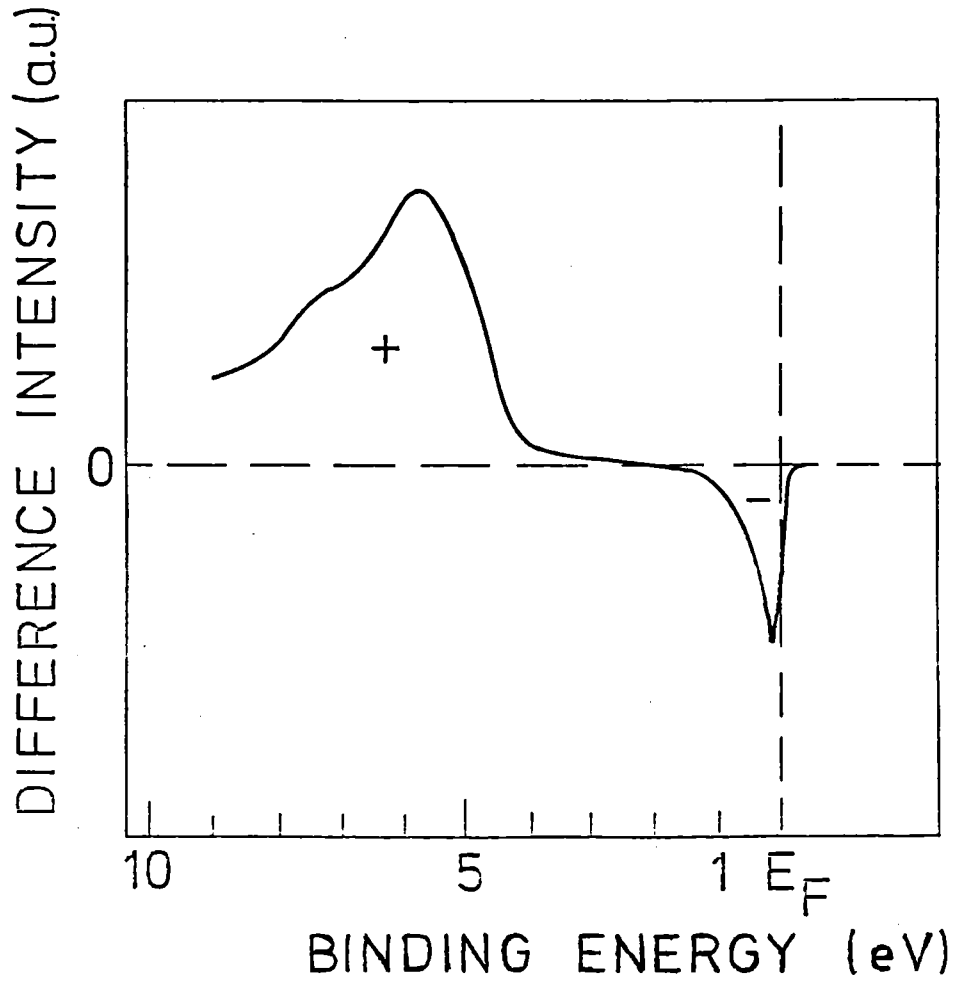
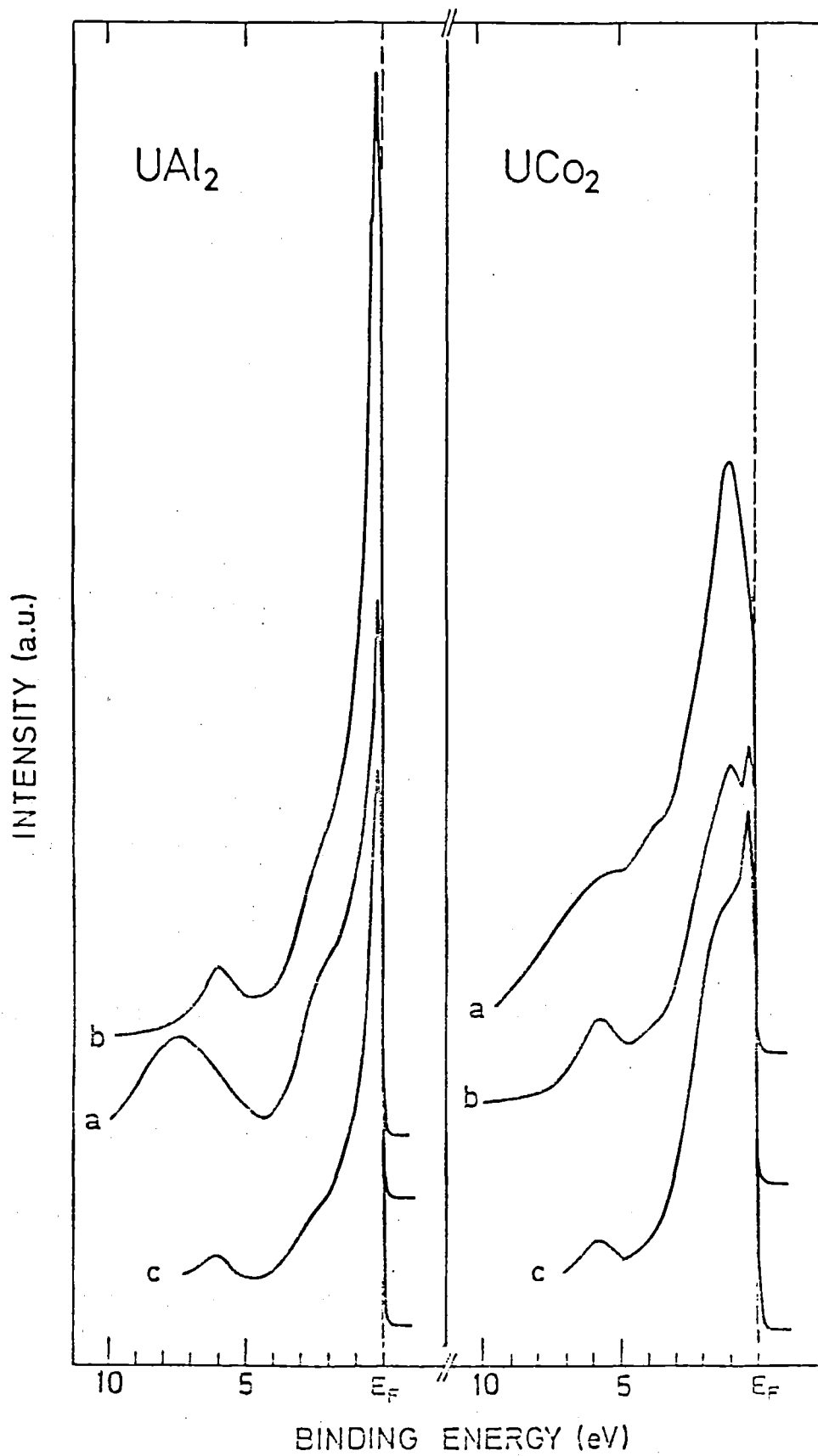


Fig.6



References

- /1/ see e.g. A.J. Freeman and J.B. Darby, Jr. The Actinides :  
Electronic structure and related properties, Vol. II, Academic  
Press, New York, 1974.
- /2/ D. Shaltiel, J. Less-Common Mat. 62 (1978) 407.
- /3/ M.B. Brodski and L.J. Trainor, Physica 91 B (1977) 271.
- /4/ J.M. Fournier, Solid State Commun. 29 (1979) 111.
- /5/ G.K. Wertheim, J. Electron Spectrosc. Rel. Phen. 15 (1979) 5.
- /6/ H.H. Hill, in Plutonium 1970 and other Actinides, W.N. Miner,  
ed. (AIME, New York, 1970) p.2.
- /7/ J.J. Verbist, J. Riga, J.J. Pireaux, and R. Caudano, J. Electron  
Spectrosc. Rel. Phen . 5 (1974) 193, and references therein.
- /8/ B.W. Veal and D.J. Lam, Phys. Rev. B 10 (1974) 4902.
- /9/ Y. Baer, R. Hauger and Ch. Zuercher, J. Electron Spectrosc. Rel. Phen  
15 (1979) 27.
- /10/ J.R. Naegele, L. Manes and G. Chauvet, to be published.
- /11/ D.E. Eastman and M. Kuznietz, Phys. Rev. Letters 26 (1971) 846.
- /12/ J.C. Fuggle, E. Källne, L.M. Watson and D.J. Fabian, Phys. Rev.  
B 16 (1977) 750.
- /13/ P. Heimann, E. Marschall, H. Neddermeyer, M. Pessa and H.F. Roloff,  
Phys. Rev. B 16 (1977) 2575.

STATE OF ANGULAR RESOLVED PHOTOEMISSION ON THE COMPOUND USb

Y. BAER<sup>+++</sup>, R. BAPTIST<sup>+</sup>, M. BELAKHOVSKY<sup>++</sup>, M.S.S. BROOKS<sup>+</sup>, O. VOGT<sup>+++</sup>

<sup>+</sup>Commission of the European Communities, Joint Research Centre  
Karlsruhe Establishment, European Institute for Transuranium Elements  
Postfach 2266, D-7500 Karlsruhe, Federal Republic of Germany

<sup>++</sup>Centre d'Etudes Nationales de Grenoble, Département de Recherche  
Fondamentale, 85 X, 38041 Grenoble, France

<sup>+++</sup>Laboratorium für Festkörperphysik, ETH, Zürich, Switzerland

ABSTRACT

Our first results of global XPS-UPS photoemission experiments on USb have shown a large density of states (with essentially f-d character) at the Fermi level in agreement with the metallic character of this compound and a small peak at 2.2 eV below  $E_F$  (with p-character) originating from the 5p orbitals of the antimony atoms. Here we report the preliminary results on a single crystal face 001 of the monpnictide USb, using synchrotron radiation. The aim of these studies is to determine the electronic states along the  $\Gamma X$  line. The spectra observed in the normal configuration emission show only strong intensity variations on varying the energy of the incident photons (from 20 eV to 60 eV) or the polarisation of the radiation. However due to the large number of flat bands in the region of interest, it is difficult to identify with certainty the resolved peaks with the predicted peaks obtained using an indirect transition model of photoemission and a band structure calculation. Finally, the effects of oxidation on the fresh in-situ cleaved sample could be followed by controlling the 0-2p peak located at about 6eV below  $E_F$ .

PRELIMINARY OBSERVATION OF LOW TEMPERATURE DEFECT INTERACTIONS IN CUBIC  
 $^{241}\text{AmO}_2$  FROM  $^{237}\text{Np}$  MÖSSBAUER EMISSION SPECTROSCOPY

J. FRIEDT, R. POINSOT and J. REBIZANT

Centre de Recherches Nucléaires  
67037 STRASBOURG Cedex (France)

and

Euratom, Institut Européen des Transuraniens  
KARLSRUHE (W. Germany)

We report the preliminary observation of low temperature defect interactions and defect complex mobility using Mössbauer spectroscopy of  $^{237}\text{Np}$  impurities created by  $\alpha$ -decay of  $^{241}\text{Am}$  in a host of  $\text{AmO}_2$ .

The  $^{237}\text{Np}$  emission spectroscopy tests microscopically the electronic configuration and lattice environment of the recoil nuclei ( $E_R \approx 93$  keV) from the  $^{241}\text{Am}$  decay, on a time scale after the decay comparable to the nuclear mean life time, i.e.  $\sim 100$  ns. The experiments are performed as a function of temperature and of the degree of self-irradiation of the oxide stored at 300 K. They are measured with respect to a single line  $\text{NpO}_2$  absorber maintained at 77 K.

The recoil nuclei are always observed to coexist in the tetravalent and the pentavalent charge states of  $^{237}\text{Np}$ , with however a relative proportion of the  $\text{Np}^{4+}$  configuration increasing with the degree of self-irradiation of the source host.

Above 15 K, independently of the degree of self-irradiation, the  $\text{Np}^{4+}$  resonance consists of a single resonance line of Lorentzian shape ; the  $\text{Np}^{5+}$  resonance reveals a broad distribution of quadrupole interactions. However, the  $\text{Np}^{4+}$  line is strongly broadened in comparison to the theoretical line width ( $W_{\text{exp}} = 3.2$  mm/s vs  $W_{\text{theor}} = 0.07$  mm/s), as always observed in  $^{237}\text{Np}$  Mössbauer spectroscopy.

Below 15 K, both the  $\text{Np}^{4+}$  and  $\text{Np}^{5+}$  resonances become more complex. The  $\text{Np}^{4+}$  component deviates increasingly from the Lorentzian shape as the temperature decreases and as the macroscopic defect concentration within the host increases. A tentative single line fit provides resonance widths at 4.2 K of 5 mm/s for a one week aged source and of  $\sim 10$  mm/s for a one year aged one. Alternately, below 15 K, the  $\text{Np}^{4+}$  resonance can be understood in terms of a superposition of a single line component plus a broad quadrupole pattern, in a proportion increasing with the degree of self-irradiation. Little information is obtained for  $\text{Np}^{5+}$  component as a result of the distribution of hyperfine interactions at this site.

Moreover, a fresh source (aged from 7 to 70 days) reveals a temperature dependence of the spectral area (both for the total resonance and the individual components) in agreement with the prediction from the Debye model with  $\theta_D = 220 \pm 10$  K. On the contrary, heavily self-irradiated sources (360 days old) reveal a deviation from the harmonic model, with a very significant maximum of the resonance area (both total and of the individual components) at 15 K. Self-irradiation experiments for storage times between 70 and 360 days are in progress.

Assuming that the anomalous dependence of the spectral areas will be recovered in this storage time range (70 - 360 days), the results are understood in terms of a low temperature ( $T < 15$  K) trapping of defects by the  $^{237}\text{Np}$  impurities and dissociation of these defect complexes above 15 K. In fresh, radiation defect free samples, the recoil nuclei reach principally substitutional recoil sites. This is in agreement with recoil model calculations ; the broadening of the lines is attributed to defects distant from the rest site (eg the vacancy cascade surrounded by the interstitial zone) and is more important at the  $\text{Np}^{5+}$  site because of the charge compensation requirement.

In self-damaged samples, the probability of interaction of the recoil nuclei with the random defects present in the host increases. The defect complexes stable below 15 K present a larger amplitude of lattice vibration, which is equivalent to a lower "microscopic Debye temperature". Comparing with defect studies in intermetallics, we suggest that the observation corresponds to the trapping of interstitial  $^{237}\text{Np}$  impurities by defects present in self-damaged  $\text{AmO}_2$ , which dissociate at 15 K. The interpretation needs however confirmation from studies of samples aged from 70 to 360 days.

The results are relevant for the understanding of the  $\alpha$ -decay self-irradiation consequences in oxide hosts. The formation of two charge states of the decay atoms, in proportions depending on the degree of self-damage, is demonstrated unambiguously. The preliminary observation of a defect trapping and of its dissociation above 15 K provides new insight into the succession of recovery steps in the thermal annealing of oxide hosts.

MOSSBAUER EFFECT AND MAGNETIC SUSCEPTIBILITY STUDIES  
OF THE NON STOICHIOMETRIC NEPTUNIUM OXIDES :  $\text{NpO}_{2+x}$

J. Gal<sup>\*\*</sup>, C. Musicas<sup>†</sup>, A. Cousson<sup>\*</sup>, J. Jové<sup>\*</sup>, M. Pagès<sup>\*</sup>

Studies of the magnetic and hyperfine properties of the neptunium oxides  $\text{NpO}_{2+x}$ , with  $x = 0, 0.15, 0.25$  have been performed by Mossbauer spectroscopy and magnetic susceptibility measurements.

The shape and the center of gravity of the transmission Mossbauer spectrum of the 60 keV resonance in  $^{237}\text{Np}$  change significantly with  $x$  and with the temperature.

The results can be well explained assuming temperature dependent charge transfert phenomena using the classical theory of electromagnetic wave packets.

The magnetic susceptibility of all the compounds  $\text{NpO}_{2+x}$  follows a Curie-Weiss law above 80 K with  $\mu_{\text{eff}} : 4.0, 2.8$  and  $\theta : -64, -21$  °K for  $x : 0, 0.25$  respectively.

\* Institut Curie, Section de Physique et Chimie. Service des Transuraniens,  
11, rue Pierre et Marie Curie, 75231 Paris Cedex 05, France.

† SHCT/DGR, B.P. N° 6, 92260 Fontenay-aux-Roses, France

MOSSBAUER EFFECT AND MAGNETISATION STUDIES  
OF THE MONOCLINIC  $\text{NpSe}_3$

J. Jové, A. Cousson, M. Pagès (Laboratoire Curie, Paris)

R. Potier, D. Damien, C. Costantini (CEN Fontenay-aux-Roses)

J. Gal (NRCN, Beer Sheva)

The Mossbauer effect studies of the 59.6 keV (E1) transition in  $^{237}\text{Np}$  of the  $\text{NpSe}_3$  show a first order magnetic phase transition at  $T_0 = 51(3)$  K and a second transition at  $T_F = 20(3)$  K. An unusual low temperature Mossbauer spectrum was observed and interpreted in terms of hyperfine field spread phenomena and a modulated wave type moment structure.

For an almost squared-up magnetic structure the magnetic hyperfine field constants  $g_n \mu_n H_{\text{eff}}$  are 2900(50)KOe and 3400(50)KOe, corresponding to ordered moments of 1.51(5)  $\mu_B$  and 1.78(8)  $\mu_B$  respectively with an average spread hyperfine field of 3180(30)KOe (1.66  $\mu_B$ ) for  $T < T_F$  and 3030(30)KOe for  $T > T_F$ . The hyperfine broadening factor constant is  $B = 8\text{mm/sec}$ .

The isomer shift of the Mossbauer spectra are + 6(0.5)mm/sec relative to  $\text{NpAl}_2$ . Above 80 K, the magnetic susceptibility showed Curie-Weiss behavior with  $\mu_{\text{eff}} = 2.88 \mu_B$  and  $\theta = -87$  K.

The two transitions at  $T_0$  and  $T_F$  are confirmed by the susceptibility measurements. It seemed probable that an incommensurate-to-commensurate or commensurate-to-incommensurate magnetic phase transition could be related to  $T_F$ .

Strongly correlated electron bands and magnetism in transition  
metals

Application to actinide metals and compounds

by

K. A. Long

Commission of the European Communities  
Joint Research Centre  
European Institute for Transuranium Elements  
Karlsruhe Establishment  
Postfach 2266  
D-7500 Karlsruhe  
Federal Republic of Germany

Abstract

In this paper electron bands and magnetism in narrow band materials are discussed. The theory which is developed in this paper is applicable to d-transition metals and their compounds, certain rare earth compounds, and to the early actinides and their compounds. Normally the magnetism of itinerant electron systems is considered by treating the atomic interactions (the electron-electron interactions) as a perturbation of the one electron theory. The approach taken in this paper is to solve the atomic problem first, including spin-orbit and crystal field interactions as well as the electron-electron interactions. These can be treated on each site if necessary, and then one can include the transfer interaction, which allows electrons to move from site to site, as a perturbation, and this leads to the formation of bands. In the limit of very strong overlap one recovers the normal one electron band theory. However in the limit of strong correlation, where  $U$  the electron-electron interaction parameter is much larger than the band width  $B$ , the bands are much different in character. It is in this narrow band limit that one expects to find magnetism, and in this method one has included the Hund's rule correlations that leads to the formation of moments on each site. These magnetic moments are then aligned by the Weiss molecular field, even when the size of the moments themselves fluctuate, due to the transfer of electrons between sites. As long as there is a sufficiently large molecular field coming from the neighbouring sites this will happen and one will have conditions favourable to magnetism. The question of whether or not moments form on the individual sites, is answered by considering the form of the crystal field interaction, and the number of electrons on each site. This problem is discussed using group theory. In the case of an even number of electrons on a site, there may be no moment, whereas in the case of an odd number of electrons on a site, a residual moment is always left due to time reversal symmetry.

The lifting of this degeneracy is discussed in the context of a magnetic impurity in a metal. Again this problem is usually developed in terms of the perturbation that the impurity causes to the electron gas of the metal. Here the opposite approach is taken, whereby the electron gas is considered as a perturbation of the atomic system. This leads to the lifting of the degeneracy of the atomic system, and the possibility of a non Curie susceptibility. The question of whether this kind of behaviour can occur in metals and alloys is discussed.

## Introduction

In the treatment of magnetism in metals and their compounds, there has arisen a dichotomy between the localised and the itinerant point of view. The itinerant approach in its pure form, consists in treating the metal as being like an electron gas, so that in a sense the constituent atoms are ignored. On the other hand, the localised approach neglects the transfer of electrons through the metal, and considers only the interactions of the electrons on each atom and the exchange interaction between the resultant moments. It was Hubbard (4,6,7,5) who first reconciled these two points of view by giving a mathematical formulation of the ideas of Van Vleck (19). However subsequent authors, by concentrating on his s-band model, made his theory indistinguishable from a form of the electron gas theory. To treat only the s-band model is to do less than justice to the significant advances made in his four papers, especially papers 2 and 4. By doing this one throws away the chance of describing the real diversity of properties of the transition metals. The chance to include both the motion of the electrons through the crystal, while also including electron-electron, spin-orbit, and crystal field interactions on each site, gives one an opportunity to include all the main ingredients needed to give an adequate description of magnetism in transition metals. This opportunity is taken in this paper and in subsequent work.

In sections one and two a treatment is given of bands in such a model as applied to the f-bands in the actinides, rare earth compounds and cerium, section one giving a phenomenological treatment and section two giving a rigorous development. In section 3, crystal field interactions are investigated, and in section 4 the problem of a magnetic impurity in a metal is investigated from a localised point of view. The results obtained are used in section 5, together with a treatment of the dynamic magnetic susceptibility to give a physical description of the occurrence and non-occurrence of magnetism in transition metals, rare earth compounds, and the actinides.

1. Electron bands in transition metals : Phenomenological treatment

Long use of the one electron band theory of metals has rendered solid state physics immune to the idea that electron bands can be based on many electron wave functions. This is well illustrated by the conviction that the  $4f^n$  states in the rare earth metals do not belong on a band structure diagram, because when an electron jumps onto a site already in such a configuration, it transforms the atom into a  $4f^{n+1}$  configuration, hence necessarily involving interaction effects, which are outside the scope of the one electron theory. It is true that an interacting theory is not compatible with a non-interacting one as we shall see below. However this means that the one electron theory is an over simplification and not that bands can not be developed from many electron states. One electron band theory is based on the hypothesis that one can ignore the electron-electron interactions, spin-orbit interactions, and crystal field effects. These terms are dropped from the Hamiltonian, along with the electron-lattice interaction. This conviction is completely invalid as is shown below, firstly in a phenomenological manner, and then in a rigorous manner.

Consider a one dimensional lattice composed of identical atoms<sup>(1)</sup>, spaced a distance  $a$  apart. Let us assume for argument's sake, that all the atoms are in a  $5f^n$  configuration, with energy  $E(5f^n)$ . This energy includes the effect of all atomic interactions, and the effect of the crystal field if necessary. Then let an extra electron be introduced into the system. This electron can exist in a virtual state on any of the sites. If it is on site  $m$ , then there will be  $n+1$  electrons on this site, and this atom will be in a  $5f^{n+1}$  configuration, with energy  $E(5f^{n+1})$ . The electron can of course move to any site, and will have the same energy. These states are equally probable, and by the superposition axiom of quantum mechanics, a general state is a linear superposition of all these states. Let the state with one electron at site  $m$  be represented by  $|m\rangle$ .

Then

$$|m\rangle = |m, \Gamma(5f^{n+1})\rangle \prod_{m=m'} |m', \Gamma(5f^n)\rangle \quad (1.1)$$

and

$$|m+1\rangle = |m+1, \Gamma(5f^{n+1})\rangle \prod_{m' \neq m+1} |m', \Gamma(5f^n)\rangle \quad (1.2)$$

A general state of the system is given by,

$$|\Phi\rangle = \sum_m |m\rangle \langle m|\Phi\rangle \quad (1.3)$$

The states  $m$  are not eigenstates of the system, because there exists an amplitude for the electron to jump to a neighbouring site equal to  $iA/n$ , where

$$A = \int \langle m|r\rangle [V_{cr}(\underline{r}) - U_{AT}(\underline{r}-\underline{r}_m)] \langle r|m+1\rangle d^3\underline{r} \quad (1.4)$$

$$V_{cr}(\underline{r}) = \sum_m U_{AT}(\underline{r}-\underline{r}_m) \quad (1.5)$$

where  $V_{cr}(\underline{r})$  is the crystal potential, and  $U_{at}(\underline{r})$  is the atomic potential at the site  $m$ . Then in this model,

$$|\langle m|\Phi\rangle|^2 = \text{the probability of an atom at site } m \text{ being in a } 5f^{n+1} \text{ state.}$$

$$1 - |\langle m|\Phi\rangle|^2 = \text{the probability of an atom at site } m \text{ being in a } 5f^n \text{ state.}$$

So even with one electron present, there is a mixed valency, which is of course very close to  $n$ . However, as more electrons are added the average valency will increase, but one must allow for the fact that an electron can not jump onto a site that is already in a  $5f^{n+1}$  state. This leads to the band becoming narrower for an added electron, as the number of electrons present increases. Putting  $C_m = \langle m|\Phi\rangle$ , one has,

$$i\hbar \frac{d}{dt} C_m(t) = (E(5f^{n+1}) - E(5f^n)) C_m - AC_{m+1} - AC_{m-1} \quad (1.6)$$

Assuming a periodic solution,  $C_m(t) = b(x_m) \exp(-iEt/n)$ ,  $b(x_m) = b e^{ikma}$ ,

one obtains a set of allowed energy values given by,

$$E(k) = E(5f^{n+1}) - E(5f^n) - 2A \cos(ka) \quad (1.7)$$

This formula is similar to the usual tight binding formula, but is only correct if there are a few electrons added to the system of atoms in a  $5f^n$  configuration. If more electrons are added one has to take account of correlation effects, as is done in the next section.

When an atom changes its configuration from  $5f^n$  to  $5f^{n+1}$ , the energy as we have seen above changes from  $E(5f^n)$  to  $E(5f^{n+1})$ . In the reverse process the extra electron according to Varma (2) becomes a one electron band electron, or according to Hirst (3) becomes part of a Fermi liquid of  $s$  electrons. In the first case,

$$E(5f^{n+1}) - E(5f^n) = E_f \quad (1.8)$$

where  $E_f$  is the energy of the highest one electron energy state that is occupied. Equation (1.7) is clearly not invariant to a change in the origin of energy. If the zero of energy is taken as the level of the potential outside the metal, and not at the bottom of the band, this would be written as,

$$-|E(5f^{n+1})| = -|E(5f^n)| - |W| \quad (1.9)$$

$$|W| = E_f, \text{ whereas } |W| \neq E_f \text{ showing an inconsistency.}$$

where  $W$  is the work function, and  $E(5f^{n+1})$  is the binding energy of an atom in this configuration. Thus to have an atom interacting with a set of non interacting electrons does not yield a consistent (in the sense of symbolic logic) theory. In other words Koopman's theory is not obeyed by the interacting theory of atoms, but is valid for the one electron theory.

Fermi liquid theory is similar in this sense to the first case, and here one has,

$$E(5f^{n+1}) - E(5f^n) = -E_o(N) + E_o(N+1) \quad (1.10)$$

where  $E_0(N+1) - E_0(N) = E_F$  is by definition the Fermi energy, and is the energy added to the system when an extra electron is added to the system. Equation (1.9) is invariant to a change in the energy origin, because it only involves energy differences. This model is a reasonable one for the case of a magnetic impurity in a simple metal, but is no use for a pure transition metal, because in this case an electron incident on an atom can not be described by a plane wave, because it has been emitted by a neighbouring atom. Since one is interested in the motion of one extra electron that is added to the system, a Green's function method is ideally suited to this problem. This is described in the next section. In this model it transpires that there is an interesting physical interpretation. Each atom is described in terms of its many electron states. The interaction term represents the transfer of electrons between the atoms. When an electron arrives on an atom, the atom's many electron state changes. So one can view the system of interacting atoms, as continuous fluctuations in their many electron states. In this model the binding energy of the solid is seen to be due to the exchange of electrons between the atoms, reminiscent of the way in which nuclear forces are caused by the exchange of mesons, or electromagnetic forces are caused by the exchange of photons. In fact if one views the atoms as black boxes which undergo transitions in their energy states, states which are denoted by  $\alpha, J, M$   $J$  being the total angular momentum and  $M$  its  $z$  component,  $\alpha$  representing any other quantum numbers, then one does not need the concept of an electron. Since it is unnecessary one can drop it. So all one is left with are atoms of states  $q, \alpha, J, M$  where  $q$  is the charge of an atom, and these states continuously fluctuate because of the presence of neighbouring atoms.

## 2. Narrow electron bands in transition metals

In table one, the characteristic energy parameters for the d-transition metals, rare earth mixed-valent compounds, and actinides are set out. In the case of the actinides this includes only the early actinides, as the later actinides become like the rare earths, with probably stronger crystal field interactions. However research on the later actinides, i.e. curium and berkelium is very much in its infancy.

Table one

	d-metals	f(rare earths)	f(actinides)
Bandwidth (one electron theory)	5ev	-	1ev
Bandwidth (with correlation)**	0.1ev <sup>+</sup>	0.1ev	0.01ev
Spin orbit splitting	0.1ev	0.1ev	0.38ev
Crystal field splitting	2ev	0.001ev	0.125ev
Coulomb energy*	5ev	5ev	5ev

\* includes screening

\*\* see below + this ignores hybridisation

This table implies that the best method of treating the electron motion in the actinides is to consider the atomic interactions first, and treat the electron transfer terms as a perturbation. The starting point for such a treatment is a generalised form of the Hubbard model (4,5,6,7). One takes the Hamiltonian for a set of electrons, written in second quantized form based on a complete set of Bloch states, and transforms it to its localised form,

$$\hat{H} = \sum_{ij} \sum_{\mu, \nu} T_{ij}^{\mu\nu} c_{i\mu}^{\dagger} c_{j\nu} + \frac{1}{2} \sum_{ij, k, l} \sum_{\substack{\mu, \nu \\ \sigma, \bar{\sigma}}} \langle i\mu, j\nu | \frac{1}{r} | k\sigma, l\bar{\sigma} \rangle c_i^{\dagger} c_j^{\dagger} c_{\sigma} c_{\bar{\sigma}} \quad (2.1)$$

where,

$$T_{ij}^{\mu\nu} = \int \phi_{\mu}^*(\underline{r} - \underline{R}_i) \left( -\frac{\hbar^2}{2m} \nabla^2 + V(\underline{r}) \right) \phi_{\nu}(\underline{r} - \underline{R}_j) d^3r \quad (2.2)$$

and,

$$V(\underline{r}) = \sum_i U_{AT}(\underline{r} - \underline{R}_i) \quad (2.3) \quad ; \langle i\mu, j\nu | \frac{1}{r} | k\sigma, l\bar{\sigma} \rangle = e^2 \int \frac{\phi_{\mu}^*(x - \underline{R}_i) \phi_{\nu}^* \phi_{\sigma} \phi_{\bar{\sigma}} dx dx'}{|x - x'|} \quad (2.4)$$

The second term in equation (2.1) represents the electron-electron interaction. In the Hubbard model this is approximated by neglecting all the terms except those on one site. Then H is written,

$$\hat{H} = \sum_{ij} \sum_{\mu, \nu} T_{ij}^{\mu\nu} c_{i\mu}^{\dagger} c_{j\nu} + \frac{1}{2} \sum_i \sum_{\substack{\mu, \nu \\ \sigma, \bar{\sigma}}} \langle \mu\nu | \frac{1}{r} | \sigma\bar{\sigma} \rangle c_{i\mu}^{\dagger} c_{i\nu}^{\dagger} c_{i\sigma} c_{i\bar{\sigma}} \\ + \sum_{ij} \sum_{\mu, \nu} T_{ij}^{s\mu} (c_{is}^{\dagger} c_{j\mu} + c_{is} c_{j\mu}^{\dagger}) \quad (2.5)$$

where the third term represents a hybridisation term. This is neglected below, but is included for completeness. The question of hybridisation, how large it is, whether it exists at all, and if so what kind exists, will be discussed in another paper.

Hubbard pointed out that in the narrow band limit, it was much better to express this operator  $\hat{H}$ , in terms of many electron transfer operators  $|\Gamma_{n'}\rangle\langle\Gamma_n|$  which transfer an atom in a state  $|\Gamma_n\rangle$  into a state  $|\Gamma_{n'}\rangle$ , where  $n' = n, n \pm 1$ . Clearly when an electron jumps from one atom to another, the number of electrons on the first atom decreases by one and the state changes from an  $l^n$  state to an  $l^{n-1}$  state, and on the second atom changes from an  $l^{n'}$  state to  $l^{n'+1}$  state. This adding of an electron, corresponds to the way atomic states are built up using fractional parentage coefficients. Therefore it is not surprising that the second quantized operator  $\hat{C}_{ij\mu}$  can be expressed linearly in terms of the many electron transfer operators. The exact expression is (8),

$$C_{ij\mu}^+ = \sum_{n=1}^{2(2l+1)} \sum_{\Gamma_n} \sum_{\Gamma_{n-1}} \sqrt{n} G_{\Gamma_{n-1}}^{\Gamma_n} C_{\mu, \Gamma_{n-1}}^{\Gamma_n} X_i(\Gamma_n, \Gamma_{n-1}) \quad (2.6)$$

$G_{\Gamma_{n-1}}^{\Gamma_n}$  are the Racah fractional parentage coefficients, and for the case of LS coupling one has,

$$C_{\mu, \Gamma_{n-1}}^{\Gamma_n} = C_{\frac{1}{2}\sigma, S_{n-1}, \mu_{n-1}}^{S_n, \mu_n} C_{l_{n-1}, L_{n-1}, M_{n-1}}^{L_n, M_n} \quad (2.7)$$

Using eqn. (2.6) eqn. (2.5) can be written as,

$$\begin{aligned} \hat{H} = & \sum_i \sum_{n=1}^P \sum_{\Gamma_n} \sum_{k=1}^P \left[ n \epsilon_i + \frac{1}{2} n_i (n_i - 1) Q_i^l(\Gamma_n) \right] X_i(\Gamma_n) \phi(k_1, \dots, k_{n-1}, \dots, k_p) \\ & + \sum_{i \neq j} \sum_{n_1=1}^P \sum_{n_2=1}^P \sum_{\Gamma_{n_1}} \sum_{\Gamma_{n_2}} B(i, \Gamma_{n_1}; j, \Gamma_{n_2-1} : i, \Gamma_{n_1-1}; j, \Gamma_{n_2}) X_i(\Gamma_{n_1}, \Gamma_{n_1-1}) \\ & \times \phi(k_1, \dots, k_{n_1-1}, \dots, k_{n_2-1}, \dots, k_p) X_j(\Gamma_{n_2-1}, \Gamma_{n_2}) \quad (2.8) \end{aligned}$$

The expressions for  $Q_i^p(\Gamma_n)$ ,  $B$  and  $\phi$  are found in /8/. In this form of the Hamiltonian it is apparent that the Coulomb interaction has been diagonalised. It is also apparent that by changing to a j-j coupling scheme one could include exactly the spin orbit coupling. In an intermediate coupling scheme (9) one could also include this and the crystal field interactions. This is very important when one considers the actinides. This is however not done exactly here but is to be considered in a later paper. However it is important to grasp that in principle the calculation is the same, and is done in terms of  $\chi(\Gamma_n^c, \Gamma_n^c)$  where  $|\Gamma_n^c\rangle$  are the states of  $l^n$  in a given symmetry of the crystal field, which are exactly the states discussed in /9/. What changes are the coefficients in eqn. (2.6). Equations of the normal tight binding type are obtained in the limit  $Q \rightarrow 0$ , which is also the limit of one electron band theory. In the limit  $B \rightarrow 0$ , one has a localised atomic description. In the cases discussed in this paper  $B$  is not zero, but  $Q > B$ . However  $Q$  is undoubtedly less than the usual value put on the Coulomb interaction as included in Table one. This intermediate situation explains why magnetic properties can seem localised in nature, whereas there is a Fermi surface and an electrical conductivity, which is albeit low.

The calculations are carried out using a Green's function technique. One considers Green's functions which describe the propagation of an excited atomic state through the lattice. This of course corresponds to the propagation of an extra electron which is added to the system. These Green's functions are of the form

$$G_{ij}(\Gamma_{n-1}, \Gamma_n, t | \Gamma_{n-1}', \Gamma_n', 0) = -i \theta(t) \langle [ \chi_i(\Gamma_{n-1}, \Gamma_n, t), \chi_j(\Gamma_{n-1}', \Gamma_n', 0) ] \rangle \quad (2.9)$$

The equation of motion is given by, in Fourier transformed form, by,

$$E G_{ij}(\Gamma_{n-1}, \Gamma_n | \Gamma_{n-1}', \Gamma_n'; E) = + \frac{1}{2\pi} \langle [ \chi_i(\Gamma_{n-1}, \Gamma_n), \chi_j(\Gamma_{n-1}', \Gamma_n') ] \rangle + \langle [ [ \chi_i(\Gamma_n, \Gamma_{n-1}, t), \hat{H} ], \chi_j(\Gamma_{n-1}', \Gamma_n', 0) ] \rangle_E \quad i, j = 1 \dots N \quad (2.10)$$

Substituting H from eqn. (2.8) and decoupling the operators belonging to different sites, one obtains,

$$\begin{aligned}
 & [E - E(\Gamma_n) \phi_{N-1}(\dots k_n=1 \dots) + E(\Gamma_{n-1}) \phi_{N-1}(\dots k_{n-1}=1 \dots k_p)] \times \\
 G_{ij}(\Gamma_{n-1}, \Gamma_n, E | \Gamma_n', \Gamma_{n-1}') &= \left[ \chi(\Gamma_n) + \chi(\Gamma_{n-1}) \right] \left[ \frac{1}{2\pi} \delta_{ij} \delta_{\Gamma_n \Gamma_n'} \delta_{\Gamma_{n-1} \Gamma_{n-1}'} \right] \\
 + \overline{\phi_{N-1}(\dots)} & \sum_{m \neq i} \sum_{n_2} \sum_{\Gamma_{n_2}'} \sum_{\Gamma_{n_2}''} B(i, \Gamma_n; m \Gamma_{n_2-1}'' : i, \Gamma_{n-1}; m \Gamma_{n_2}'') \\
 & \times G_{mj}(\Gamma_{n_2-1}'', \Gamma_{n_2}' | \Gamma_n', \Gamma_{n-1}') \quad (2.11)
 \end{aligned}$$

These equations have to be solved for specific configurations. One should note that if  $\Gamma_n' = \Gamma_n, \Gamma_{n-1}' = \Gamma_{n-1}$ , B is a constant, then the one equation left will yield the same results as eqn. (1.6). In (8) the configurations  $d^1(\text{Sc, Lu})$  and  $d^2(\text{Ti, Zr, Hf})$  were considered. For an example of the application to the actinides, we will choose the  $f^2$  configuration. This may correspond to the case of uranium, whereas  $f^4$  corresponds to neptunium,  $f^6$  to plutonium and  $f^7$  to americium. There are of course many more terms in the f series, and one has ignored the existence of d electrons which may also be localised. Accordingly an application to the actinides represents a more severe approximation. However this criticism applies to any theory of the actinides. The actinides are just very complicated!

In Table 2 one compares the terms considered for the  $f^2$  and  $d^2$  configurations. Some atoms are in  $f^1$  and  $f^3$  configurations.

TABLE 2

No. of els	Terms : d	Terms :
1	$2_D$	$2_F$
2	'S, 'D, 'G ; $3_F$	'S, 'D, 'G, 'I ; $3_H$
3	$4_F$	$4_I$

Consider eqn. (2.11) for the singlet states 'L = ('S, 'D, 'G, 'H) :

$$\begin{aligned}
 & [E - E('L) \overline{\Phi}_{N-1}(k_2-1) + E(^2F) \overline{\Phi}_{N-1}(k_1-1)] G_{ij} (^2F, 'L | 'L, ^2F) \\
 & = \frac{1}{2\pi} \delta_{ij} [ \overline{\chi}('L) + \overline{\chi}(^2F) ] + [ \overline{\chi}('L) + \overline{\chi}(^2F) ] \sum_{m \neq i} \\
 & [ \sum_{\Gamma_2'', ^2F} B(i, 'L, m, ^2F; i, ^2F, m, \Gamma_2'') \times \overline{\Phi}_{N-2}(k_1-1, k_2-1) G_{mj} (^2F, \Gamma_2'' | 'L, ^2F) \\
 & + \sum_{\Gamma_2'', \Gamma_3''} B(i, 'L, m, \Gamma_2''; i, ^2F, m, \Gamma_3'') \times \overline{\Phi}_{N-2}(k_2-2) G_{mj} (\Gamma_2'', \Gamma_3'' | 'L, ^2F) ] \\
 & \hspace{20em} (2.12)
 \end{aligned}$$

where  $^2F$  corresponds to  $f = m\sigma$ , and these 14 states should be summed over,  $'L = 0, L, 0, M_1, \Gamma_2'' = ^3H, 'L$ , and  $\Gamma_3'' = ^4F$ . The terms on the right hand side of eqn.(2.12) which involve overlap terms B must satisfy conservation of spin and angular momentum, as is the case for  $d^n$  configurations. The transition  $[ 'L, 'L ]$  into  $[ ^2F, ^4I ]$  are impossible because total spin is not conserved ( $S_{IN}^{TOT} = 0$  is not equal to  $S_{FIN}^{TOT} = 2, 1$ ). The terms for which this is true can be written and so far the singlet states one obtains

$$E = E('L) - E(^2F) + \sum_{f'', \Gamma_2'' = 'L, ^4I} \widetilde{B}_K ('L, f''; f, \Gamma_2'')$$

where  $f, f''$  represents any of the 14  $^2F$  states, and

$$\widetilde{B}_K = [ \overline{\chi}(\Gamma_{n-1}) + \overline{\chi}(\Gamma_{n-1}') ] \overline{\Phi}_N B_K$$

and  $B_K$  is the Fourier transform of  $B_{VV}$ , where translational invariance has been assumed.

For the states of the ground term of the  $f^2$  configuration, normally  $^3H$  the creation and annihilation processes satisfy the S and L conservation laws ( $^3H + ^3H \rightarrow ^2F + ^4I$ ;  $S_{IN}^{TOT} = 2, 1, 0$ ;  $S_{FIN}^{TOT} = 2, 1$ ;  $L_{IN}^{TOT} = 8, 7, \dots, 0$ ;  $L_{FIN}^{TOT} = (8, \dots, 2)$ ) and therefore these processes are retained. In this case one obtains, from eqn. (2.12),

$$\begin{aligned}
 (E - \epsilon_2) G_{22} + b_{0'2} G_{0'2} + b_{23} G_{32} &= a_2 \\
 b_{20'} G_{22} + (E - \epsilon_0') G_{0'2} + b_{30'} G_{32} &= 0
 \end{aligned} \tag{2.14}$$

where 0' corresponds to  $^1L$ , 2 to  $^3H$  and 3 to  $^4I(f^3)$ , so that

$$\begin{aligned} \epsilon_2 &= E_2 - \epsilon_f + b_{22} \quad ; \quad a_2 = [\bar{X}(f) + \bar{X}(2)] / 2\pi N \\ b_{22} &= [\bar{X}(f) + \bar{X}(2)] \bar{\phi}_{N-1}(k_2-1, k_3) B_{12}(2, f, f, 2) \\ \text{etc.} & \end{aligned} \tag{2.15}$$

One can estimate the values of  $\bar{\phi}$  and  $b_{\alpha\beta}$  in terms of  $\bar{X}(f)$ , which is the number of quasiparticles in the states  $^2F$ , due to the increase in the Coulomb energy, and one would expect  $\bar{X}(f) \ll 1$ . One then keeps only the largest terms in eqn. (2.14) and one obtains for the  $^3H$  band,

$$\begin{aligned} E(\underline{k}) &= \frac{1}{2} [E(^4I) - \epsilon_f] \pm \frac{1}{2} [(2E(^3H) - \epsilon_f - E(^4I))^2 \\ &+ |\tilde{B}_k(^3H, ^3H; f, ^4I)|^2]^{\frac{1}{2}} \end{aligned} \tag{2.16}$$

Therefore the bandwidth is determined by the processes  $^3H + ^3H$

$$\bar{X}(f) \cong [\exp(\Delta E/kT) + 1]^{-1} \tag{2.17}$$

where  $E = E(f) + E(f^3) - 2E(f^2)$ . Assuming similar values to the case of  $d^2$ , and assuming the initial width of the band  $B(k) \cong 1\text{ev}$  (from single electron calculations), one obtains a band width of 0.2ev for the  $^3H$  band, and 0.001ev for the singlet band. This band is narrowed by the factor  $\bar{X}(f)$ , and the conservation laws. This means that there is a very sharp maximum in the density of states, which has been suspected for a long time in the actinides (10), (11), (12). This has been previously explained as simply coming out of band structure calculations (12), and not specifically associated with any particular features of the system. Here it is associated at least in the  $f^2$  configuration with the singlet excited states,  $^1S$ ,  $^1D$ ,  $^1G$ ,  $^1I$ . In  $d$  transition metals this occurs for all even configurations, but this may not be the case in the  $f$  elements. One must remember that one has not included the  $6d$  electrons. Below one will also see that even and odd numbers of electrons are also important for the tendency to magnetism. This may explain why  $T_c$  the superconducting transition temperature, is so sensitive to the number of electrons, on

each site, i.e. the valency. The even configurations tend to rule out magnetism, which in turn means superconductivity is more likely, but one would also have to consider how the electron-phonon interaction changes. However one would expect this to be stronger, the narrower the f or d band is. Normally (13) narrow bands mean magnetism, but this is not necessarily the case in this framework.

The narrowness of the 'L band, and the fact that it has a capacity of one electron per atom, mean that the Fermi energy will lie in this band. This would seem to be the case in uranium, neptunium, and plutonium, and many of the intermetallic compounds of these metals. It is also the case in compounds such as SmS and CeAl<sub>3</sub>. These electrons are "heavy" and slow moving electrons, which means a poor conductivity, and a rapidly rising resistivity. The effect of the electron-phonon interaction on such electrons was discussed in a previous paper (11).

### 3. Magnetism in the transition metals ; Magnetic impurities, symmetry, and crystal fields.

The origin of magnetism lies in the effects of the Coulomb interaction between the electrons, together with the Pauli exclusion principle. In the atomic localised model, there are two stages, namely the formation of moments on each site, and their alignment through a coupling interaction. Amongst the choice of many-electron states, the ground state can be found from Hund's rules, for an isolated atom in a given configuration. In the rare earths for instance, except for the f<sup>6</sup> configuration, the ground state has a finite value of J in the ground state. The f<sup>6</sup> configuration has J = 0, for its ground state because the value of L can cancel out the value of S. The moments are coupled by the exchange interaction of the form,

$$\hat{H} = - \sum_{i \neq j} K(R_i - R_j) \underline{S}_i \cdot \underline{S}_j \quad (3.1)$$

This assumes a well defined moment at each site, or in other words, a given multiplet of states at each site. The ground state of the Hamiltonian (1), is magnetic at zero temperature and the transition temperature depends on the value of K.

Above  $T_c$ , the susceptibility follows a Curie-Weiss law, because of the  $2J + 1$  degeneracy at each site. In a real metal the environment of each site is not spherically symmetric. Thus the  $2J + 1$  degeneracy is removed by the crystal field. The degree to which the degeneracy is removed depends on the crystal symmetry. In this general case the susceptibility is given by (9),

$$\chi(T) = \frac{\mu_B^2}{Z} \left( \frac{1}{kT} \sum_{\Gamma} e^{-E_{\Gamma}/kT} \sum'_{\Gamma'} |\langle \Gamma | \mu | \Gamma' \rangle|^2 + \sum_{\Gamma} \sum''_{\Gamma'} |\langle \Gamma | \mu | \Gamma' \rangle|^2 \right) \times [e^{-E_{\Gamma}/kT} - e^{-E_{\Gamma'}/kT}] / (E_{\Gamma} - E_{\Gamma'}) \quad (3.2)$$

where  $|\Gamma\rangle$  are the crystal field states,  $\sum'$  sums over states  $|\Gamma'\rangle$  that are identical or degenerate to  $|\Gamma\rangle$ , and  $\sum''$  sums over states  $|\Gamma'\rangle$  that are distinct from and nondegenerate with  $|\Gamma\rangle$ . If there is no degeneracy, there is often no remnants of a Curie-Weiss law.

The problem of the removal of the degeneracy is solved by using group theory. The maximum degree to which removal is possible is determined by whether the original configuration had an even or odd number of electrons. This is because of time reversal degeneracy. The symmetry of motion with respect to time means that if  $\psi(\underline{r})$  is a possible wave function of a stationary state then so is  $\psi^*(\underline{r})$ , and this state has the same energy.

$$i \frac{\partial}{\partial t} \psi(\underline{r}, t) = \hat{H} \psi(\underline{r}, t) = E \psi(\underline{r}, t) \quad (3.3)$$

Operating with the time reversal operator  $T$ ,

$$\begin{aligned} -i \frac{\partial}{\partial t} \psi(\underline{r}, -t) &= T H T^{-1} T \psi(\underline{r}, -t) = E \psi(\underline{r}, -t) \\ &= H T \psi(\underline{r}, -t) = E \psi(\underline{r}, -t) \end{aligned} \quad (3.4)$$

Taking the complex conjugate of (3.3),

$$-i \frac{\partial}{\partial t} \psi^*(\underline{r}, t) = \hat{H} \psi^*(\underline{r}, t) = E \psi^*(\underline{r}, t)$$

$\therefore \psi$  and  $\psi^*$  satisfy the same equation. If one is to have a non degenerate level

and

$$\begin{aligned} \psi &= C \psi^* \\ |C|^2 &= 1 \end{aligned} \quad (3.5)$$

and  $\psi(\underline{r})$  must be real or pure imaginary. When spin is involved the situation

is more complicated. Then the wave function of the system are spinors  $\psi^{\lambda\mu\dots}$  whose rank is twice the sum of the spins  $S_a$  of all the particles. The wave function and its time reversed state corresponds to states of the same energy.

If a level is non-degenerate, these states must be identical to within a constant,

$$\psi_{\lambda\mu\dots}^{\text{rev}} = C \psi_{\lambda\mu\dots} = \psi^{\lambda\mu\dots*} \quad (3.7)$$

$$C^* \psi_{\lambda\mu\dots}^* = \psi_{\lambda\mu\dots} \quad (3.8)$$

$$\therefore \psi_{\lambda\mu\dots} = C^* (-1)^n \psi^{\lambda\mu\dots*} \quad (3.9)$$

using  $g_{\alpha\lambda} g_{\beta\mu} = (-1)^n g^{\lambda\alpha} g^{\mu\beta} \quad (3.10)$

$$\therefore \psi_{\lambda\mu\dots} = (-1)^n C C^* \psi_{\lambda\mu\dots} \quad (3.11)$$

$$\therefore (-1)^n C C^* = 1, \quad |C|^2 > 0, \quad (3.12)$$

and therefore  $n$  must be even. For

odd  $n$  this can not be fulfilled. Any angular momentum can be built up from several spins  $\frac{1}{2}$ . Orbital angular momentum always correspond to an even number. Therefore oddness or evenness is determined solely by the spin. If one has  $S$  half integral,  $J$  must be half integral, and the crystal field can not remove all the degeneracy. This means that in this case one usually has a Curie-Weiss susceptibility, because one has at least two states degenerate. If the ground state is non-magnetic,  $\langle r|\mu|r'\rangle^2 = 0$ , and there is no Curie-Weiss law from the single state.

The removal of the degeneracy for even numbers of electrons, and the non-removal for odd numbers of electrons, is connected to the existence of single and double valued representations of the rotation group. For single valued representations one can have a one dimensional representation of the various crystal groups. For double valued representations, all representations are double valued or come in complex conjugate pairs. The basis functions for these pairs are of course a spinor and its complex conjugate. Therefore the minimum degeneracy for any level is two in this case.

The next interesting question is under what circumstances even this degeneracy is removed. There are two possibilities and both are reflected by suggested "solutions" to the problem of a magnetic impurity in a metal. If an impurity such as manganese is in copper, then degeneracy of the many electron state is reduced by the crystal field. If the number of electrons in this state are odd, the degeneracy is reduced to four or two. As we saw above the double degeneracy is more general, as this is the minimum value allowed by time reversal invariance. Let's describe this two state system by allowing the atom to have a spin  $\frac{1}{2}$ . This may however not be general enough. This spin  $\frac{1}{2}$  system then couples to the conduction electrons of the host metal via a Hamiltonian of the form

$$H_{imp} = - \int \mathcal{J} \underline{s}(\underline{r}) \cdot \underline{\sigma} d^3\underline{r} \quad (3.13)$$

In order to calculate the resistivity one needs to calculate the spin flip amplitude, which is the probability amplitude with which the spin  $\uparrow$ , is flipped by the local spin. This gives the scattering amplitude for an electron  $k$ , to go to a final state  $k'$ . In second order perturbation theory this is found to diverge as the temperature decreases. Thus the resistivity rises as the temperature falls. At this point perturbation theory breaks down, and one has to look for a new mode of description. Nagaoka, Wilson and Nozières have pioneered one method of solution. This we call making odd, even. At low temperatures, for  $J$  negative, the only case for which one gets divergence, a kind of bound state is formed by a conduction electron and the moment. Then instead of having one electron at the site, one has two. The total angular momentum is no longer  $\frac{1}{2}$ , but 0 and 1. The state  $S = 0$  is

$$|S=0\rangle = \frac{1}{\sqrt{2}} [ |\frac{1}{2}\rangle_1 |-\frac{1}{2}\rangle_2 - |-\frac{1}{2}\rangle_1 |\frac{1}{2}\rangle_2 ] \quad (3.14)$$

This state lies below the states  $S = 1$ , i.e. it has lower energy. It is a singlet state with  $\langle S_z \rangle = 0$ , and therefore one has no Curie-Weiss behaviour of the susceptibility.  $\chi(T)$  goes from a  $T^{-1}$  behaviour to a roughly temperature independent behaviour.

There is however another type of solution which one might expect. The

previous method of solution concentrates on the behaviour of the electron gas, which because of its many degrees of freedom is a complicated system. One can however "invert" the method and concentrate on the local moment as a two state problem. All two state problems can be solved with the same mathematical apparatus. Each physical system is a representation of this mathematical solution. The conduction electrons cause the local spin to flip from  $|\frac{1}{2}\rangle$  to  $|\frac{-1}{2}\rangle$  and vice versa. If the amplitude of this process is  $A(T)$ , where  $T$  is the temperature, the Hamiltonian can be written as

$$H_{ij} \equiv \begin{bmatrix} E_0 & -A^* \\ -A & E_0 \end{bmatrix} \quad (3.15)$$

The solution to this problem, for the eigenvalues,

$$\begin{vmatrix} E - E_0 & A^* \\ A & E - E_0 \end{vmatrix} = 0 \quad (3.16)$$

Therefore the spin flip processes raise the degeneracy of the states.

$$E = E_0 \pm \sqrt{|A|^2} \quad (3.17.)$$

$$|I\rangle = \frac{1}{\sqrt{2}} \left[ |\frac{1}{2}\rangle + |\frac{-1}{2}\rangle \right] \quad (3.18)$$

$$|II\rangle = \frac{1}{\sqrt{2}} \left[ |\frac{1}{2}\rangle - |\frac{-1}{2}\rangle \right] \quad (3.19)$$

Now clearly,  $A$  can not go to infinity, When  $\sqrt{|A|^2} > kT$  it is no longer correct to calculate the spin flip amplitude using the original bases states  $|\frac{1}{2}\rangle$  and  $|\frac{-1}{2}\rangle$ . When  $\sqrt{|A|^2} > kT$ , one has only a one state system, and one would predict that the spin flip scattering rate will saturate. This problem must be solved self consistently. Since for the lower energy state,  $\langle \mu_z \rangle = 0$ , there is no Curie-Weiss behaviour of the local moment. However,  $S_{TOT} = \frac{1}{2}$ , and not zero. There is no compensation of the local spin. The final degeneracy due to time reversal invariance is raised by a time reversal breaking interaction from the local spin's point of view.

There are two methods of calculating the susceptibility. In the first method one calculates the value of  $\langle \mu_z \rangle$  in the presence of a magnetic field. Then

$$\chi(T) = \lim_{H \rightarrow 0} \frac{\partial \langle \mu_z \rangle}{\partial H} \quad (3.20)$$

When there is a magnetic field on,

$$\begin{aligned} H_{11} &= E_0 + \mu_B H & H_{21} &= -A \\ H_{12} &= -A^* & H_{22} &= E_0 - \mu_B H \end{aligned} \quad (3.21)$$

Then the eigenvalues are given by the two solutions of,

$$\begin{vmatrix} E - E_0 - \mu_B H & -A \\ -A^* & E - E_0 + \mu_B H \end{vmatrix} = 0 \quad (3.22)$$

$$E_{I,II} = E_0 \pm \sqrt{[\mu_B^2 H^2 + |A|^2]} \quad (3.23)$$

The two states are,

$$|I\rangle = a_1^I |1\rangle + a_2^I |2\rangle \quad (3.24)$$

$$|II\rangle = a_1^{II} |1\rangle + a_2^{II} |2\rangle \quad (3.25)$$

$$\langle \hat{S}_z \rangle_H = \frac{\text{Tr} [ e^{-\beta \hat{H}} \hat{S}_z ]}{Z} \quad (3.26)$$

$$\begin{aligned} Z = \text{Tr} [ e^{-\beta \hat{H}} ] &= \exp[-\beta(E_0 + \sqrt{X})] + \exp[-\beta(E_0 - \sqrt{X})] \quad (3.27) \\ &= 2 \exp(-\beta E_0) \cosh \beta \sqrt{X} \end{aligned}$$

where,  $X = [\mu_B^2 H^2 + A^2] \quad (3.28)$

then,  $\langle \hat{S}_z \rangle_H = \frac{[-\frac{1}{2} + |a_1^I|^2] e^{-\beta \sqrt{X}} + [\frac{1}{2} - |a_2^I|^2] e^{+\beta \sqrt{X}}}{[2 \cosh \beta \sqrt{X}]}^{-1} \quad (3.30)$

where,  $|a_1^I|^2 = \frac{|H_{12}|^2}{(E_I - H_{11})^2 + H_{12} H_{21}^*}$ ;  $|a_2^I|^2 = \frac{(E_{II} - H_{11})^2}{(E_{II} - H_{11})^2 + H_{12} H_{21}^*} \quad (3.31)$

It is however simpler, if one only wants  $\chi(T)$  and not  $\langle S_z \rangle_t$ , to start from eqn. (3.2), where

$$\langle I | S_z | I \rangle = 0 \quad \langle II | S_z | II \rangle = 0 \quad (3.32)$$

$$\therefore \chi(T) = \frac{g^2 \mu_B^2}{\cosh \beta |A|} \frac{1}{4} \left[ \exp(|A|/kT) - \exp(-|A|/kT) \right] [2|A|]^{-1} \quad (3.33)$$

$$= \frac{g^2 \mu_B^2}{4|A|} \tanh \beta |A| \quad (3.34)$$

For large  $T$ ;  $\chi(T) = \frac{g^2 \mu_B^2}{4} \frac{1}{k_B T} \quad (3.35)$

For small  $T$ ;  $\chi(T) = \frac{g^2 \mu_B^2}{4|A|} \quad (3.36)$

Therefore  $\chi(T)$  at low  $T$  depends on the temperature dependence of  $A$ , the splitting caused by the interaction with the conduction electrons.

Experimentally one should be able to measure  $A$  by a resonance experiment, using a transverse oscillating magnetic field  $h(t) = h \exp i \omega t$ .

Then at resonance  $2|A| = \hbar \omega_0$ , or  $|A| = \hbar \omega_0 / 2$ . Thus the physics of a magnetic impurity in a metal would seem to show strong similarities to the physics of a maser. However one could not separate those impurities in state  $|II\rangle$  from those in state  $|I\rangle$ .

#### 4. The dynamical susceptibility

In extended materials, metals and their compounds, in the formalism developed in section 1, one can derive an expression for the dynamic susceptibility which allows one to discuss their magnetic properties. This is given by,

$$\chi_{MM}(\underline{r}, t) = i \theta(t) \langle [ \hat{M}(\underline{r}, t), \hat{M}(0, 0) ] \rangle \quad (4.1)$$

$$\hat{M}(\underline{r}, t) = \mu_B \sum_{\nu} \hat{J}_{\nu}(t) \delta(\underline{r} - \underline{r}_{\nu}) \quad (4.2)$$

where  $\hat{J}_v$  is the total angular momentum operator at site  $v$ , and  $M(r, t)$  is the magnetisation.

Using the closure relation twice,

$$\hat{M}(r, t) = \mu_B \sum_{\Gamma_{n_1}} \sum_{\Gamma_{n_2}} \sum_{\mathcal{D}} \langle \Gamma_{n_1} | \hat{J}_v | \Gamma_{n_2} \rangle \hat{X}(\Gamma_{n_1}, \Gamma_{n_2}, t) \delta(r - r_v) \quad (4.3)$$

$$\therefore \chi_{M, M}(r, r', t) = \mu_B^2 \sum_{\Gamma_{n_1}} \sum_{\substack{\Gamma_{n_2} \\ \mathcal{D}_1, \mathcal{D}_2}} \sum_{\Gamma_{n_3}} \sum_{\Gamma_{n_4}} \langle \Gamma_{n_1} | \hat{J}_{v_1} | \Gamma_{n_2} \rangle \langle \Gamma_{n_3} | \hat{J}_{v_2} | \Gamma_{n_4} \rangle G_{v_1, v_2}(\Gamma_{n_1}, \Gamma_{n_2}; \Gamma_{n_3}, \Gamma_{n_4}, t) \times \delta(r - r_{v_1}) \delta(r' - r_{v_2}) \quad (4.4)$$

where one has used,

$$\begin{aligned} \hat{J}_v(t) &= e^{i\hat{H}t} \hat{J}_v(0) e^{-i\hat{H}t} = \sum_{\Gamma_{n_1}} \sum_{\Gamma_{n_2}} e^{i\hat{H}t} |\Gamma_{n_1}\rangle \langle \Gamma_{n_1} | \hat{J}_v(0) | \Gamma_{n_2}\rangle \langle \Gamma_{n_2} | e^{-i\hat{H}t} \\ &= \sum_{\Gamma_{n_1}} \sum_{\Gamma_{n_2}} \langle \Gamma_{n_1} | \hat{J}_v(0) | \Gamma_{n_2}\rangle \hat{X}(\Gamma_{n_1}, \Gamma_{n_2}, t) \end{aligned} \quad (4.5)$$

Fourier transforming, one finds that,

$$\chi_{MM}(q, q', t) = \mu_B^2 \sum_{\Gamma_{n_1}, \Gamma_{n_2}} \sum_{\Gamma_{n_3}, \Gamma_{n_4}} \langle \Gamma_{n_1} | \hat{J}_{v_1} | \Gamma_{n_2}\rangle \langle \Gamma_{n_3} | \hat{J}_{v_2} | \Gamma_{n_4}\rangle G_{q, q'}(\Gamma_{n_1}, \Gamma_{n_2}; \Gamma_{n_3}, \Gamma_{n_4}, t) \quad (4.6)$$

or for translationally invariant systems,

$$\chi_{MM}(q, \omega) = \mu_B^2 \sum_{\Gamma_{n_1}, \Gamma_{n_2}} \sum_{\Gamma_{n_3}, \Gamma_{n_4}} \langle \Gamma_{n_1} | \hat{J}_{v_1} | \Gamma_{n_2}\rangle \langle \Gamma_{n_3} | \hat{J}_{v_2} | \Gamma_{n_4}\rangle G_q(\Gamma_{n_1}, \Gamma_{n_2}; \Gamma_{n_3}, \Gamma_{n_4}, t) \quad (4.7)$$

The factors  $\langle \Gamma_{n_1} | \hat{J}_{v_1} | \Gamma_{n_2}\rangle$  are independent of the site  $v_1$ .

Assuming that  $\langle \chi_v(\Gamma_n, \Gamma_{n'}) \rangle = 0$  for  $\Gamma_n \neq \Gamma_{n'}$ , and remembering the form of the Green's function, as being proportional to,

$$\begin{aligned} &\langle |\Gamma_{n_1}\rangle \langle \Gamma_{n_4}| \rangle \delta_{\Gamma_{n_2}, \Gamma_{n_3}} - \langle |\Gamma_{n_3}\rangle \langle \Gamma_{n_4}| \rangle \delta_{\Gamma_{n_1}, \Gamma_{n_2}} \\ &= \delta_{\Gamma_{n_1}, \Gamma_{n_4}} \delta_{\Gamma_{n_2}, \Gamma_{n_3}} \left[ \langle \chi(\Gamma_{n_1}) \rangle - \langle \chi(\Gamma_{n_2}) \rangle \right] \end{aligned} \quad (4.8)$$

equation (4.7) becomes,

$$\chi_{MM}(q, \omega) = \sum_{\Gamma_{n_1}, \Gamma_{n_2}} \mu_B^2 \langle \Gamma_{n_1} | \hat{J} | \Gamma_{n_2}\rangle \langle \Gamma_{n_2} | \hat{J} | \Gamma_{n_1}\rangle G_q(\Gamma_{n_1}, \Gamma_{n_2}; \Gamma_{n_2}, \Gamma_{n_1}, \omega) \quad (4.9)$$

$$= \sum_{\Gamma_{n_1}} \sum_{\Gamma_{n_2}} |\langle \Gamma_{n_1} | \hat{J} | \Gamma_{n_2}\rangle|^2 G_q(\Gamma_{n_1}, \Gamma_{n_2}; \Gamma_{n_2}, \Gamma_{n_1}, \omega) \quad (4.10)$$

In the case of a completely localised system, one can see from the definition of  $G_q$ , that

$$G_q^{LOC}(\Gamma_{n_1}, \Gamma_{n_2}; \Gamma_{n_2}, \Gamma_{n_1}; \omega) = \frac{\delta(q=0) [\exp[-E_{\Gamma_{n_1}}/kT] - \exp[-E_{\Gamma_{n_2}}/kT]]}{Z_0 [\omega - (E_{\Gamma_{n_1}} - E_{\Gamma_{n_2}})]} \delta_{n_1, n_2} \quad (4.11)$$

$$\chi_{MM}^{LOC}(q, \omega) = \frac{\sum_{\Gamma_{n_1}, \Gamma_{n_2}} |\langle \Gamma_{n_1} | \hat{x} | \Gamma_{n_2} \rangle|^2 \delta(q=0) [\exp[-E_{\Gamma_{n_1}}/kT] - \exp[-E_{\Gamma_{n_2}}/kT]]}{\mu_B^2 Z_0 [\omega - (E_{\Gamma_{n_1}} - E_{\Gamma_{n_2}})]} \quad (4.12)$$

where the summations are over the possible states of  $n_1 = n_2$  electrons.

Where

$$\langle \chi(\Gamma_{n_1}) \rangle_{LOC} = \sum_{\Gamma_{n_1}'} \langle \Gamma_{n_1}' | e^{-\beta \hat{H}} \hat{x}(\Gamma_{n_1}) | \Gamma_{n_1}' \rangle / Z_0 \quad (4.13)$$

$$= \langle \Gamma_{n_1} | e^{-E_{\Gamma_{n_1}}/kT} | \Gamma_{n_1} \rangle / Z_0$$

$$= \exp(-E_{\Gamma_{n_1}}/kT) / \sum_{\Gamma_n} \exp(-E_{\Gamma_n}/kT) \quad (4.14)$$

This is then a derivation of eqn. (3.2), when allowance is made for degeneracy.

This formula is however not easy to calculate with. Although it is relatively easy (Sec. 2) to obtain the energy spectrum from the Green's function, it is not simple to obtain a useful form for  $G_q$  sufficient to describe the susceptibility. This is because one needs considerable modification to the ensemble average. In an occupied band, the energy levels need to be filled up to the level of the chemical potential, and this ensemble needs to be used in calculating the magnetic susceptibility.

However, one can clear up one problem posed by the experimental results immediately. In mixed valency compounds, the magnetic susceptibility is not of a Curie-Weiss type, but is independent of temperature. There is however the exception of TmSe, which does have a Curie contribution. In this case both configurations are magnetic. Hence  $\langle \Gamma_{n_1} | \underline{J} | \Gamma_{n_2} \rangle \neq 0$ , and one can expect a Curie contribution. In most other cases, one of the configurations is a non-magnetic one, and  $\langle \Gamma_{n_1} | \underline{J} | \Gamma_{n_2} \rangle = 0$ , and therefore this band can be expected not to contribute to the susceptibility. Thus the absence of a Curie behaviour is connected to the value of the matrix elements between configurations. There need not be any complicated compensation of the local moments by conduction electrons (2). To be more specific though one needs a much better approximation to  $G_q$ , than the one used in this paper.

In the actinides and actinide compounds, there are several materials in which there are "mixed valency" f-bands, which are very narrow, and which lie at the Fermi energy /11/. This includes the pure metals, neptunium,  $\alpha$  and  $\beta$  -plutonium, and compounds such as  $\text{PuAl}_2$  and  $\text{UAl}_2$ .

The weak temperature dependence of the susceptibilities of these materials shows that the very narrow bands are non-magnetic. In  $\text{PuAl}_2$  the susceptibility becomes Curie like at higher temperatures, and in this case either a magnetic band becomes occupied at higher temperatures, or the f-states become localised at higher temperatures due to the electron-phonon interaction /11/. The final interpretation must be decided by experiment, perhaps on the specific heat.

### Conclusion

In this paper a method for treating the generalised Hubbard model in d-transition metals is extended to treat f-transition metals, and mixed valency compounds. In doing this it has been assumed that only f-electrons interact strongly on each site, and that d-electrons are not involved. The method however could be extended to treat this case where both d and f-electrons interact strongly on each site, but this would only change the details of the results, and would not change any of the fundamental results. By allowing for  $n-1$ ,  $n$ , and  $n+1$  electrons on each site, it has

been shown that the transfer of electrons between sites leads to the formation of electron bands. In this method one can include on site electron-electron interactions, spin orbit interactions, and crystal field interactions.

It has been shown that if non magnetic configurations are involved in the formation of mixed valency bands, then these bands are non-magnetic. In this connection it is important to know when and how such non-magnetic configurations arise. A discussion of this problem has been given in terms of crystal field theory. In the case of an even number of electrons, the degeneracy can be lifted by electric forces alone, but in the case of an odd number of electrons all states are at least doubly degenerate. The lifting of this degeneracy by interaction with the conduction electrons has been discussed and this may lead to a temperature independent susceptibility at low temperatures.

#### Acknowledgements

Some of the ideas contained in this work were conceived while the author was supported by an EMR contract from the Atomic Energy Authority, Harwell, while working at the University of Surrey. The author would like to thank Dr. J.A. Lee, Dr. M.J. Mortimer, Dr. A.G. Crocker, and Mr. R.O.A. Hall for helpful conversations and for their continued interest in this work. The author would also like to thank Dr. V. Dallacasa, Dr. G. Amoretti and Dr. L. Manes for reading the manuscript and suggesting corrections. The author would also like to thank his wife, Christina Long, without whose help and support this work would not have been carried out.

References

- /1/ Feynman R.P. "Lectures on physics" (Addison-Wesley; Reading, Mass.) Vol.3, Ch .13 (1965)
- /2/ Varma C.M., Rev. Mod. Phys., 48,219,(1976)
- /3/ Hirst L.L., Phys. Kondens. Mater., 11, 255, (1970)
- /4/ Hubbard J., Proc. Roy. Soc., A276, 238, (1963)
- /5/ Hubbard J., Proc. Roy. Soc., A277, 237, (1964)
- /6/ Hubbard J., Proc. Roy. Soc., A281, 401, (1964)
- /7/ Hubbard J., Proc. Roy. Soc., A285, 542, (1965)
- /8/ Irkhin Yu.P., Sov. Phys., 39, 490, (1974)
- /9/ Chan S.K., and Lam D.J., "The Actinides", Eds. Freeman A.J. and Darby J.B., Vol. 1, Ch.1, (1974), (Academic Press, New York)
- /10/ Fradin F.Y., Phys. Rev. Letters, 33, 158, (1974)
- /11/ Long K.A., Phys. Stat. Sol. (b), 74, 155, (1977)
- /12/ Freeman A.J., "The Actinides", Eds., Freeman A.J. and Darby J.B., Academic Press, New York, Vol.1, Ch.2
- /13/ Doniach S., "Green's functions for solid state physicists", Benjamin, New York, 1974
- /14/ Landau L.D., and Lifshitz E.M., "Quantum Mechanics", Permagon, London, (1965)
- /15/ Nagaoka Y., Phys. Rev., A138, 1112, (1965)
- /16/ Wilson K.G., Rev. Mod. Phys. 47, 773, (1974)
- /17/ Nozières P., J. Low Temp. Phys. 17, 31, (1975)
- /18/ Feynman R.P., "Lectures on Physics", Vol.3, Ch.9, (Addison-Wesley, Reading, Mass.), (1965)
- /19/ Van Vleck J.H., in "Quantum Theory of atoms, molecules, and the solid state", Ed. P. Löwdin, Academic Press (1966) and Rev. Mod. Phys. 25, 226, (1953).

On the regularity of the cohesive energy of the lanthanide elements

Börje Johansson, Sekt. 214, FOA, S-104 50 Stockholm 80, Sweden

It is well-known that the quasi-irregular behaviour of the cohesive energy of the lanthanides is due to the divalent free atom configuration,  $f^{n+1}s^2$ . When the cohesive energy is referred to the trivalent atomic configuration,  $f^n ds^2$ , a much more regular variation through the series is obtained. Nugent et. al.<sup>1)</sup> proposed that the remaining variation is due to the nephelauxetic variation in the inter-f-electron repulsion energy between the gaseous  $f^n ds^2$  atoms and the corresponding atoms in the crystalline metal. However, we will show that the reason for this variation is exclusively an atomic property, namely the coupling between the open  $f^n$  and d shells.

This finding also lead us to somewhat question the appropriateness of using the P(M)-function<sup>1-3)</sup> for interpolations and predictions of various thermodynamical data. However, the P(M)-function can be readily redefined for the lanthanides so that it is no longer influenced by the atomic ( $f^n, d$ ) coupling.

Attention should now be paid to the corresponding atomic ( $f^n, d$ ) coupling for the actinides, so that the P(M)-function can be appropriately redefined also for this series of elements. Thereby, hopefully, the puzzling experimental result for the cohesive energy of americium will be clarified.

1) L.J. Nugent, J.L. Burnett and L.R. Morss, *J. Chem. Thermodynamics* 5, 665 (1973).

2) F. David, K. Samhoun, R. Guillaumont and L.J. Nugent, Heavy Element Properties, eds. W. Müller and H. Blank (North Holland, Amsterdam 1976), p. 97.

3) F. David, K. Samhoun, R. Guillaumont and N. Edelstein, *J. Inorg. Nucl. Chem.* 40, 69 (1978).

KONDO EFFECT IN U, Np AND Pu METALS <sup>+</sup>.

V.Dallacasa

Istituto di Fisica, GNSM, Parma, Italy.

Abstract. A theory is presented for the resistivity of U, Np and Pu metals. The acoustic phonon contribution is calculated taking the temperature dependence of the sound velocity in the f band into account and subtracted from the experimental curves. The remaining contribution to the resistivity can be explained in terms of magnetic scattering of conduction electrons from the f electrons, with values of the exchange constant much bigger than  $kT$ . These large values suggest an explanation to the constant susceptibilities as a function of temperature in terms of f spin fluctuations.

## 1. INTRODUCTION

The peculiar properties of actinides have raised several theoretical efforts in last years. The reach variety of experimental results can be attributed to the presence of f electron bands, as well as d and s bands, at the Fermi level.

From band structure calculations (Kmeto and Hill 1970; Freeman and Koelling 1974) it is known that for the lightest actinide metals, up to Pu, the f electrons belong to bands, whose bandwidth is of the order of 1 eV. This assigns them a non-localized behaviour, contrary to those of the second half of the series, which are more similar to rare-earth metals. This is also confirmed by consideration of metallic radii through the series (Fournier 1975, 1976). At the middle of the series, specifically for Pu, it has been pointed out by Johansson (1975) that the Hubbard U becomes comparable with the bandwidth, as calculated in a band approach. This would make a one-electron band structure calculation probably not appropriate there. Note that it is this metal, by the way, that shows the most anomalous electrical properties.

From the other hand, sound attempts to take correlation into account have not been produced, except for some (Jullien et al. 1972; Doniach 1974; Long 1977) so that the situation for Pu is not clear. This is even more so, on noting that for Am, immediately next to Pu in the Periodic Table, a picture of localized f electrons is appropriate (Freeman and Koelling 1974; Fournier 1975; Johansson 1975; Jullien 1974). The d and f electrons are supposed to form broad bands but, as pointed out by Coqblin et al. (1978) there is a strong f-d hybridization. We will make use of this to treat the d and f electrons together in calculations.

On the basis of these considerations, one is led to a two-band model (Coqblin et al.1978) an s-like broad and flat band and a narrow f-d band, containing the Fermi energy. The existence of a sharp f band is required by the large value of the coefficient  $\gamma$  of the low-temperature electronic specific heat (Fournier 1975; Jullien 1974; Coqblin et al.1978).

In this paper we present a theory for the resistivity of actinide metals which is able to explain the observed behaviour as a function of temperature for U, Np and Pu. It can also account for the high and almost temperature-independent magnetic susceptibility (Fournier 1975; Nellis and Brodsky 1974; Brodsky 1978).

The most successful calculation for the electrical resistivity so far (see Coqblin et al.1978; Brodsky et al.1974 for a review and appropriate references) has been proposed by Jullien et al.(1974) on the basis of a spin fluctuation model, in which electrons of a broad s-like band are coupled with the electrons of a narrow d-f band through an exchange interaction. The spin-fluctuation scattering arises as the system is supposed to be close to magnetism. This model suffers from two difficulties, the first is that strong enhancement Stoner factors  $S \sim 10$  are needed to have agreement with experiments, the second is that no explanation can be given of the observed constant susceptibilities.

It is important to realize that, in order to understand the actual scattering mechanisms, especially at high temperatures, a correct <sup>phonon</sup> subtraction is to be made. When the f band is expected to be narrow or have a relatively small Fermi energy, the usual linear dependence of the resisti-

vity on temperature (for  $T \gg \Theta$  where  $\Theta$  is the Debye temperature) may become invalid (Fradin 1974). The resistivity may bend towards the real axis in a plot vs. temperature and eventually saturate at very high temperatures. We note in this respect that the procedure by Coqblin et al. (1978) to subtract the resistivity of Th neglects the f phonon contribution, while in effect the Fermi temperatures of the f band arising from their fits are very small ( $T_F = 280^\circ\text{K}$  for Pu). In view of this, the phonon contribution of the narrow band is treated in this paper. The principal aim is in the high temperature region, typically  $T \sim 300^\circ\text{K}$ , because at low temperatures the presence of a  $T^2$  term, where phonons contribute a  $T^5$  term, could be consistent with spin fluctuations (Jullien et al. 1974; Long 1977; Coqblin et al. 1978).

## 2. MODEL FOR PHONON-LIMITED RESISTIVITY

Following Jullien et al. (1974) we assume essentially a two-band model. Only the electrons of the broad band, termed conventionally the s electrons, will be assumed to carry the current, while the f electrons are supposed to form a narrow band around the Fermi level.

The scattering mechanisms consist of phonon scattering and a second mechanism that will become apparent once the phonon subtraction is made. Thus, let us first calculate the phonon-limited resistivity. In a Debye model this is given by (Ziman 1965)

$$\rho = \frac{\hbar k_F}{n_s e^2 \lambda} \quad (2.1)$$

where  $k_F$  is the Fermi wave-vector of the s electrons,  $n_s$  their number per unit volume,  $e$  the electron charge and the mean

free path is given by

$$\frac{1}{\Lambda} = N \bar{\sigma}_a \frac{\hbar^2 q_D^2 T}{M K_D e^2 (\Theta)^4} \int_0^{\Theta/T} \frac{4z^5 dz}{(e^z - 1)(1 - e^{-z})} \quad (2.2)$$

This is a particular form of a general formula, proposed by Kaiser and Doniach (1970) for the resistivity due to excitations of boson type. Here,  $N$  is the number of atoms per unit volume,  $\bar{\sigma}_a$  an average cross section of a single atom,  $q_D$  the Debye cut-off wave-vector,  $M$  the atomic mass and  $\Theta$  the Debye temperature. To get (2.2) one has to assume that  $q_D > 2k_F$  (Tosi 1975) and that only acoustic phonons contribute to the scattering so that the effect of optical phonons can be neglected (Ziman 1965). This latter effect has been considered by Long (1977). Further, only normal processes are included, the Umklapp scattering being neglected (Ziman 1965).

The existence and inclusion of optical phonons, as discussed by Long, implies the consideration of the complicated crystal structure of the actinides, with many atoms in the unit cell and the estimate of their energy  $\omega_o$  at zero wave-vector. Their contribution is smaller than the acoustic one by a factor  $(\omega_D/\omega_o)^2$ , where  $\omega_D$  is the Debye energy (Long 1977).

The inclusion of Umklapp processes, from the other hand is not easy to perform, so we simply assume they are negligible, checking at the end the consistency of this assumption.

When  $T \gg \Theta$  we can calculate (2.2) as follows

$$\frac{1}{\Lambda} = N \bar{\sigma}_a \frac{kT}{M s_{ph}^2} + o((\Theta/T)^2) \quad (2.3)$$

where  $s_{ph}$  is the sound velocity such that  $\Theta = \hbar q_D s_{ph}/k$ . In a usual approach (Ziman 1965) one would now conclude that  $\frac{1}{\Lambda} \propto T$ . However, this is the result of assuming that  $s_{ph}$  is independent

of temperature, which is not the case. In fact, we can connect  $S_{pn}^2$  in a general way to the response function of the electron gas, so that we have to consider the full temperature dependence of the latter. This results because of screening effects, the sound velocity being related to the plasma frequency of the atoms, renormalized by the dielectric constant of the electrons. Thus we have for the frequency of sound waves (Pines and Nozieres 1966)

$$\omega^2 = \Omega_p^2 / \epsilon(q) \quad (2.4)$$

the plasma frequency being  $\Omega_p^2 = 4\pi N Z e^2 / M$  with  $Z$  the valency and the dielectric constant being connected to the response function  $\chi(q, T)$  by the general formula

$$1/\epsilon(q, T) = 1 - \frac{4\pi e^2}{q^2} \chi(q, T) \quad (2.5)$$

Actually, this equation holds for electrons interacting by means of Coulomb forces in a positive background without external potentials (Pines and Nozieres 1966). Thus, if as in our case, electrons belong to a band, (2.5) would be inapplicable and to overcome the difficulty we assume an effective-mass approximation. This appears justified for s electrons, but less for f electrons. However, the gross features of the physical quantities of interest to us, like the resistivity and the susceptibility, are expected not to depend on details of the density of states. Thus, with the limitation of not describe any fine structure, we can expect that the parabolic approximation, even in the f band, is legitimate. We shall in any case come back to this point later.

Next, the actual computation of  $\chi(q, T)$  is difficult in general. But, in the present case we can use the RPA (Coqblin et al. 1978) so that

$$\chi_{\text{RPA}}(q, T) = \chi_0(q, T) / \left(1 - \frac{4\pi e^2}{q^2} \chi_0(q, T)\right) \quad (2.6)$$

where  $\chi_0(q, T)$  is the response function of the electrons in the band, reduced to free-like particles (Pines and Nozieres 1966).

Thus

$$\epsilon(q, T) = 1 + \frac{4\pi e^2}{q^2} \chi_0(q, T) \quad (2.7)$$

so that, in the limit  $q \rightarrow 0$  we find for the atomic vibration frequency

$$\omega^2 = \frac{v_{\text{sp}}^2}{\epsilon(q, T)} = \frac{v_{\text{sp}}^2}{4\pi e^2 \chi_0(q, T)} q^2 = s_{\text{ph}}^2 q^2, \quad q \rightarrow 0 \quad (2.8)$$

which gives (Pines and Nozieres 1966)

$$s_{\text{ph}}^2 = NZ^2/M \chi_0(0, T) \quad (2.9)$$

This equation should be used twice, for s and for f electrons. In each case the valency  $Z_s$  and  $Z_f$  should be used, respectively. Thus, using (2.9) in (2.3), eq.(2.1) becomes, summing the s and f contributions separately

$$\rho = \rho_s + \rho_f \quad (2.10)$$

with

$$\rho_{s(f)} = \frac{\hbar k_F}{k_s e^2} N \bar{v}_a kT \frac{\chi_0^{s(f)}(0, T)}{N Z_{s(f)}^2} \quad (2.11)$$

The response function  $\chi_0(0, T)$  can be written (Pines and Nozieres 1966)

$$\chi_0(0, T) = - \int_0^\infty d\varepsilon N(\varepsilon) \frac{df(\varepsilon)}{d\varepsilon} \quad (2.12)$$

where  $N(\varepsilon)$  is the density of states appropriate to the band in consideration and  $f(\varepsilon)$  is the Fermi-Dirac distribution function. For s electrons the strong degeneracy ( $\varepsilon_F^s \gg kT$ ) allows to write

$$\chi_0^s(0, T) = N^s(\varepsilon_F^s) \quad (2.13)$$

Thus, the s contribution to (2.11) can be worked out readily and we find

$$\rho_s = AT \quad (2.14)$$

with

$$A = \frac{\hbar k_F \bar{\sigma}_a}{n_s e^2} \frac{K N^s(\epsilon_F^s)}{Z_s^2} \quad (2.15)$$

i.e. the usual linear dependence of a normal metal (Ziman 1965). We note that this relation holds whenever the Fermi energy is much larger than  $kT$  and is not necessarily related to s electrons.

For a narrow f-like band the situation is different. The correct formula to be used is still (2.11) but now the full temperature dependence, arising from the Fermi function in (2.12) has to be taken into account (Fradin 1974). It is then convenient to introduce the dimensionless variables (Coqblin et al. 1978; Jullien et al. 1974)

$$\bar{T} = T/T_c, \quad \bar{\chi}_o(o, \bar{T}) = \chi_o(o, T) / \chi_o(o, 0); \quad \left( T_c = \frac{2}{3} T_F^f \right) \quad (2.16)$$

in terms of which we can write from (2.11) the f contribution

$$\frac{\rho_f}{\rho_\infty} = \bar{T} \bar{\chi}_o^f(o, \bar{T}) \quad (2.17)$$

with

$$\rho_\infty = \frac{\hbar k_F N \bar{\sigma}_a}{n_s e^2 Z_f} \quad (2.18)$$

The evaluation of  $\bar{\chi}$  can be done numerically and the universal curve obtained for  $\rho_f/\rho_\infty$  is reported in fig.1 as a function of

$\bar{T}$ . We note the monotonic behaviour up to the value  $\rho_\infty$ . This arises because when  $\bar{T} \rightarrow \infty$ ,  $\bar{\chi} \propto 1/\bar{T}$  becomes a Curie law. Physically  $\rho_\infty$  is the resistivity that corresponds to isolated atoms so that in fact when  $\bar{T} \rightarrow \infty$ ;  $\rho_f \rightarrow \rho_\infty$  as the atomic motions become uncorrelated. From a mathematical point of view, a saturation value as  $\bar{T} \rightarrow \infty$  is not peculiar of phonon excitations

but is a general property. This follows from the formula of Kaiser and Doniach (1970) on using Kramers-Kronig relations for the response function (Jullien et al. 1974 for an example of spin excitations).

As shown in fig.1, there is little difference between the use of a parabolic and a rectangular density of states in the band and the general trend of the curve is the same. This justifies, at least in part, our particular choice of a parabolic band.

If eq.(2.17) is used to fit an experimental curve, as shown in fig.2, it is seen that  $T_c$  coincides with the abscissa of the intercept of the tangent from the origin to the experimental curve with  $\rho_\infty$ . This may be used as a criterion for a fast choice of  $T_c$ .

We note that the non-enhanced susceptibility of the band electrons appear in eq.(2.8) as already pointed out by Fradin (1974) in a similar calculation. Thus, the actual susceptibility of the system can differ from  $\chi_o(o,T)$  and include enhancement factors. This is important as in fact the behaviour of  $\chi_o(o,T)$  at large  $T$  becomes Curie, while the experimental susceptibility is almost constant with temperature in the cases we consider here (Fournier 1975; Brodsky 1978).

As follows from (2.3) the present calculation is confined to high temperatures such that  $T \gg \Theta$ . From the definition of  $\Theta$  and eq.(2.9) this inequality leads to the restriction, using the asymptotic value  $\chi_o(o,T) \rightarrow NZ/KT$  ( $T \rightarrow \infty$ )

$$T \gg T_o = \frac{\hbar^2 q_D^2 Z}{M K} \quad (2.19)$$

For  $q_D = (6\pi^2 N)^{1/3}$  (Ziman 1965) we find the following values:

$T_o = 1.60$  °K for U,  $T_o = 2.2$  °K for Np and  $T_o = 1.9$  °K for Pu, where we used in the three cases respectively  $Z_U = 4$ ,  $N_U = 4.8 \cdot 10^{22} \text{ cm}^{-3}$ ,

$M_U = 397 \cdot 10^{-24} g$  ;  $Z_{Np} = 5$ ,  $N_{Np} = 5.2 \cdot 10^{22} cm^{-3}$ ,  $M_{Np} = 393 \cdot 10^{-24} g$   
 and  $Z_{Pu} = 6$ ,  $N_{Pu} = 4.26 \cdot 10^{22} cm^{-3}$ ,  $M_{Pu} = 465 \cdot 10^{-24} g$  for the f band.

For the s band we find values around  $T_0 = 250^\circ K$ , following the same estimation method.

### 3. APPLICATION TO U, Np AND Pu.

The calculation of the previous paragraph is oversimplified, but at the relatively high temperatures of our interest, is expected to be general enough. In particular, the crystal structure does not appear to introduce serious limitations. Thus, in this paragraph the theory will be applied to the problem of the electrical resistivity for U, Np and Pu, which show an anomalous behaviour (fig.2) with respect to the normal T dependence as exhibited by Th.

First of all, it is convenient to estimate  $\rho_\infty$  in eq. (2.18). The Fermi wave-vector can be deduced from the density of states/atom of band s electrons  $\sim 0.25$  ev /atom (Fournier 1975), putting it equal to the free-electron expression  $\frac{3}{2} \frac{Z_s}{\epsilon_F^s}$ . This gives  $\epsilon_F^s \sim 12$ ev or  $k_F = 1.78 \cdot 10^8 cm^{-1}$  for  $Z_s = 2$ . Next we estimate  $\bar{V}_a = 4\pi a^2$  where  $a$  is the metallic radius. Available values (Fournier 1975) are  $a = 1.6 \text{ \AA}$  for U,  $a = 1.55 \text{ \AA}$  for Np and  $a = 1.65 \text{ \AA}$  for Pu. This gives values around  $\rho_\infty = 200 \mu\Omega cm$ . We note that the inclusion of a typical Umklapp process magnitude would result in too large values (Ziman 1965) of the resistivity as compared to the experimental ones, which are less than  $150 \mu\Omega cm$ . Thus, they do not appear to play an important role.

According to the discussion of the previous paragraph we can now estimate quickly the value of  $\bar{T}_c$ , by drawing the tangent from the origin to the experimental curves and looking

at the abscissa of the intercept with  $\rho_{\infty}$ . This leads to  $T_F^f = 3.686 \cdot 10^3$  °K for U,  $T_F^f = 5.17 \cdot 10^2$  °K for Np and  $T_F^f = 1.02 \cdot 10^2$  °K for Pu. The true experimental curves are obtained by subtracting the normal behaviour set equal to the resistivity of Th, which is assumed to have no or little f character, to have the f contribution alone. The results of the fittings with the above mentioned values are reported in figs.3-4-5. The phonon contribution is seen not to exhaust the full temperature dependence and a second mechanism is clearly revealed.

Before we go on discussing this, it is worth noting the small values of the Fermi temperatures within the f band. The smallness of these values is similar to that deduced by Coqblin et al.(1978). Such very small values are mentioned by Long (1977) for the bandwidth of the f band as a result of the effects of correlation, when the Hubbard U dominates the bandwidth deduced from one-electron theories (Long 1977). From Johansson's (1975) estimates of their ratio this seems to be appropriate for Pu and maybe for Np, i.e. near the localization threshold at Am. Consistently with these arguments, we see that the resultant Fermi energy of U is much larger and closer to the values predicted by the one-electron theory.

From the other hand, such small  $\varepsilon_F^f$  values would lead to a density of states/atom, within the assumed parabolic f band  $\sim 100 \text{eV}^{-1} / \text{atom}$  absurdly high and incompatible with the low temperature specific heat data (Fournier 1975; Jullien 1974; Coqblin et al.1978) indicating a density of states/atom of some  $\text{eV}^{-1} / \text{atom}$ . This can be reconciled with our picture by assuming that the f band has a sharp structure around  $\varepsilon_F^f$  as also pointed out by Coqblin et al.(1978). The parabolic approximation is a poor one as far as the detailed shape is

concerned, as noted previously, representing only an average shape. We obtain qualitatively a density of states possibly as in fig.6.

We note, however, that the value of  $\varepsilon_F^f$  is not connected in our approach with the width  $W$  of the band and, in particular, in our model we cannot infer  $W$  from  $\varepsilon_F^f$ . The width can be much larger than  $\varepsilon_F^f$  leading possibly to values of  $W$  even comparable with those obtained from energy band calculations (Freeman and Koelling 1974). This conclusion would seem to be enhanced by the observation that quantitatively similar fits as those in figs.3-4-5 can be done with the curve B in fig.1, which corresponds to  $\varepsilon_F^f \ll W$ . We cannot thus unambiguously favour one of the models. In this second case we still end with a picture like in fig.6 with a larger bandwidth, a split band model very similar to the covalent model proposed by Friedel (1956) and extensively used by Fournier (1975) in connection with actinides.

The curves C in figs.3-4-5 are the fittings to the difference between the phonon and the experimental contributions. In all the three cases considered we found them to be very well described by a logarithmic expression  $\rho = \rho_0 \ln \frac{T}{T_0}$ , with the values of  $\rho_0$  and  $T_0$  as indicated in the captions to the figures. This can be related to a magnetic scattering, i.e. a Kondo effect (Kondo 1964) originating from an antiferromagnetic coupling between the s conduction electrons and the f band electrons. Although such an interpretation requires that the f electrons are paramagnetic in the sense of a non-zero spin giving rise to spin-flip processes in the conduction band, it does not require a Curie susceptibility in the f band. We shall make this point clear later in connection with the

explanation of the constant susceptibilities. Thus, assuming a Kondo effect we can try to determine the exchange coupling constant  $J$ . Although the  $f$  spins belong to band electrons so that a rigorous treatment of the magnetic scattering would require the introduction of suitable form factors, like in spin fluctuation theories (Kaiser and Doniach 1970; Mills and Lederer 1966) at relatively high temperatures this effect can be neglected. Thus the magnetic scattering contribution can be expressed, according to Kondo (1964) as

$$\rho = \rho_M \left( 1 - \frac{3Z_s J}{\epsilon_F^s} \ln T \right) \quad (3.1)$$

where  $\rho_M$  is the result of the Born approximation, proportional to  $J^2$ . Comparing this with the expression used to fit the curves C in figs.3-4-5, we find

$$\frac{3Z_s J}{\epsilon_F^s} = \ln^{-1} T_0 \quad (3.2)$$

so that we can infer the value of  $J$  from the temperature  $T_0$  at which curves C cross the temperature axis. Assuming  $\epsilon_F^s \sim 12$  ev as previously estimated and  $Z_s = 2$  we find  $J = 0.367$  ev for U,  $J = 0.385$  ev for Np and  $J = 0.456$  for Pu. We note that these values are 3-4% smaller than  $\epsilon_F^s$ , consistent with the use of perturbation theory necessary for (3.1) to hold (Kondo 1964), but much larger than  $kT$ . On the basis of this one expects strong fluctuations of the  $f$  spins to occur, because a large value of the coupling  $J$  will induce transitions between states of up and down spin. In next paragraph we shall try to show how this feature can be useful for the explanation of the constant value of the susceptibility.

A magnetic scattering of the form proposed here is expected to be reasonable when the center of gravity of the  $f$  band is not too close to the Fermi level so that one can assign

a well defined number of electrons to the f band. This would not be true anymore if the f levels are very close to the Fermi energy and the system exhibits mixed-valence behaviour (Atoyan et al.1978)

#### 4.RESISTIVITY AND MAGNETIC SUSCEPTIBILITY

The results of the previous paragraph indicate that magnetic scattering of conduction electrons from fluctuating spins in the f band can provide an explanation of the high temperature resistivity of the lightest actinides U, Np and Pu for which electrical measurements are available. The analysis implies that the magnetic contribution vanishes at  $T_0$ , where the fit of experimental curves can be accomplished by assuming only a phonon mechanism. This suggests that the present theory could be extended to the low temperature region too as in fact we would argue to be, for  $T \ll T_0$  in the compensated, singlet ground state of the Kondo problem (Kondo 1969). It is known that such a state is similar to that of a normal Fermi liquid to which one can apply Landau's theory and in particular one expects a  $T^2$  contribution to the resistivity a result of the exclusion principle (Nozieres 1974). Such a result is in agreement with the observed  $T^2$  dependence (Brodsky et al.1974) of the resistivity. Thus, we obtain a picture where at low temperatures the normal  $T^2$  law of the interacting liquid dominates the phonon contribution but, gradually, as the temperature raises, the compensated state goes over to a strongly fluctuating spin state due to the high value of the coupling J. Correspondingly the resistivity, after a  $T^2$  dependence, decreases and for  $T > T_0$  shows a logarithmic

dependence.

The existence of fluctuating spins offers an explanation to the almost constant susceptibilities. In fact, due to the strong  $J$ , we expect a splitting in the otherwise degenerate two-spin state of the  $f$  spins such that a spin fluctuation lifetime of the order  $\tau_{sf} \sim J^{-1}$  is produced. Correspondingly, the susceptibility can be expressed in the form (Rivier 1968; Heeger 1969)

$$\chi = NZ_f / (1/\tau_{sf}) \quad (4.1)$$

provided, as previously found  $J \gg kT$ . Results for  $\chi$ , using the previously found values of  $J$ , are reported in table 1. For  $Z_f$  we used the number of  $f$  and  $d$  electrons together and the comparison with experimental data is made after subtraction of a normal contribution, identified with that of Th. As one can see, the theoretical results compare favourably well with the experiments, the difference being  $0.1-0.2 \cdot 10^{-6}$  emu/g. This could be attributed to cross terms,  $s$ - $f$ ,  $s$ - $d$  and so on, which are difficult to evaluate, their magnitude being reasonably smaller than the small contribution of  $s$  electrons  $0.4 \cdot 10^{-6}$  emu/g of Th. In particular the theory predicts a slightly higher value for the susceptibility on Np as compared to that of Pu, as is observed (Fournier 1975; Brodsky et al. 1974).

An interesting connection can be established between resistivity and susceptibility by simple inspection of the figs. 3-4-5 and fig.7, reporting the experimental results of Fournier (1975). It is seen that at the temperatures  $T_0$  the susceptibility shows a variation with respect to the overall constant values, although in a different fashion for the three metals. We could attribute this tentatively to the cross-over

from the spin-fluctuating to the compensated state, or at least to the tendency of the system to change its spin-fluctuating state. Being broad in temperature, these changes can hardly be attributed to a structure in the density of states as a function of energy.

## 5. DISCUSSION AND CONCLUSIONS

Let us summarize the principal aspects and results. The main point was to give an expression for the lattice resistivity from phonons originating in the f band as rigorous as possible, although simplified. When this is subtracted from the experimental curve, the possibility of a spin fluctuation mechanism becomes apparent, i.e. a Kondo scattering of s electrons from the electronic spins in the f band with a value of the coupling constant  $J$  greater than  $kT$ . This is then responsible for fluctuations of the f spins, leading to a constant susceptibility. Thus, a single mechanism allows to explain the experimental electrical and magnetic data through the series U, Np and Pu.

The small values of the Fermi temperatures in the f bands are suggestive of strongly correlated bands close to Np and Pu, in agreement with the localization threshold at Am.

The present theory could be extended to treat compounds or alloys of actinides. Many of them show properties analogous to those of the pure metals, in particular the maximum in the resistivity as in Pu and susceptibilities ranging from temperature-independent to Curie-Weiss behaviour (Jullien 1974; Coqblin et al. 1978; Jullien et al. 1974). Possibly some other cases could be treated along these lines, specifically the case of Cm. This metal also exhibits a resistivity very

similar to that of Pu (Schenkel 1977) and a Curie-Weiss susceptibility ( Kanellakopulos et al.1975). Also, the case of Am is of interest. The measured electrical resistivity of this metal (Schenkel and Muller 1977) does not fit in the model developed here. But, as noted previously, the electron states in Am are believed to be localized and hence our model inapplicable to it in its present form. These and similar problems are currently being investigated.

Figure captions

Fig.1. Universal curve for  $\rho_f/\rho_\infty$  as a function of  $\bar{T}$ .

Curve A: free-electron approximation; curve B: rectangular density of states with the Fermi energy much smaller than the bandwidth.

Fig.2. Geometrical interpretation of  $T_c$ . Draw the tangent to the experimental curve (Np in this example) and intercept it with  $\rho_\infty$ . The abscissa of the intercept is  $T_c$ . This figure also illustrates the behaviour of the resistivity of U, Np and Pu.

Fig.3. Experimental resistivity of U as a function of temperature (upper curve A) and after the subtraction of the Th contribution (lower curve A). Curve B is the phonon contribution. Curve C is the result of the subtraction between curve B and the lower curve A. It can be fitted by the logarithmic expression  $\rho = \rho_0 \ln \frac{T}{T_0}$  with  $\rho_0 = 24.4$  and  $T_0 = 230$ . Units are  $\mu\Omega$  cm.  $\rho_\infty = 196$ .

Fig.4. Experimental resistivity of Np as a function of temperature after the subtraction of the Th contribution (curve A). The points B are the phonon f-like fitting and the curve C the difference. This can be fitted with a logarithm as in fig.3 with  $\rho_0 = 68.51$  and  $T_0 = 180$ . Units are the same as in fig.3.  $\rho_\infty = 213$ .

Fig.5. Experimental resistivity of Pu as a function of temperature after the subtraction of the Th contribution (curve A). The dashed curve B is the phonon-like contribution and C

the difference. All as in the previous figures with  $\rho_0 = 67.61$   
 $T_0 = 80$  and  $\rho_\infty = 213$ .

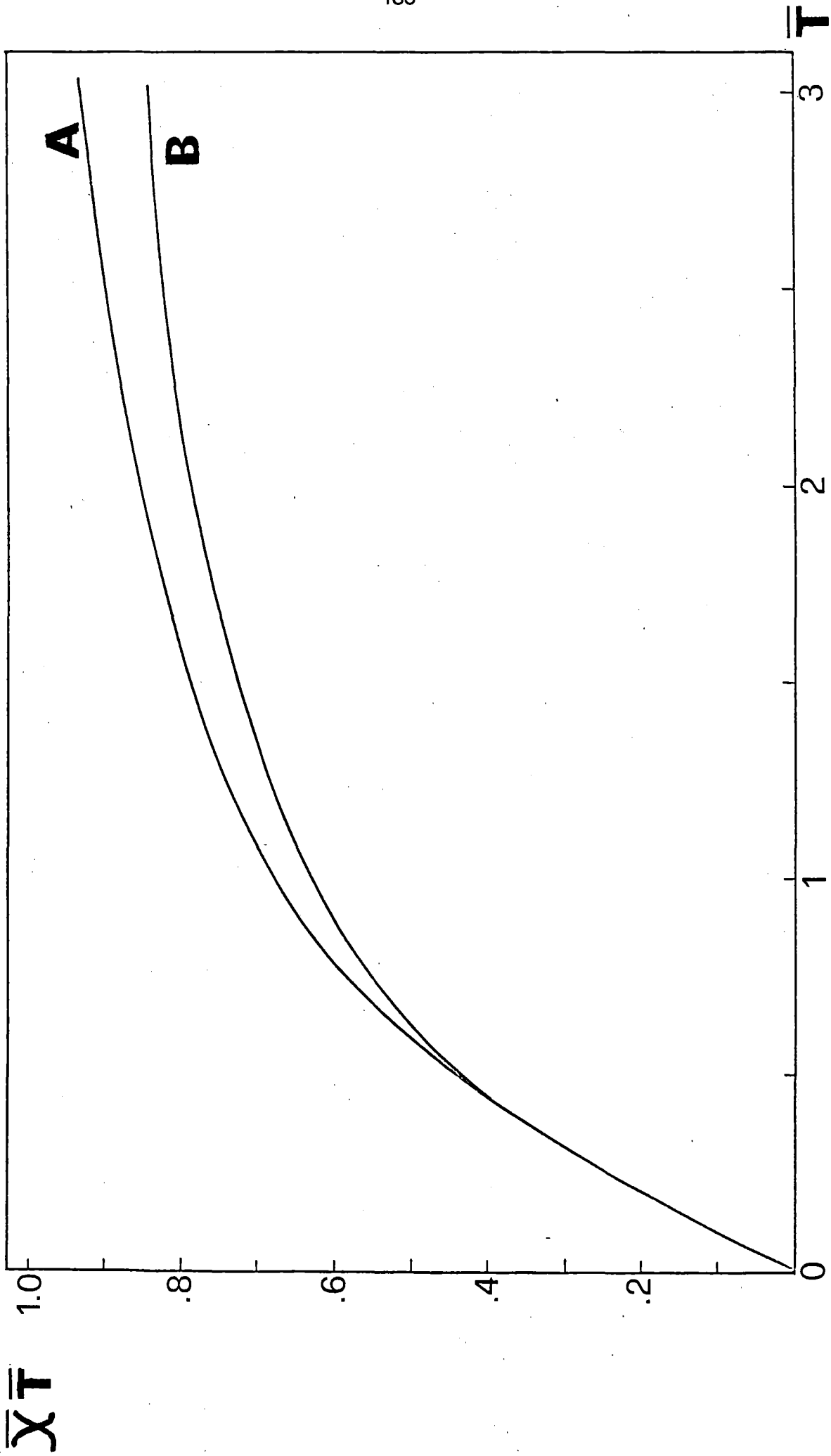
Fig.6. Possible shape of the density of states in the f band (arbitrary units) arising from the results of this paper, in order to agree with low-temperature electronic specific heat data.

Fig.7. Experimental magnetic susceptibilities (from Fournier 1975). Note the changes at  $T=80^\circ\text{K}$  in Pu, at  $T=180^\circ\text{K}$  in Np and at  $T=230^\circ\text{K}$  in U. These values correspond fairly well to the  $T_0$  values of the logarithmic resistivity, indicating a relation between the temperature at which the magnetic scattering vanishes and the values at which the susceptibility changes its constant value.

	U	Np	Pu
J(ev)	0.367	0.385	0.456
$\chi \cdot 10^6$ emu/g (theory)	1.47	1.77	1.51
$\chi \cdot 10^6$ emu/g (exper)	1.23	1.90	1.80

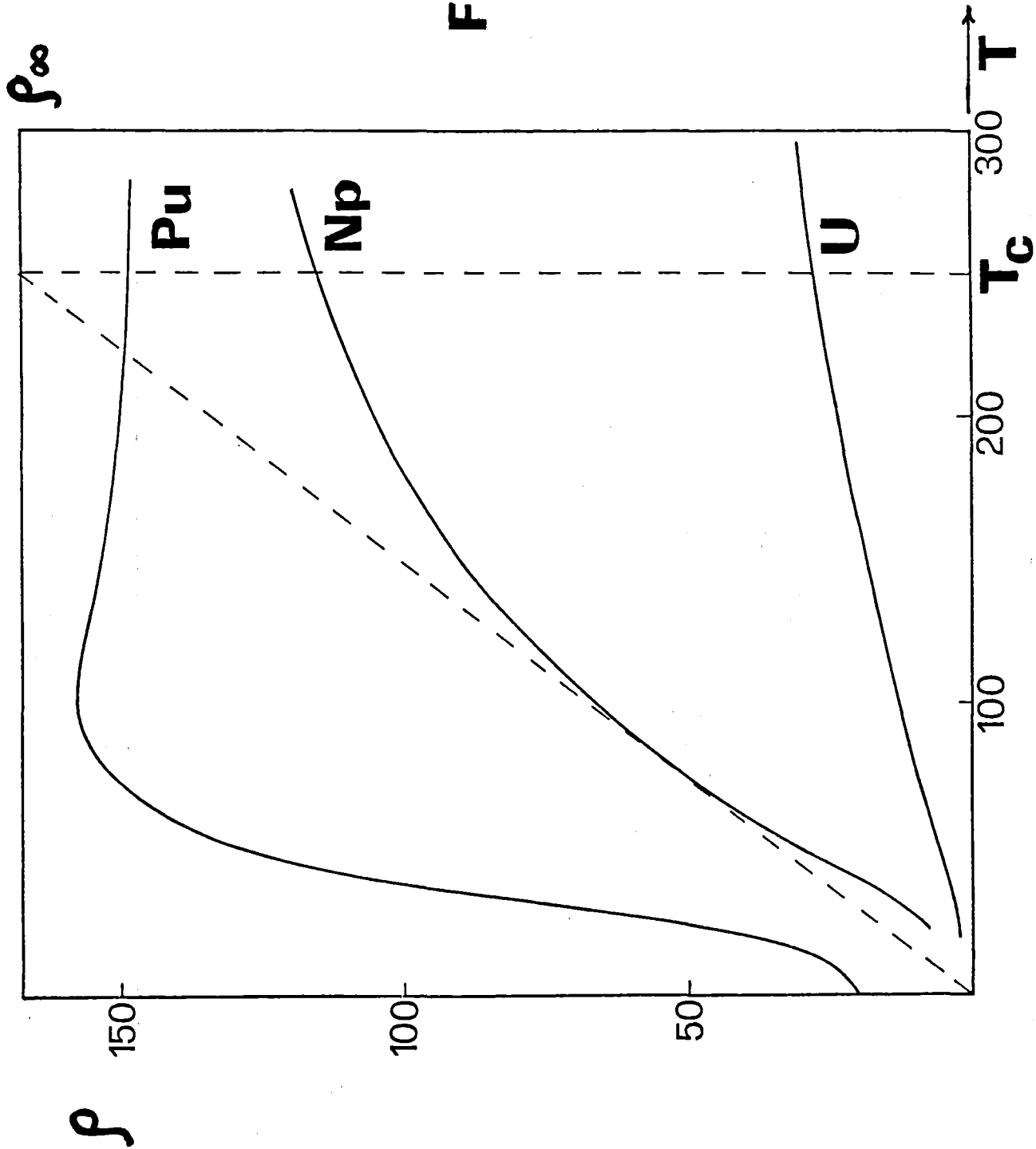
Table 1.

Table caption. Values of the coupling J deduced from the resistivity fits and corresponding calculated  $\chi$  from (4.1). The last row reports the experimental values for comparison, after subtraction of the Th contribution  $\sim 0.4 \cdot 10^{-6}$  emu/g (from Nellis and Brodsky 1974)



**FIG.1**

FIG. 2



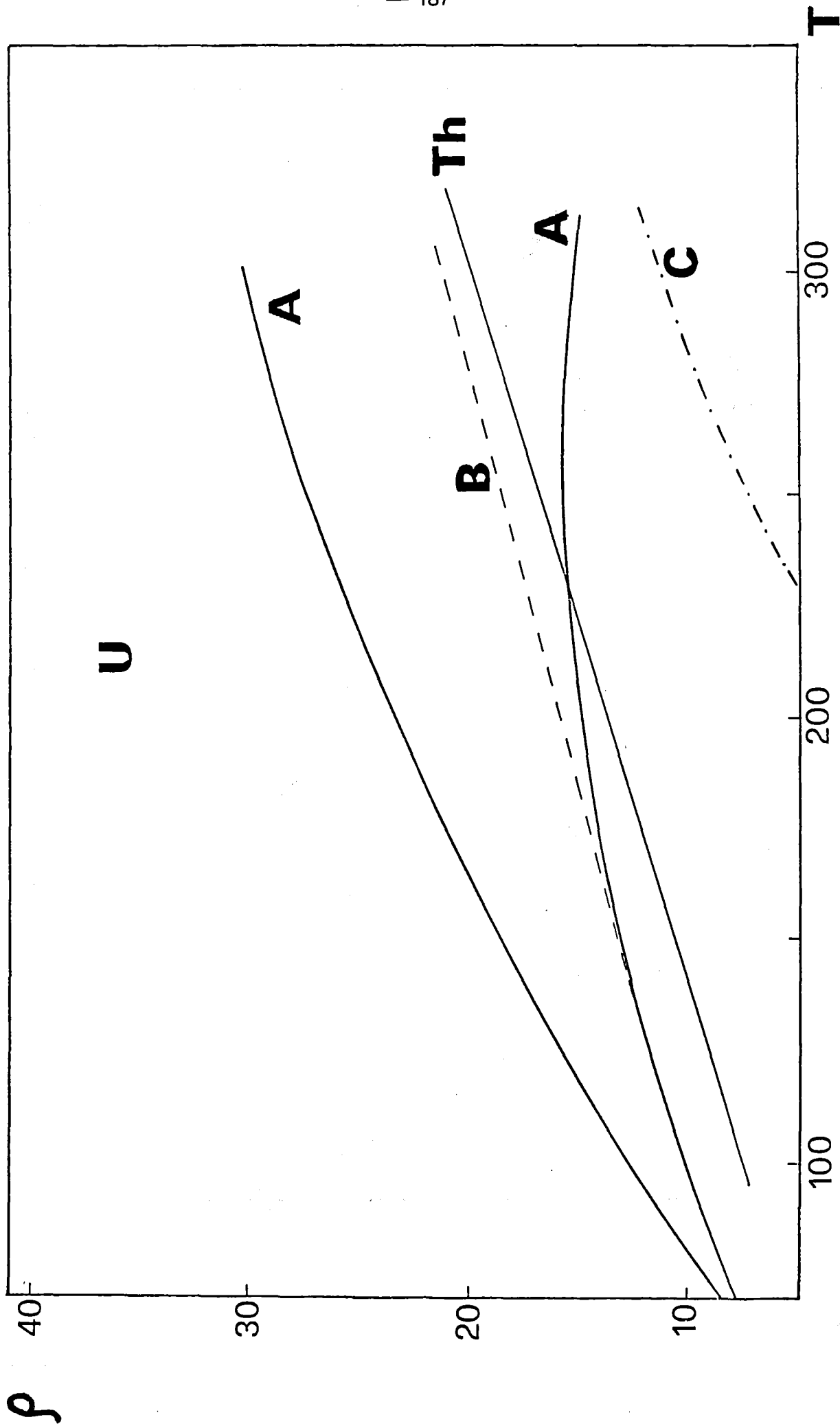


**FIG.3**

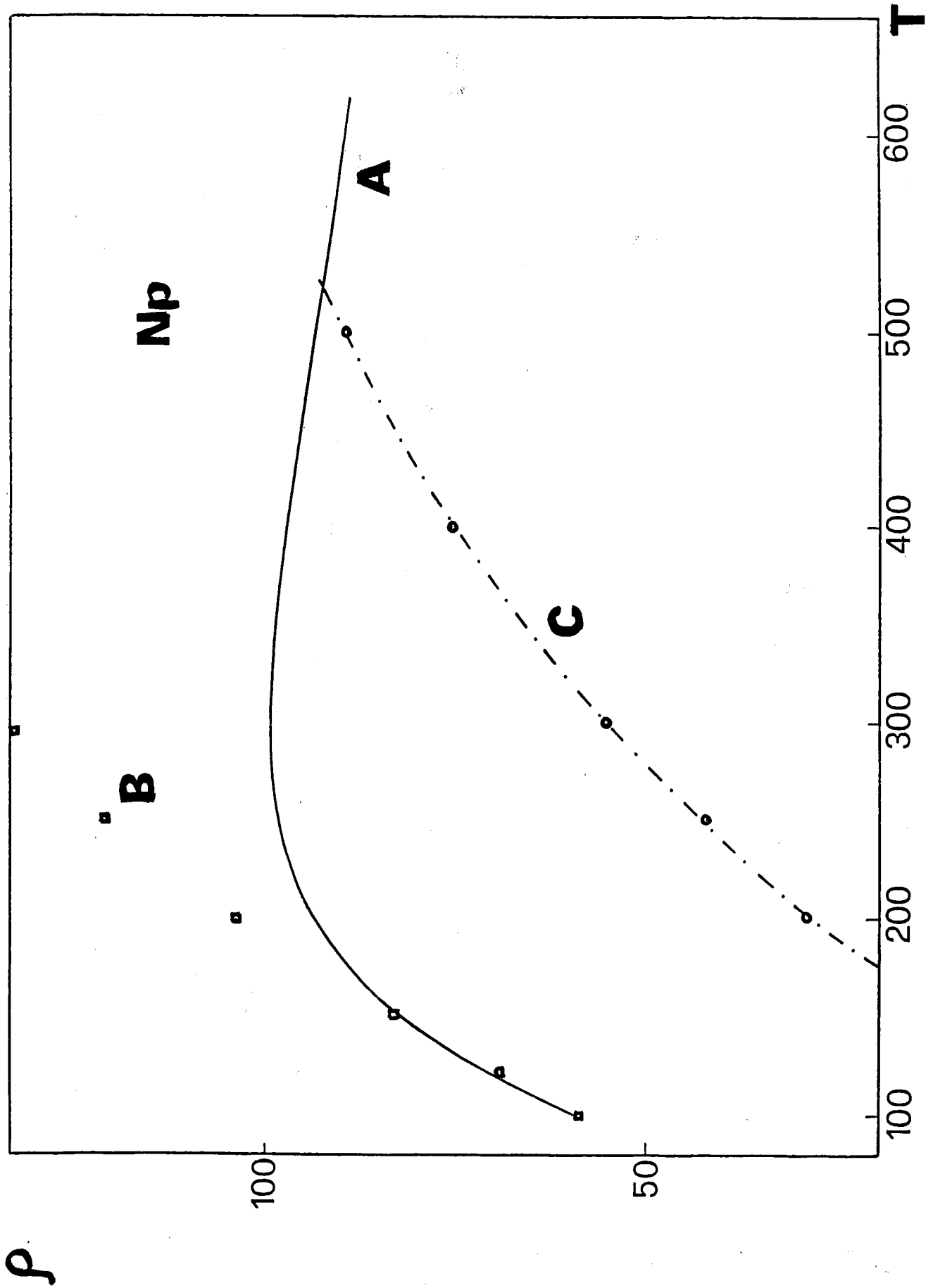
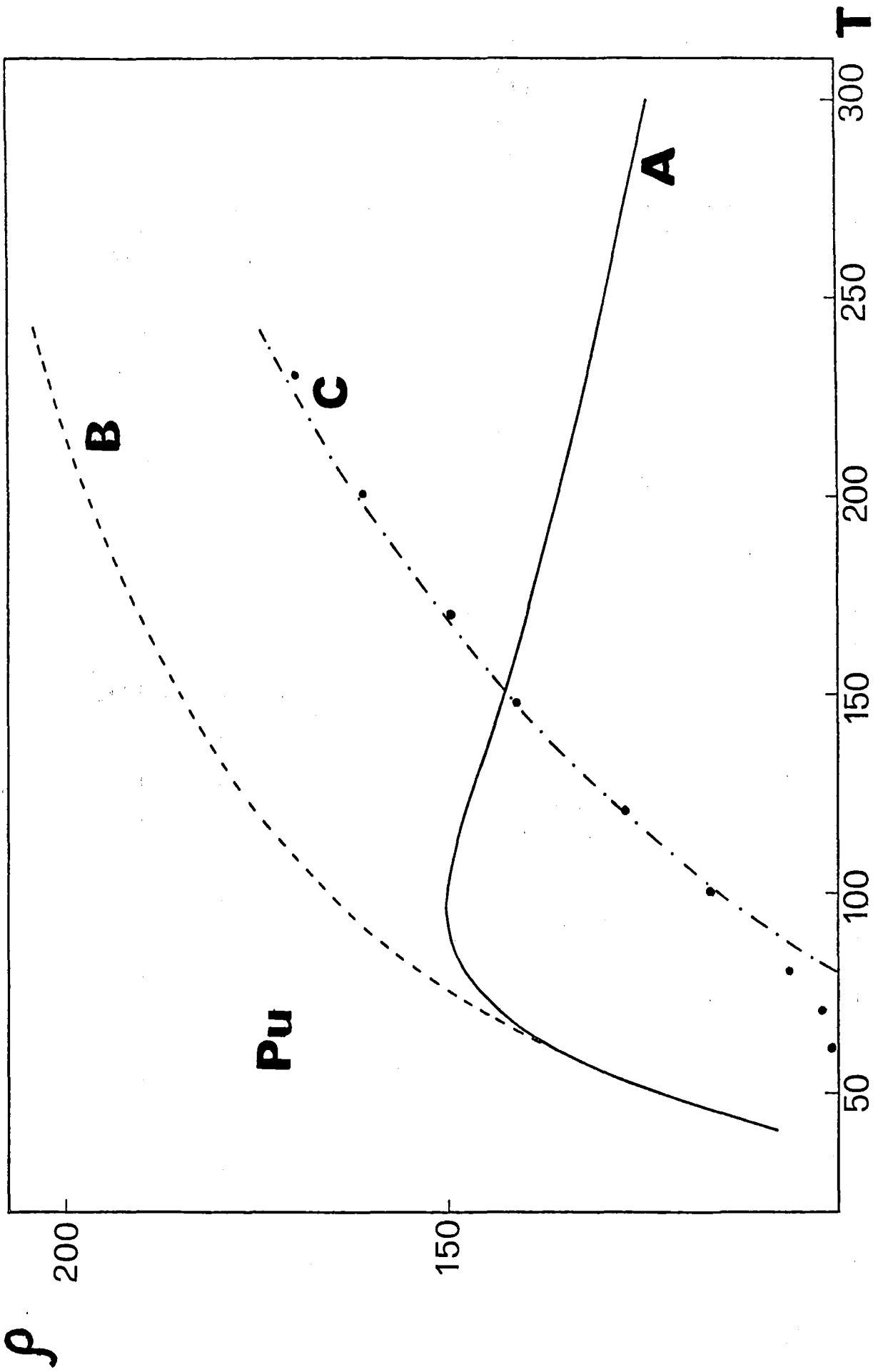
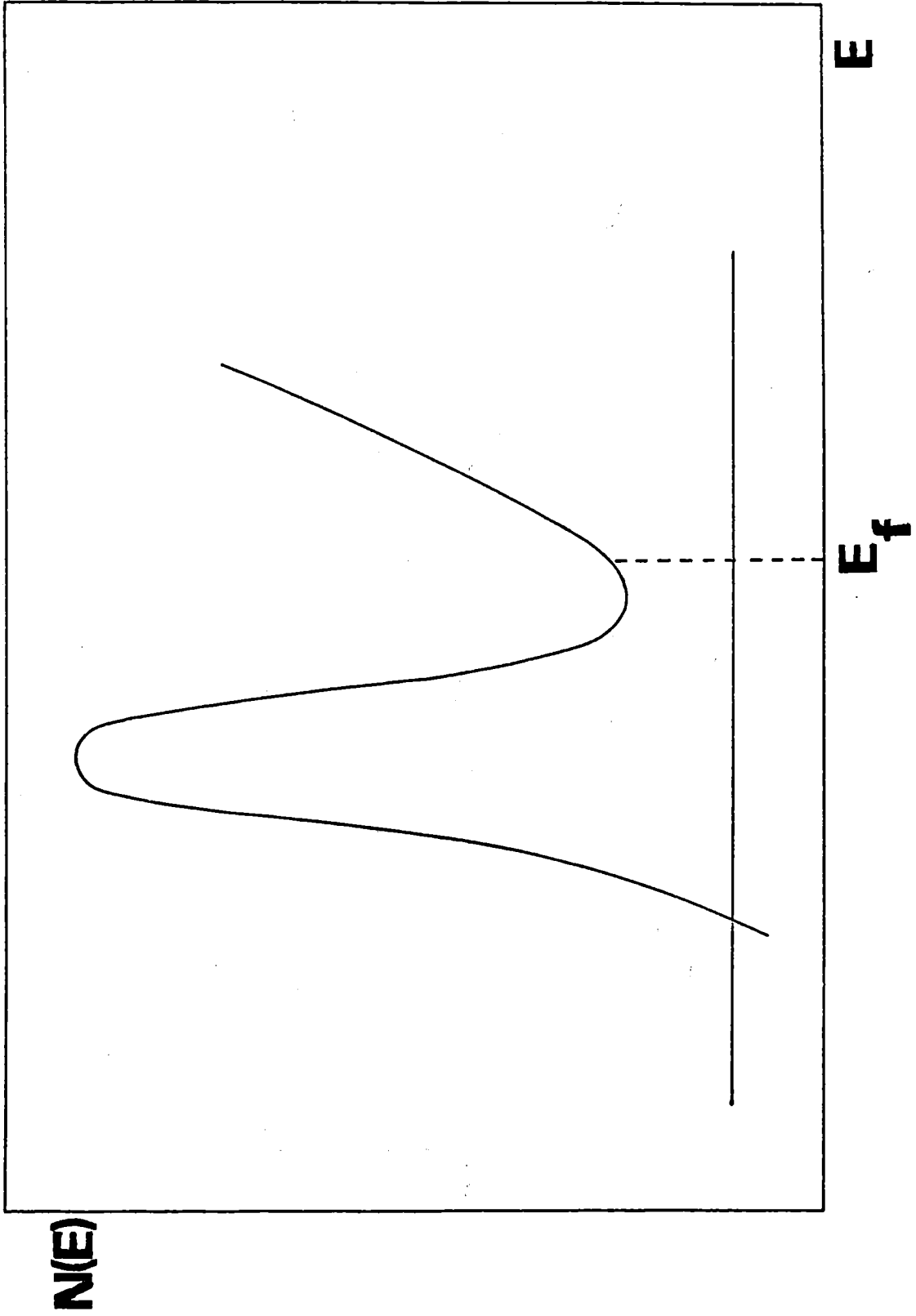


FIG. 4



**FIG. 5**

**FIG. 6**



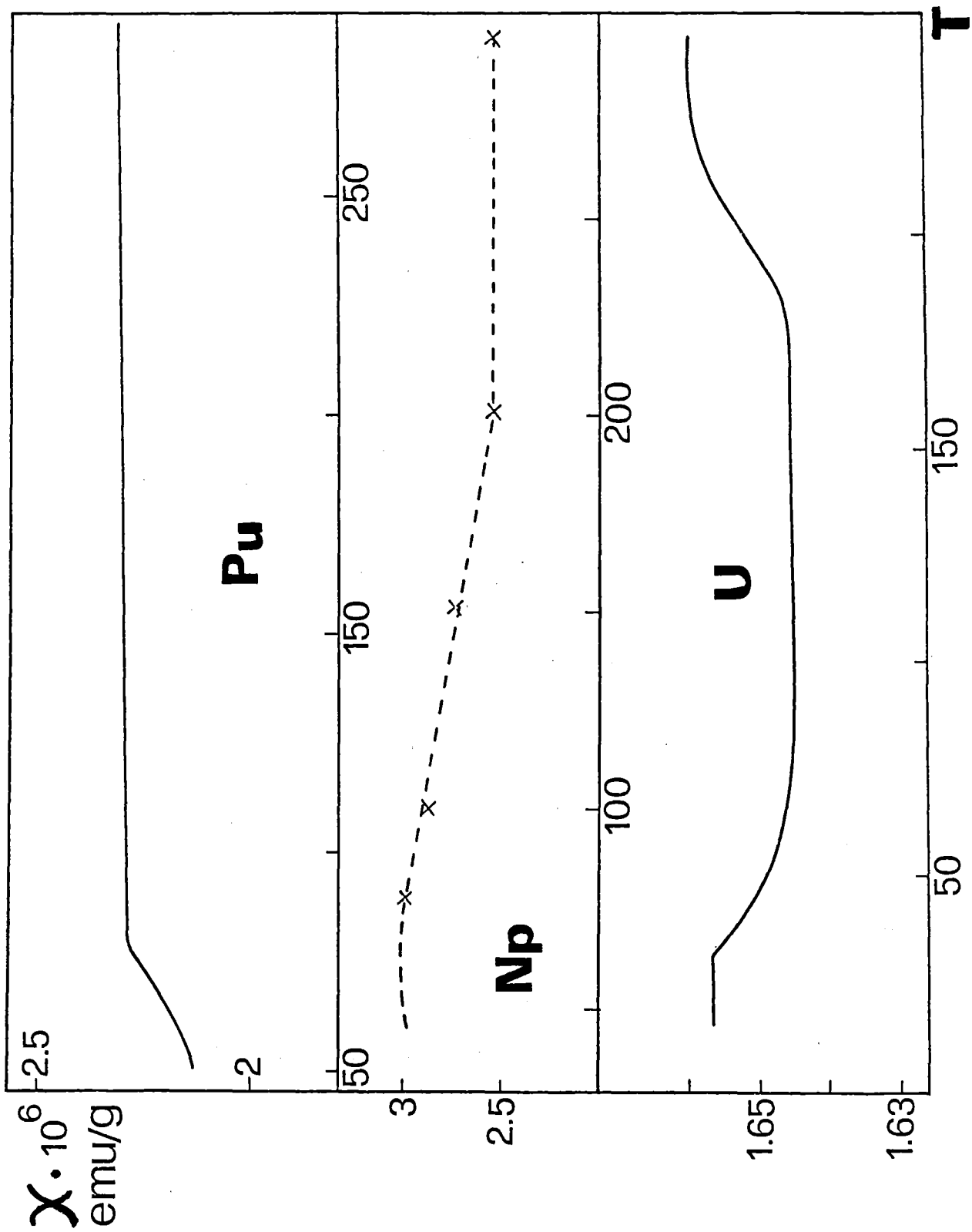


**FIG. 7**

REFERENCES

- Atoyan A.M, Barabanov A F and Maksimov L A 1978 Sov.Phys. JETP 47,1155.
- Brodsky M D, Arko A J, Harvey A R and Nellis W J 1974 in The Actinides, Electronic Structure and Related Properties (Academic Press, New York) Vol.II
- Brodsky M D 1978 Rep.Progr.Physics 41,1547
- Coqblin B, Iglesias-Sicardi J R and Jullien R 1978 Cont.Phys. 19,327
- Doniach S 1974 in The Actinides, Electronic Structure and Related Properties (Academic Press, New York)Vol.II
- Fournier J M 1975 Thesis Grenoble Univ.(unpublished);1976 J.Phys.Chem.Solids 37,235
- Fradin F Y 1974 Phys.Rev.Lett.33,158
- Freeman A J and Koelling D D 1974 in The Actinides, Electronic Structure and Related Properties (Academic Press, New York) Vol.II
- Friedel J 1956 J.Phys.Chem.Solids 1,175
- Heeger A J 1969 Sol.St.Phys.23,283
- Johansson B 1975 Phys.Rev.11,2740
- Jullien R 1974 Thesis Orsay (unpublished)
- Jullien R, Galleani D'Agliano E and Coqblin B 1972 Phys.Rev. 6,2139
- Jullien R, Beal-Monod M T and Coqblin B 1974 Phys.Rev.9,1441
- Kaiser A B and Doniach S 1970 Intern.J.Magnetism 1,11
- Kanellakopoulos B, Blaise A, Fournier J M and Muller W 1975 Sol.St.Comm.17,713
- Kmeto D A and Hill H H 1970 in Proc.Metallurg.Soc.AIME
- Kondo J 1964 Prog.Theor.Phys.32,37; 1969 Sol.St.Phys.23,183
- Long K A 1977 Phys.St.Solidi (b) 79,155

- Mills D L and Lederer P 1966 *J.Phys.Chem.Solids* 27,1805
- Nellis D L and Brodsky M B 1974 in *The Actinides, Electronic Structure and Related Properties* (Academic Press, New York)Vol.II
- Nozieres P 1974 *J.Low Temp.Phys.*17,31 .
- Pines D and Nozieres P 1966 *The Theory of Quantum Liquids* (Benjamin, New York)
- Rivier N. 1968 Thesis Cambridge Univ.
- Schenkel R 1977 *Sol.St.Comm.*23,389
- Tosi M P 1975 *Lectures on The Many Body Problem*, Parma Univ. (Italy)
- Ziman M. J. 1965 *Principles of The Theory of Solids* (Cambridge Univ.Press)

Self-consistent band structure calculations for fluorite  
structure compounds

M.S.S. Brooks and P.J. Kelly

Commission of the European Communities  
Joint Research Centre  
European Institute for Transuranium Elements  
Karlsruhe Establishment  
Postfach 2266  
D-7500 Karlsruhe  
Federal Republic of Germany

Abstract

We present electronic band structures and densities of states for  $UO_2$  and  $CaF_2$  calculated self-consistently using the linear muffin tin orbitals (LMTO) method in the atomic sphere approximation (ASA) and a local density approximation to exchange and correlation. Using the form of the pressure cell boundary relation appropriate to an atomic sphere the contributions to the pressure are calculated. Earlier non self-consistent band structures were calculated with atomic spheres of equal size. We now examine the effects of changing the sphere sizes on charge transfer and on the pressures.

The text contains also results on NaCl-structure actinide compounds, which were not presented at the "9<sup>ème</sup> Journée des Actinides".

## 1. Fully Relativistic Non-Selfconsistent Band Structures.

Spin-orbit terms have been added to the band structure programmes for actinide metals and compounds. Two methods were employed:

a) Following Andersen<sup>1</sup> the spin-orbit Hamiltonian and overlap matrices are added to the normal band structure programs. The process is lengthy in computer time due to several interior summations that must be performed. However, the method has been applied to thorium and the results are identical to the Augmented Plane Wave results of Koelling and Freeman.<sup>2</sup>

b) the speed of spin-orbit calculations may be increased by applying a unitary transformation to the structure constants of the Atomic Sphere Approximation<sup>1</sup> and computing the coupled j-bands. This is particularly useful for actinide compounds, where the band calculations are anyway lengthy. In Fig. 1 we show the  $\Gamma$ -X bands for USb with and without spin-orbit coupling. The largest effect is seen in the uranium 6p band where the original triplet (plus spin states) is split into a quartet and a doublet separated by approximately 0.5 Ryd at  $\Gamma$ . Crossings are also removed in the complex valence and f-band structures.

## 2. Self-Consistent Energy Band Calculations

Self-consistent energy band calculations for actinide metals and compounds have been developed. Thus ionicities (or charge transfer), electron occupation numbers in various atoms and angular momentum states, radial charge densities, and partial densities of states, may be computed. To date  $\text{CaF}_2$ ,  $\text{UO}_2$ , USb, UN, UC and PuP have been studied. In uranium and plutonium mononictides the hybridisation of the actinide f, with pnictogen p electrons has been demonstrated. As an example we show (Fig. 2) the partial contributions to the densities of states, for both uranium and antimony, analysed according to angular momentum character. We note especially how the uranium f and d in addition to the pnictogen p electrons populate the valence band and how the pnictogen p-character re-appears at the Fermi-level in what is normally called the f-band. Just such a mixing is what is required to explain the anisotropy observed in inelastic neutron scattering experiments on USb<sup>3</sup>. Another interesting example is the partial density of states of  $\text{UO}_2$  (Fig. 3). The f-electrons were excluded from this calculation. One may observe how the empty conduction bands are of primarily uranium d-character, and how the uranium d-states contribute to the valence band of the compound. This is the covalent contribution to the bond.

### 3. Energy Bands and Physical Properties: Zero Temperature Equation of State

The self-consistent energy band theory, described in the previous section, is now being used to compute physical properties, starting with the zero temperature equation of state. A change of energy uniform compression is given by

$$\delta E = PV$$

which defines the pressure  $P$ . A computation of the pressure requires many self-consistent band calculations at different lattice parameters. Zero pressure should correspond to the experimentally determined equilibrium lattice parameter. In addition the contributions to the bonding are determined in the calculation. Systematic studies have been made of  $\text{CaF}_2$  and  $\text{UO}_2$ . Some of the results for  $\text{CaF}_2$  and  $\text{UO}_2$  are summarised in Tab. 1. Fig. 4 shows the  $\text{UO}_2$  zero temperature equation of state and various bonding contributions as a function of lattice parameter. We find that  $\text{UO}_2$  is primarily an ionic compound (although less so than  $\text{CaF}_2$ ), but with a considerable uranium d-contribution to cohesion.

In additional computations we have arbitrarily excluded the d-contributions to bonding by restricting our basis states to sp-electrons. This forces the compound to become fully ionic. In  $\text{CaF}_2$  the equilibrium lattice parameter changes by only 2 %, the loss of the d-electron covalent contribution being almost exactly compensated by an increase in the Madelung term. This similarity of the energy of the covalent and ionic bonds explains why simple ionic theories often give good values for the cohesive energies of partially ionic crystals.

In uranium mononictides uranium f- and d-electrons are responsible for the bonding. Although the calculations are at present in progress; we show in Tab. 2 preliminary results for UC and UN. The large negative f and d contributions are closely connected with their hybridisation with the pnictogen p-electrons i.e. their contribution to the valence band density of states.

A very recent computation of the bulk modulus ( $B$ ) of  $\text{UO}_2$  yields a value of  $B = 2.44 \cdot 10^{12} \text{ dyn cm}^{-2}$  compared to an experimental result of  $2.09 \cdot 10^{12} \text{ dyn cm}^{-2}$ .

We would emphasize that the only input to the calculations are the atomic numbers of the atoms of the compound and the crystal structure.

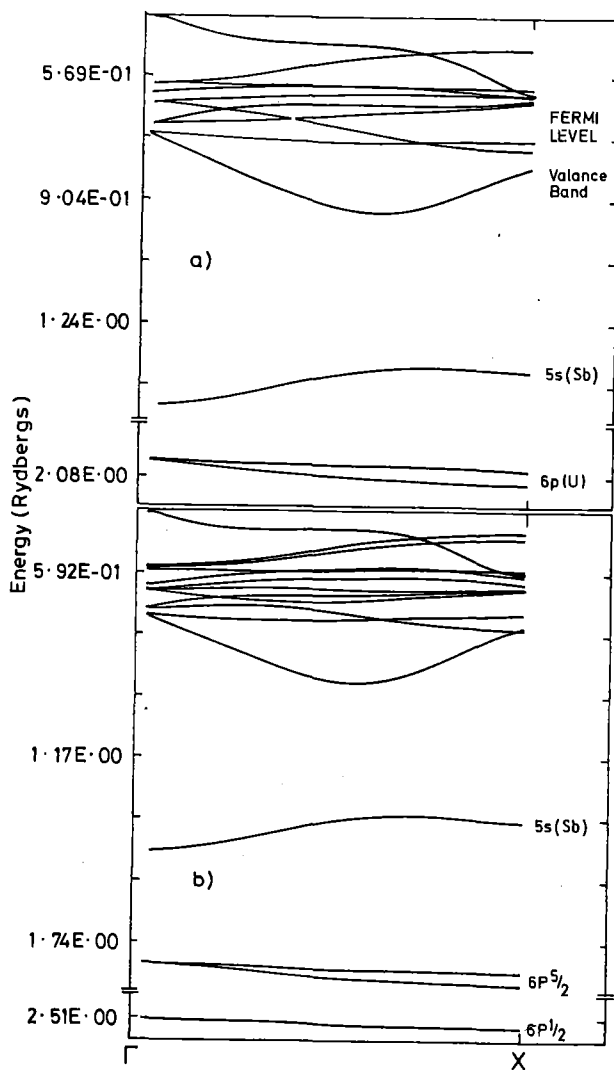


Fig. 1: Energy bands of uranium antimonide; (a) without spin-orbit coupling. The uranium 6p state is at the bottom, (b) with spin-orbit coupling; the  $6p_{3/2}$ ,  $6p_{1/2}$  states separated by about 0.5 Ryd. Several band crossings are replaced by anti-crossings near the Fermi level.

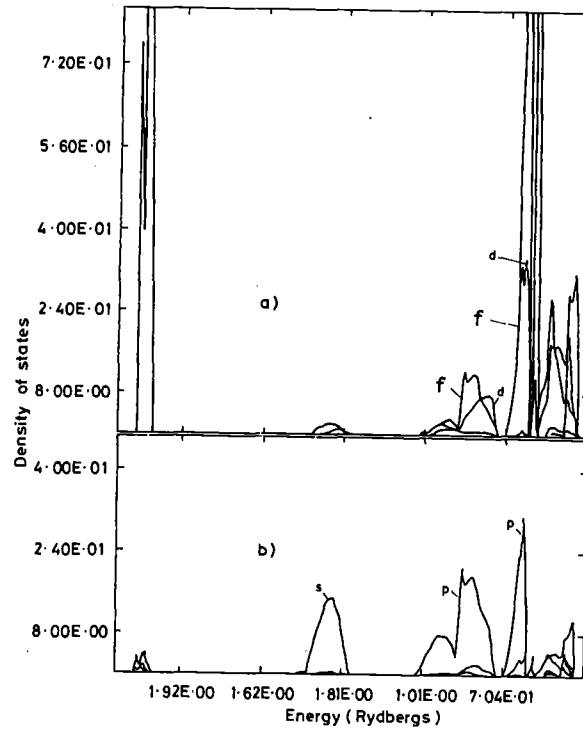


Fig. 2: Partial densities of states in uranium antimonide: (a) uranium, (b) antimony. The principle feature is the f-p-d mixing.

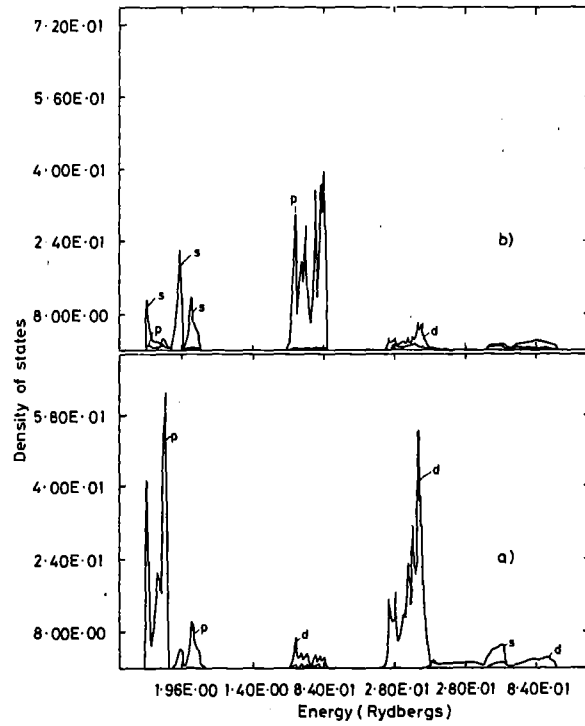


Fig. 3: Partial densities of states of  $UO_2$ : (a) uranium, (b) oxygen. The uranium d-electrons make a contribution to the valence band reducing the ionicity but providing a covalent contribution.

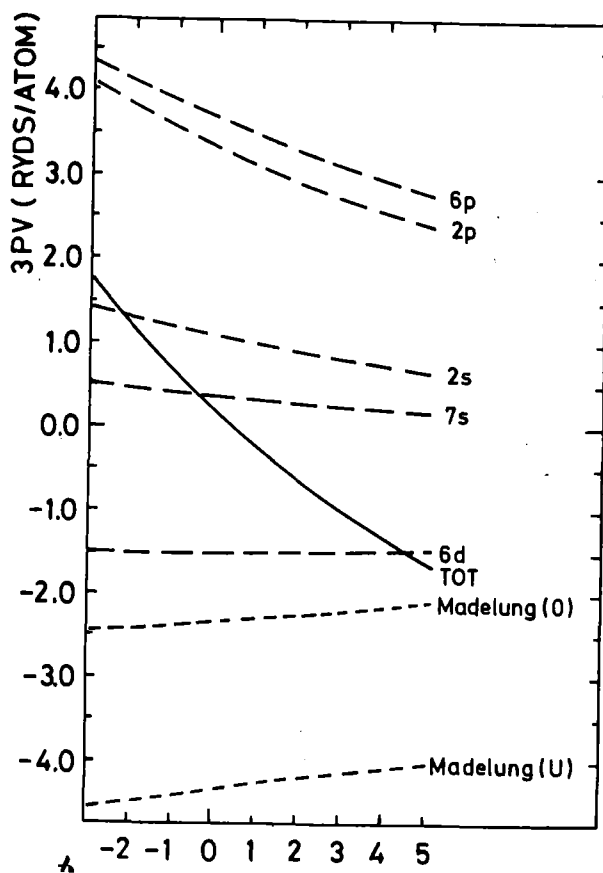


Fig. 4: Zero temperature equation of state of  $UO_2$  (abscissa is the % deviation from experimental equilibrium lattice parameter). The theoretical and experimental lattice parameters differ by about 0.5 %. The electronic pressure contributions (analysed for atom and angular momentum character) are shown along with the Madelung contribution. Only the uranium d-contribution is bonding.

	CaF <sub>2</sub>	UO <sub>2</sub>
Cation charge	1.86	3.4
Theoretical lattice parameter	3% < Experiments	1/2% < Experiments
No. of anion electrons		
s(core)	2.0	2.0
s(conduction)	0.0	0.0
p	5.9	5.7
No. of cation electrons		
s(core)	1.98	2.0
s(conduction)	0.0	0.13
p	5.87	5.61
d	0.29	0.82
d-bonding contribution to 3pv	-0.68	-1.53
Madelung contribution to 3 pv	-2.01	-6.50

Tab. 1: Calcium fluoride and uranium dioxide: a comparison of electronic structure according to band calculations.

	UC	UN
Cation charge	1.5	1.4
No. of anion electrons		
s	1.72	1.90
p	3.86	4.49
No. of cation electrons		
s	0.93	0.25
p	5.94	5.88
d	1.29	1.22
f	2.85	3.25
Contribution to 3p <sub>v</sub>		
cation s	0.24	0.24
p	3.19	2.96
d	-1.42	-1.04
f	-1.99	-1.56
Madelung	-0.84	-0.69
anion s	0.67	0.81
p	0.94	0.72
Madelung	-0.84	-0.69

Tab. 2: Uranium carbide and uranium nitride: bonding contributions from partially converged energy band calculations.

REFERENCES

- 1) O.K. Andersen, Phys. Rev. 12B(1975) 3s060.
- 2) A.J. Freeman, and D.D. Koelling, in The Actinides, Electronic Structure and Related Properties), Vol. 1, A.J. Freeman, and B. Darby, eds., Academic Press, New York, 1974, p. 51.
- 3) O. Vogt, Phys. Rev. Letters 40 (1978)523.

List of Participants

H. Abazli	R.C. Jenkins	M. Thevenin
G. Amoretti	B. Johansson	E. Thibaut
Ch. Apostolidis	J. Jove	R. Troc
R. Baptist	B. Kanellakopulos	V. Varacca
F. Baumgärtner	C. Keller	J.-L. Vasamillette
O. Beck	P. Kelly	P.A. Vigato
M. Belakhowsky	F. Kinnart	J. Verbist
U. Benedigt	R. Klenze	V. Verdingh
A. Blaise	J.C. Krupa	A. Wojakowski
M. Boge	H. Kutter	P. Zanella
G. Bombieri	G. Le Marois	
G. Boussières	J.C. Levet	
M.S.S. Brooks	R. Lindner	
M. Brunelli	K. Long	
K.-C. Buschbeck	G. Lugli	
G.L. Calestani	J. McConik	
J.M. Costantini	L. Manes	
A. Cousson	E. Mastoroudi	
V. Dallacasa	E. Mohs	
D. Damien	L.R. Morss	
F. David	M.J. Mortimer	
P. Delamoye	W. Müller	
G. De Paoli	C. Musikas	
E. Dornberger	J. Naegele	
H. Eschbach	H. Noël	
R.D. Fischer	M. Pagès	
R. Fitoussi	L. Pellegrini	
G. Folcher	R. Poinot	
P. Fulde	F. Rustichelli	
J. Gal	J.P. Silvestre	
R. Gauthier	J.C. Spirlet	
D.C. Giori	A. Stollenwerk	
R. Guillaumont	A. Tabuteau	